



Master of research

Fluid mechanics - fundamentals and applications

Aerodynamics and aeroacoustics

Pressure reconstruction at the interface in Direct Numerical Simulations of two-phase bubbly flows: evaluation of interfacial terms in the averaged modeling

Student :

ANNAMISIA BERTUGNO

Supervisor :

GUILLAUME BOIS - CEA-DEN/STMF

Supervisor :

ANTOINE DU CLUZEAU - CEA-DEN/STMF

This internship has been carried out at
Laboratoire de modélisation et simulation en mécanique des fluides
DEN/DANS/DM2S/STMF/LMSF



Academic year:

2018 - 2019

Abstract

This report details the work carried out during the internship at the LMSF laboratory of the CEA.

Dynamics, pseudo-turbulence and turbulence of two-phase bubbly flows, frequently occurring in the reactors of Nuclear Power Plants, may be analysed performing Direct Numerical Simulations (DNS) of simplified configurations. They may be considered as *numerical experiments* since they provide the instantaneous evolution of the microscopic properties of the flow. These data are available to reconstruct averaged (RANS) equations in order to produce a macroscopic description of the flow, more meaningful for industrial applications and useful for validating and developing new turbulence models. In particular the Two-fluid formulation, where the phases are treated separately, is proved to be a powerful tool to investigate how the presence and the properties of the dispersed phase affect turbulence of the liquid carrier phase. Indeed, when this *up-scaling* procedure is followed, equations for turbulent quantities may be derived too with the aim of having a better insight on the fluctuations induced both by the inhomogeneity of the flow and by its chaotic behavior.

The open-source code TrioIJK developed at the LMSF is devoted to DNS. It resorts to the Front-Tracking method to advect the interfaces and solves the One-fluid formulation of the Navier-Stokes equations for incompressible fluids. The interfacial cells of the fixed-Eulerian grid show an averaged value of pressure because of the discontinuity induced by the surface tension. In the previous application the explicit assessment of the interfacial terms arising in the averaged equations was bypassed. An algorithm devoted to the reconstruction of this discontinuity at the bubble interface has been implemented in order to consider the interfacial cells as ghost cells for both the liquid and the vapor phase. The details of this implementation are presented along with test cases for its validation. The averaged momentum equation is then computed considering adiabatic conditions and neglecting phase-change. The interfacial force M_κ is evaluated explicitly for the first time, as it is pivotal to better point out the role of surface tension in bubble migration, already highlighted by the researches carried out at the LMSF. Under the same hypothesis the Reynolds stress balance equation for the liquid phase is computed too. The presence of a purely liquid microscopic pressure allows a new esteem of the pressure-affected terms. Their influence and the ratio between the interfacial production and the redistribution are investigated. The results obtained on two simple configurations are reported in order to validate the previous application of the code TrioIJK. Additional use of this post-processing tool on different configurations is feasible to confirm the models developed in [1].

Contents

1	Introduction	5
2	General context	7
2.1	Two-phase flows in nuclear reactors	7
2.2	The role of Computational Fluid Dynamics	9
2.3	Single-phase turbulence dynamics and main modelling strategies	10
3	Method	13
3.1	One-fluid formulation	13
3.2	Front-Tracking	14
3.3	Local instantaneous "Two-fluid" formulation	17
3.4	Up-scaling, turbulence and averaged formulation	17
4	General physical remarks	22
4.1	Momentum balance and surface tension	22
4.2	Reynolds stress tensor transport equations	24
5	Pressure reconstruction	26
5.1	The Algorithm	26
5.2	Validation	28
6	Computation of the statistics	31
6.1	Interfacial pressure force	31
6.2	Interfacial viscous force	33
7	Single rising bubble	34
7.1	Mesh convergence	35
7.2	Momentum budget	38
7.3	Reynolds stress budget	48
8	Swarm of bubbles	59
8.1	Settings	59
8.2	Results	60
9	Conclusions and Perspectives	62
A	Alternative method	64
B	Derivation of the Reynolds stress transport equation	68
C	Code for pressure reconstruction	69

List of Figures

2.1	Functional scheme of a PWR	7
2.2	Functional scheme of a BWR	8
2.3	Flow patterns in a vertical boiling channel	9
3.1	Solved pressure field	16
3.2	Solved velocity field	16
3.3	Planes of the average	18
5.1	Different types of point defined for the pressure evaluation by Santarelli and al.	26
5.2	Example of the currently implemented algorithm.	27
5.3	Trend of extended and computed pressure at $y = 0.131$ m and $z = 0.18$ m	29
5.4	Pseudocolor of liquid pressure	30
6.1	Averaged momentum equation along z - direction	32
6.2	Averaged momentum equation - vapor phase	32
7.1	Configuration of the test case	34
7.2	Evolution in time of liquid (U_l) and gas (U_v) velocity.	35
7.3	Mesh convergence - Interfacial production	37
7.4	Averaged momentum equation - liquid phase	39
7.5	Velocity distribution on a plane $z = 0.0025$ m and $t=??$	40
7.6	Integral of the momentum equation - liquid phase	41
7.7	Confront between the two methodology	42
7.8	Averaged momentum equation - vapor phase	42
7.9	Integral of the momentum equation - liquid phase	44
7.10	Confront between the two methodology	44
7.11	Momentum equation for the mixture	45
7.12	Contributions in the equation 3.21	46
7.13	Contributions in the equation 3.21-Integral version	46
7.14	Influence of the liquid extended pressure field on the pressure diffusion	49
7.15	Influence of the liquid extended pressure field on the redistribution	50
7.16	Check on the consistency of the viscous contributions in 3.22	51
7.16	Contributions to the R_{ij} balance equation	53
7.17	Contributions to the K balance equation	55
7.17	Contributions to the R_{ij} balance equation	57
7.18	Confront between the explicit and implicit esteem of Π_{ij}	58
8.1	Initial position of the bubbles in the box.	59
8.2	Evolution in time of liquid (U_l) and gas (U_v) velocity.	60
8.3	Extended liquid pressure field on a plane at $y = 0.0025m$ after 4 time-steps.	61
A.1	Pressure extended field in the liquid phase on a slice along the z axis. Time step=100	65
A.2	Pressure extended field in the vapor phase on a slice along the z axis. Time step=100	66
A.3	Difference between the liquid extended field and the on-fluid pressure field on a slice along the z axis. Time step=100	66

List of Tables

5.1	Geometrical parameters for the single bubble test case	28
5.2	Parameters of the colliding bubbles test case	29
7.1	Physical and geometrical parameters of the test case	34
7.2	Mesh converge study: the component along the streamwise direction is considered.	36
8.1	Geometrical and physical parameters - swarm of bubbles case	59
8.2	Interfacial pressure contributions and redistribution.	61
A.1	Physical and geometrical parameters of the studied configuration. The grid is uniform and the initial velocity profile for the component along x is quadratic.	65

1 Introduction

Two-phase flows made up of a gas and a liquid occur in several contexts, both in natural phenomena and engineering applications: rain, breaking waves on one hand, cavitation in pumps, combustion of liquid fuels, boiling water in the reactor of a nuclear power plant on the other, are just few examples. Thus, accurately analyzing and predicting the behavior of such systems has a remarkable scientific, technological and economic relevance.

These flows may appear in different forms, such as stratified or dispersed, depending on the relative concentration of the two phases, on their properties and on the flow regime. Each of them implies its own characteristic length and time scale, its own type of interaction between the phases and therefore needs a different mathematical and numerical model. Indeed, two phase-flows are of major importance because the continuum approach, namely the use of the Navier-Stokes equations, solves the entire range of scales involved which is wide when the size of the system analysed is huge with respect to the smallest continuum scale, as happens often. Then, questions on how to extract significant information through average and models arise and, as a unique answer is clearly not possible, this stands as a major issue in multiphase computational fluid dynamics. Moreover, although the behavior and the governing equations of both the phases are well known, setting up an adequate way to describe their interaction is an open challenge.

The present work focuses on the dispersed bubbly flows, where the low vapor concentration induces it to occur in small bubbles and the carrier continuous liquid phase is solved. This regime often emerges in the reactors of Nuclear Power plants. The behavior of these flows is similar to the one of the homogenous flows, with the only huge exception that the small scale dynamics is incredibly reacher. This circumstance has an impact on the transition to turbulence and on its development. Thus the description and the study of this multiscale and chaotic phenomenon, frequent in industrial applications, becomes a challenging issue also because experiments able to provide detailed information about the interaction of the bubbles with each other and the flow are often too complicated or expensive to be carried out. The Direct Numerical Simulation, resolving all flow scales, still remains the most powerful investigative tool, acting like a 'numerical experiment', whose importance is destined to increase along with the High Performance Computing development.

As stated before, the complexities caused by both turbulence and by the interfacial phenomena might be addressed resorting to several approaches and mathematical models, rather than relying on the huge amount of information describing them at a local scale. Averaged equations are found out to be a useful tool as they follow a Reynolds decomposition and are suitable for obtaining information on quantities traditionally employed to characterize turbulence. Therefore DNS could be involved in an *up-scaling* procedure: the data they provide on the instantaneus fields are used to build the averaged equations. Then the resulting information could be relevant both for a physical analysis and to improve turbulence models more practical than DNS in engineering applications. In case the bubbles are considered and resolved as finite-size particles, the presence of the interface results in the showing up of new terms in first and second order averaged governing equations that play a relevant role as they cannot be neglected or reduced. Consequently their precise esteem becomes crucial to understand the underlying physical phenomena and elaborate performing models. Accurate reference data for the averaging should be provided by the DNS and therefore the need for proper and stable algorithm is significant.

The main aim of this work is to develop and then implement an algorithm for the reconstruction of the discontinuous pressure field at the very interface in order to rely on these precise values in both the averaged momentum and in the Reynolds stress balance equations, as they are proposed in [1].

This algorithm must fit for the open source code TrioIJK developed at the CEA, devoted to

the resolution of two phase flows and based on a Front-Tracking method. Its structural formula prevents us to have a value of liquid and vapor pressure in the interfacial cells of the mesh since an unique value for the entire mixture is assigned to them by the Navier-Stokes solver.

The report is organized as follows: the section 2 presents the motivations of the research carried out by the CEA and thus of the present work, focusing firstly on the occurrence of bubbly flows in Nuclear Power Plants, then on the numerical issues their study entails, with a particular emphasis on the study and modelling of turbulence. Then a general outline of the numerical method implemented in the code TrioIJK and in particular of the Front - Tracking is provided in 3, along with the formulation of the governing equations determining the final shape of the interfacial terms. The section 4 is devoted to a short resume of the main features of bubbly flows dynamics considering its effect both on the motion of the bubbles and on the turbulence in the liquid phase. The section 5 deals with the accurate description of the algorithm coded to extend the single phase pressure to the interface and the tests carried out to validate it are presented. The section 6 is devoted to the exposition of the results obtained computin the averaged equations on a test configuration with the aim of displaying the effect of the interfacial forces. Firstly the pressure contribution is highlighted, then the viscous stress effects on the interface and the numerical problems it entails. The section ?? and ?? contain the results obtained applying the new algorithm and then the whole up-scaling procedure on a simple configuration with a single bubble rising in a periodic box and then on a swarm of bubbles.

Finally in ?? the conclusions drawn from this work are presented along with suggestions and perspectives on the topic. The appendix provides an insight of an alternative method tested to recompute the interfacial pressure which takes inspiration from numerical methods for multiphase flows.

2 General context

The work described in the present report is related to the studies carried out by LMSF laboratory of the CEA and have numerical, mathematical and physical motivations. In order to understand them it is required to take a step back and expose the context: the industrial applications of bubbly flows are presented here alongside to the role played by Computational Fluid Dynamics (CFD) in their study, especially when a turbulent configuration is taken into account. For this reason a description of turbulence is presented too.

2.1 Two-phase flows in nuclear reactors

Before detailing the numerical method adopted in the study of the bubbly flows, a short overview on the context of their application in reference to the Nuclear Power Plants is needed.

The main purpose of a Nuclear Power Plant is to productively use the heat originated by the splitting of the radioactive atoms in the core of the reactor. This heat is then retained in various form and employed in the production of steam that is the major actor in electric energy production or in propulsion systems. Clearly water is the main vector fluid to accomplish this heat storage and transfert due to its well - known and tested features. Nevertheless its final thermo - hydraulics is affected by the specific technological layout adopted.

The most common type of Nuclear Reactor is the Pressurized water reactor (PWR), where water in primary cooling loop is pressurized to prevent boiling, whereas the phase change only takes place in a secondary loop, less exposed to radioactive contaminations. In order to reach this aim some pressurizers are introduced in the reactor to establish a pressure of approximately 155 atm necessary not to induce vaporization into the hot water flow at a temperature of $300^\circ\text{C} - 330^\circ\text{C}$.

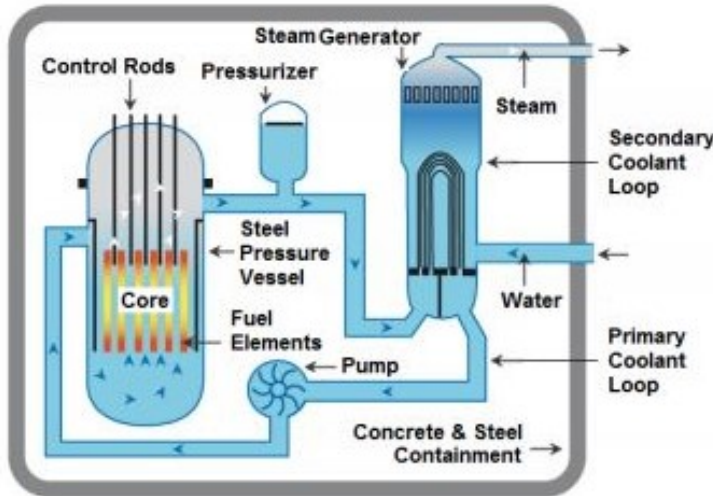


Figure 2.1: Functional scheme of a PWR

Some of the critical issues connected to the need for an extremely high pressure are overcome by the Boiling Water Reactors (BWR), whose main feature is a primary coolant loop which lets the water boil and produce the steam needed to generate electricity.

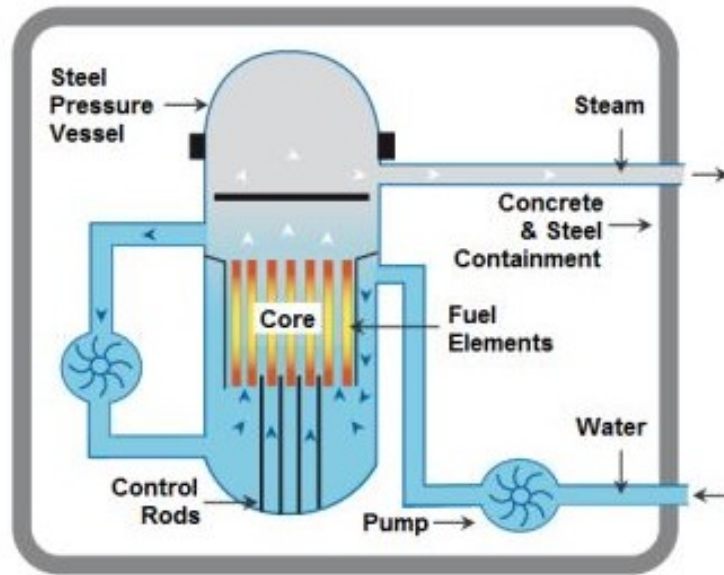


Figure 2.2: Functional scheme of a BWR

In both of the examples provided (and that are not intended to be thorough) multiphase flows emerge from boiling, but the interaction between vapor and liquid are much more pivotal in the BWR, where the characteristics of the mixture determine the working condition in the reactor. As a matter of fact in the vertical channels of the cooling loops where boiling is allowed, the flow undergoes successive transformations once the boiling temperature is reached, changing its regime. As displayed in figure 2.3 one can distinguish:

- Bubbly flows, where the vapor is dispersed, although their shape is not unique and depends on multiple factors;
- Slug flows. The bubbles coalesce and aggregate thus causing some slugs into the channel, whose wakes include an immensely rich topology and dynamics;
- Annular flows. When the void fraction (namely the ratio between the volume of gas and the total volume occupied by the flow) increases the gas extends over the center of the channel, whereas the liquid phase concentrates along the walls and in tiny droplets into the channel.

The above-mentioned classification is evidently only a simplification of complex unsteady transitional phenomena where the boundaries between one pattern and the other is not unambiguously defined.

Bubbly flow, the object of this work, is then the very first step in this progress and the developments it activates into the ducts may pilotate the entire boiling process. As a consequence the comprehension of its physical inner workings where dynamics and heat transfer are highly connected results essential to predict the evolution of the flow patterns and avoid conditions that may be critical or dangerous for the reactor. For instance, if the bubbles gathers on the walls of the channels and create an internal dry film, there may be local peaks of temperature that provokes a risk of melting and collapsing of the system. The flux responsible for this sudden increased temperature is called the Critical Heat Flux and must be avoided. Broadly speaking two - phase flow play not only a functional but also a control role in nuclear reactors and furthermore in the undesired case of accident, the presence of multiphase flows is almost unavoidable.

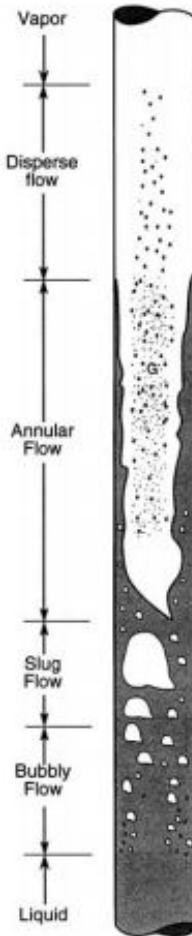


Figure 2.3: Flow patterns in a vertical boiling channel

2.2 The role of Computational Fluid Dynamics

In this framework the knowledge of the characteristics of the flow and above all their *prediction* is needed to design a safe reactor. Evidently not all the conditions can be analysed with experiments and, as the scientific community acknowledged long ago, the Multiphase Computational Fluid Dynamics (see [1]) suits the aim as it allows to reproduce numerically the behavior of this kind of flows. Models are clearly needed in this procedure and in most of the established CFD codes they are developed following on an empirical basis. In order to provide reliable information on turbulence, multi-phase interaction, heat transfer, they ought to be validated by comparison with trustworthy data and all the simulations should be carried out under full control over numerical errors and uncertainties. It is a huge challenge because of the high complexity of multiphase flows, whose governing equations add new terms to the already complex Navier - Stokes equations, and because the progress made in this field are too recent to enable an extensive database.

The STMF (*Sérvice de thermo-hydraulique et de mécanique des fluides*) of the CEA (*Commissariat à l'énergie atomique et aux énergies alternatives*) makes an effort to develop CFD tools to reproduce and analyse bubbly flows and the present work is connected to these studies (see [1], [2], [3].)

In order to avoid the above - mentioned problems of modelling that affect most of the current numerical simulation of multiphase flows, this analysis is grounded on the DNS. It is recalled that this approach consists in solving the governing equations setting on the proper boundary and initial conditions to describe a single realization of the flow. This simulation has the immeasurable advantage of not needing any model to close the equations and therefore does not rely on any

simplifying hypothesis whose validity may be questionable. On the other hand the computational cost is still too high and this approach is then not conceivable at all to simulate real industrial applications especially for two-phase turbulent flows. This limitations notwithstanding, the DNS is the only tool to provide a "numerical experiment" and proceed with an analysis of the dynamics, still not completely known, of this type of flows. Evidently the configuration under investigation cannot be complex, but they allow a first, fundamental insight to develop further theories and models.

The present work is based on the tools provided by the code TrioIJK developed by CEA specifically for the DNS of two - phase flows. The relevance of this internship is connected to the procedure of the *up-scaling*: the microscopic data obtained thanks to DNS are the fundamental material of an averaging procedure aimed at providing more tractable and meaningful information on the flow properties.

It is necessary in this context to recall that this procedure and as a consequence the numerical issues this work deals with have as main aim the study of turbulence and how the properties of the liquid phase undergo changes because of the presence of bubbles. An insight on the main features of this phenomenon and of the problems it poses in modeling (and then in CFD) is needed. It is noted that most of the concepts exposed in the following refer to the single-phase dynamics. New problems arising in connection with the presence of the second phase will be detailed in other sections.

2.3 Single-phase turbulence dynamics and main modelling strategies

Turbulent flows are found almost everywhere in natural and industrial context, but still a precise knowledge and an accurate description of what exactly happens in such flows are not available. As a matter of fact they are characterized by a velocity field changing randomly in both space and time. Therefore turbulent flows are *chaotic*: though the Navier-Stokes equations are perfectly able to describe their behavior in a deterministic way, owing to their non-linearity, they show an extremely high sensitivity to initial and boundary conditions that makes unpredictable the time evolution of the system beyond some point. Nevertheless the major impact of turbulence on practical applications is due to its unique *phenomenology*: turbulent flows are able to transport and mix fluid in a much more effective way than laminar ones, precisely because of the velocity fluctuations. The viscous phenomena are not relevant anymore in determining the characteristic scales of motions and molecular viscosity can be adopted as a reference quantity to distinguish the turbulent regime. Indeed it is involved in the definition of the dimensionless Reynolds number $Re = \frac{UL}{\nu}$, which expresses the ratio between the inertial and viscous forces: when its value is high the prevalent dynamic phenomena have a different origin and may be addressed to as turbulent. It is noted that in the previous definition U is a velocity , L the characteristic dimension of the flow and finally ν the kinematic viscosity.

The importance of these features of turbulent flows is manifest, since they can define the rate of transport of matter, momentum and heat in a flow. In the context of the thermohydraulics of nuclear reactors, as stated before, the turbulent regime is almost unavoidable and its characteristics have an extremely strong impact on the framework previously described. The presence of the bubbles is an additional factor that makes even more complicate the phenomena under investigation. This is the reason why the study carried out by the STMF with the software TrioIJK and to whom the present work is at the service, focuses as a first step on the modelisation of turbulent bubbly flows in adiabatic conditions, neglecting phase-change, break-up and coalescence. The DNS performed are able to resolve all the scales of motion, but it is necessary to precise that they are extremely influenced by the Reynolds number. A brief recall of the turbulent scales for single-phase flows is here discussed in order to give to the reader an idea of the computational cost of the DNS. The most spread theories on the development of turbulence (Richardson and Kolmogorov) en-

visage a transfer of energy between the scales due essentially to the convective phenomena present in fluid dynamics. This transfer, usually referred to as *cascade*, is governed by mechanisms of instability and results in the generation of vortices that become smaller and smaller. A limit to this cascade emerges when the viscous effects become relevant and are able to transform the energy into heat. Kolmogorov, on the basis of its theory (not detailed here) and on a dimensional analysis, estimated these scales, the smallest ones where turbulence is remarkable, as follows:

$$\begin{aligned}\eta &= \left(\frac{\nu^3}{\epsilon}\right)^{\frac{1}{4}}, \\ u_\eta &= (\nu\epsilon)^{\frac{1}{4}}, \\ t_\eta &= \left(\frac{\nu}{\epsilon}\right)^{\frac{1}{2}}\end{aligned}\tag{2.1}$$

respectively for space, velocity and time. It is noted that in these definitions appear both the kinematic viscosity ν and the dissipation ϵ . On this basis an esteem could be done on the ratios between the largest and the smallest scale of turbulence resorting to the definition of dissipation on the Reynolds number:

$$\begin{aligned}\frac{L}{\eta} &= Re^{\frac{3}{4}} \\ \frac{T}{t_\eta} &= Re^{\frac{1}{2}} \\ \frac{U}{u_\eta} &= Re^{\frac{1}{4}}\end{aligned}\tag{2.2}$$

To provide an exhaustive description of the dynamics of a turbulent flow, DNS ought to be able to resolve all of these scales. This circumstance limits the configurations that could be studied in this way to relatively low Reynolds numbers. In two-phase flows turbulence assumes different features that will be further detailed in [3.4.3](#).

This is the reason why in most of industrial and engineering applications, turbulent flows are traditionally studied resorting to modeling. The two principal approaches used are briefly described in this section.

- R.A.N.S. Reynolds Averaged Navier-Stokes Equations. The main aim is to study the averaged velocity field $\langle \mathbf{U}(x, t) \rangle$ instead of the instantaneous field. The number of quantities under scrutiny clearly reduces, but in the new governing equations some terms can not be reduced and they express the effect of the neglected features of the flow. These terms are embodied by the covariance of the velocity fluctuations $\mathbf{u}' = \mathbf{U} - \langle \mathbf{U} \rangle$, namely $\langle u'_i u'_j \rangle$ (tensor commonly referred to as *Reynolds stress tensor* and indicated in the following as R_{ij}) and their presence results in a closure problem as the number of unknowns is bigger than the one of the available governing equations. Consequently, most of the research on the turbulence is devoted to the development of models based on a variable number of transport equations to solve this closure issue.
- L.E.S. Large Eddy Simulations. This approach resorts to an intermediate level of approximation between DNS and RANS, since only the dissipative smallest-scale structures are modeled because of their universal features. The largest scale motions, deeply influenced by the geometry of the configuration, are explicitly resolved as happens in a DNS. Such partition is achieved filtering the velocity field on the basis of energetic considerations. As happens for RANS, this approach too is affected by modelling issues that won't be described in this report.

Only the RANS approach is taken into account in the present work, where all the averaging operators need to be specified for the two-phase flows. The closure model is complicated by their

physical properties: in any case the so-called Boussinesq hypothesis is satisfied since the flow is anisotropic. It is not possible, then to verify that the deviatoric part of the Reynolds stress tensor a_{ij} is linearly proportional to the mean velocity gradient, as happens for the viscous stress in the Newtonian fluid. The expression of R_{ij} is then approached as $R_{ij} = -\nu_t \langle S_{ij} \rangle + \frac{2}{3} \rho K \delta_{ij}$, where $\langle S_{ij} \rangle$ is the mean strain rate tensor, $K = \sum_{i=1}^3 \langle u'_i u'_i \rangle$ is the turbulent kinetic energy (responsible for the isotropic contribution) and the coefficient of proportionality ν_t is called *turbulent or eddy viscosity*. Most of the models used for the single-phase flows ($\kappa - \epsilon$, $\kappa - \omega$ or algebraic models) resorts to this notion and just one or two equations to provide characteristics length and time scales and then close the problem.

Since these models are unusable for two phase flows, a different method is worth considering: evolution equations for higher order correlations, namely the components of Reynolds stress tensor $R_{ij} = \langle u' u' \rangle$ themselves are needed along with a closure equation (usually for the dissipation ϵ or for the rate of dissipation ω). This equation then becomes for the generic component in a single phase flow:

$$\begin{aligned} \frac{\partial R_{ij}}{\partial t} + \frac{\partial}{\partial x_l} \left(R_{ij} \langle u_l \rangle \right) &= - \left(R_{jl} \frac{\partial \langle u_i \rangle}{\partial x_l} + R_{il} \frac{\partial \langle u_j \rangle}{\partial x_l} \right) - 2\nu \left(\langle \frac{\partial u'_i}{\partial x_l} \frac{\partial u'_j}{\partial x_l} \rangle \right) \\ &\quad - \frac{1}{\rho} \langle p' \left(\frac{\partial u'_i}{\partial x_j} + \frac{\partial u'_j}{\partial x_i} \right) \rangle - \frac{\partial}{\partial x_l} \left(\langle u'_i u'_j u'_l \rangle + \frac{1}{\rho} \langle p' (u'_i \delta_{li} + u'_j \delta_{lj}) \rangle - \nu \frac{\partial R_{ij}}{\partial x_l} \right) \end{aligned} \quad (2.3)$$

When writing down this equation the only available quantities are the mean velocity and pressure field and the velocity covariance, thus all the terms appearing in the LHS of 2.3 and the so-called *production* are available. In literature the production is embodied by $- \left(R_{jl} \frac{\partial \langle u_i \rangle}{\partial x_l} + R_{il} \frac{\partial \langle u_j \rangle}{\partial x_l} \right)$ and stands for the production of turbulence by means of the mean velocity gradient. As all the other terms it will be further detailed and specialized for the two-phase flows in the sections 3.4.3 and 4.2. All the other quantities are not known in closed form, namely the pressure-rate of strain $\langle p' \left(\frac{\partial u'_i}{\partial x_j} + \frac{\partial u'_j}{\partial x_i} \right) \rangle + \frac{\partial}{\partial x_l} \langle p' (u'_i \delta_{li} + u'_j \delta_{lj}) \rangle$, the dissipation $\epsilon_{ij} = -2\nu \left(\langle \frac{\partial u'_i}{\partial x_l} \frac{\partial u'_j}{\partial x_l} \rangle \right)$ and the Reynolds stress diffusion $\frac{\partial}{\partial x_l} \langle u'_i u'_j u'_l \rangle$. All of them contain covariances not immediately accessible and thus models are needed.

As stated before, DNS produces information on all the flows variables, the raw material to build these correlations computing the proper averages.

The present work deals with both numerical and modelling issues faced in the up-scaling applied to two phase flows: on one hand the data provided by the DNS are conditioned by numerical methods intended to simulate the dispersed phase, often preventing the access to the exact fields over the whole domain, and on the other hand by the statistical procedure chosen which shapes the final form of terms in the averaged equations. Typically in the case of the two-phase flows these terms convey the presence of the interface and mutual influence between liquid and gas. The importance of such study is manifest since it is precisely on these exchanges that the scientific community lacks of knowledge and they are needed to characterize the behavior of these so frequently occurring flows.

3 Method

As the main aim of this work is to test an algorithm to compute the pressure field at the interface and then to provide correct information about the interfacial terms arising in the dynamics of the flow, the mathematical and numerical method employed needs to be explained in detail.

3.1 One-fluid formulation

The code TrioIJK used to run the simulations solves a "one-fluid" formulation of the conservation equations resorting to a Front-Tracking method to take into account the presence and the movements of the bubbles inside the liquid phase. Most of the common methods for two-phase flows, like Level set and Volume of Fluid, relies on the same mathematical formulation aimed at obtaining the characteristic fields for the mixture treated like a single fluid with variable properties. This means that a single set of equations is used to describe the entire evolution of the flow, whereas the interfacial contributions are expressed through singularity distributions. This is not the only way to perform DNS of two-phase flows, as it is the counterpart of a most intuitive and equivalent approach where the equations are written for each phase separately and then the jump conditions are derived to link the two solutions at the interface. The following equations may be written when the continuum hypothesis holds, the physical properties of each phase are constant and both of the phases are incompressible.

Assuming the validity of the constitutive relation for the Newtonian fluid, the following governing equations, firstly proposed by Kataoka (1986) (see [8]), are implemented:

$$\nabla \cdot \mathbf{u} = 0 \quad (3.1)$$

$$\frac{\partial \rho \mathbf{u}}{\partial t} + \nabla \cdot (\rho \mathbf{u} \otimes \mathbf{u}) = -\nabla P + \rho \mathbf{g} + \nabla \cdot [\mu(\nabla \mathbf{u} + \nabla^T \mathbf{u})] + \sigma \kappa \mathbf{n}_v \delta^i \quad (3.2)$$

where all the variables are defined as a mixture of the two phases $\phi = \sum_k \chi_k \phi_k$, admitting the symbol ϕ_k stands for a generic fluid variable in the phase κ .

χ_κ is the phase indicator function defined as follows:

$$\chi_\kappa = \begin{cases} 1, & \text{in the phase } \kappa \\ 0 & \text{otherwise} \end{cases} \quad (3.3)$$

and that in absence of phase change satisfies the transport equation $\frac{\partial \chi_k}{\partial t} + \mathbf{u}_i \cdot \nabla \chi_k = 0$ where \mathbf{u}_i is the velocity of the front. In the same circumstance no source term localized at the interface appears in the mass conservation. The presence of the two phases gives rise to the body force in last term of 3.2 which is computed as the product of the surface tension σ and the local curvature $\kappa = -\nabla \cdot \mathbf{n}_v$, holding only if the surface tension itself is a constant property. \mathbf{n}_v is employed to indicate the direction normal to interface and oriented toward the liquid phase, strictly defined as $\nabla \chi_v = -\mathbf{n}_v \delta^i$, where δ^i is the Dirac impulse at the interface.

It is here recalled that the energy balance equation for the mixture is implemented too, although is not here presented because the work proposed in this report has been developed notably for adiabatic conditions. Moreover a first note on the implementation of 3.2 into TrioIJK is required, since the equation actually solved is:

$$\frac{\partial \rho \mathbf{u}}{\partial t} + \nabla \cdot (\rho \mathbf{u} \otimes \mathbf{u}) = -\nabla P_{num} + \left(\rho - \langle \rho \rangle \right) \mathbf{g} - \beta \mathbf{e}_x + \nabla \cdot [\mu(\nabla \mathbf{u} + \nabla^T \mathbf{u})] + \sigma \kappa \mathbf{n}_v \delta^i \quad (3.4)$$

A new term appears along the vertical direction (\mathbf{e}_x is the versor of this direction). It takes into account the eventual shear stress at wall which is equal to the misbalance between the hydrodynamic force (the pressure gradient over the whole domain) and the weight of the mixture averaged

on the total volume: $\beta = \nabla \langle P \rangle - \langle \rho \rangle \mathbf{g}$ (the notation $\langle \rangle$ stands for the average over the whole domain). Consequently the gradient operator is applied only on the remaining part of the pressure $P_{num} = P - \rho \mathbf{g} \cdot \mathbf{x}$, where \mathbf{x} is the position vector of the interface. ($P_{num} = P - \langle P \rangle$) with the aim of dealing with periodic boundary conditions in the direction of gravity. In order to solve directly this set of equations a Front-Tracking method as it is suggested by Tryggvason is implemented in the code.

In broad terms the Front-Tracking is aimed at improving the numerical resolution of gradients or discontinuities in variables and surfaces or lines are used as computational degrees of freedom to accomplish this purpose. Referring to the case of dispersed gas-liquid multiphase flows, this idea leads to describe the interface between the fluids with marker points that are advected at an imposed velocity. This results in the use of two different grids: an Eulerian fixed one, necessary to discretize the whole domain and to compute all the relevant physical quantities for both of the phases, and a dynamic mesh (made up by triangular elements) used to discretize the interface, usually called front or lagrangian mesh. Both the data structure of the front (that in the case of this work includes the surface of all the bubbles) and the grid provide essential informations concerning the flow field. The interfacial contributions, for instance, are associated to the lagrangian mesh. The effective implementation of the Front Tracking method depends on how the front is described and how the communications between the grids are dealt with.

In TrioIJK this algorithm is performed into a solver based on a finite-difference method. In order to understand which problems it causes, a brief explanation of the main steps followed is needed.

3.2 Front-Tracking

- At the generical time step n the Navier-Stokes equation 3.2 is solved by a prediction-correction method resorting to a fourth order central differentiation for both the diffusive and the convective term. Firstly the velocity field is updated disregarding the contribution of pressure, thus providing the predicted velocity \mathbf{u}^* :

$$\hat{\mathbf{v}} = \frac{\partial \mathbf{u}^*}{\partial t} = -\nabla(\mathbf{u}^n \otimes \mathbf{u}^n) + \frac{1}{\rho^n} \nabla \cdot \left(\mu^n (\nabla \mathbf{u}^n + \nabla^T \mathbf{u}^n) \right) - \frac{1}{\rho^n} \left(\phi(\rho_v - \rho_l) + \kappa^n \sigma \right) \nabla \chi_v^n. \quad (3.5)$$

$$\mathbf{u}^* = \mathbf{u}^n + \Delta t \hat{\mathbf{v}} \quad (3.6)$$

Then the Poisson equation for the pressure field is computed by means of a multigrid method to respect the constraint of incompressibility.

$$\nabla \cdot \left(\frac{1}{\rho^n} \nabla P^{n+1} \right) = \frac{1}{\Delta t} \nabla \cdot \mathbf{u}^* \quad (3.7)$$

Once this constraint has been accomplished, the velocity field may be finally updated resorting to a three-steps Runge-Kutta scheme for the time integration.

$$\mathbf{u}^{n+1} = \mathbf{u}^* - \frac{1}{\rho} \nabla P^{n+1} \quad (3.8)$$

This procedure is accurate at the third order. It should be pointed out the velocity field is known at the interface between the cells, whereas both the density and the pressure are computed directly at the grid centers and therefore the term ρ in the previous equation is always linearly interpolated to the faces. As regards to the mesh, a uniform Cartesian discretization of the computational domain is involved in the steps described above. The indices are listed as $i - j - k$ in order to ease the access to close cells with respect to the standard algorithm of the software TrioCFD.

- Once \mathbf{u} and P are known at the time step $n+1$ on the Cartesian mesh, the front is advected. It is constituted by a structured surface mesh made of triangles. The velocity of the lagrangian

mesh is obtained thanks to a (tri-)linear interpolation to the markers locations of the discret velocities in the vicinity of the interface. The new position of all the marker points is then defined:

$$\mathbf{x}_j^{n+1} = \mathbf{x}_j^n + \Delta t \mathbf{u}_i^n \quad (3.9)$$

where the vector \mathbf{x}_j indicates the position of the generical marker point j and \mathbf{u}_i^n stands for the projection of the interpolated velocity along the direction normal to the front.

- A remeshing procedure is performed in order to ensure an optimal distribution of the nodes, conserve the mass of each phase and preserve the length of the segments of the front in a prescribed range. In addition it is noted that Volume of Fluid-like variables are build as a semi-local correction of the mass.
- The phase indicator function χ_{n+1} is then recomputed at the new time step.
- All the other physical properties are updated on the Eulerian mesh, as well as secondary variables computed from the Front position and involved in the numerical method, namely the local curvature and the normal to the front itself.

As stated before the main problem the Front-tracking has to deal with is how to transfer to the fixed grid the information carried by the front, or in other words, how to impose on the continuos solution fields the discontinuities rapresented by the front itself. The discret Dirac impulse smooths the quantities across the interface over a single cell in order to preserve msharp distributions. This means a single and uniform value of the main quantities is assigned to the interfacial cell, properly averaged between liquid and vapor ones. As a consequence these cells characterise the mixture and it is impossible to define a liquid or vapor field in them. Depending on the type of analysis carried out these sharp differences between the purely liquid or the vapor might pose problems. In the studied cases, where the temperature is not a thermodynamic variable because of the incompressibility constraint and only adiabatic conditions are simulated, the fundamental discontinuity is undoubtedly the surface tension contribution linked to the local curvature of the front (see equation 3.2). This has a direct impact on the pressure field. An example of the computed pressure obtained by TrioIJK is shown in the following picture:

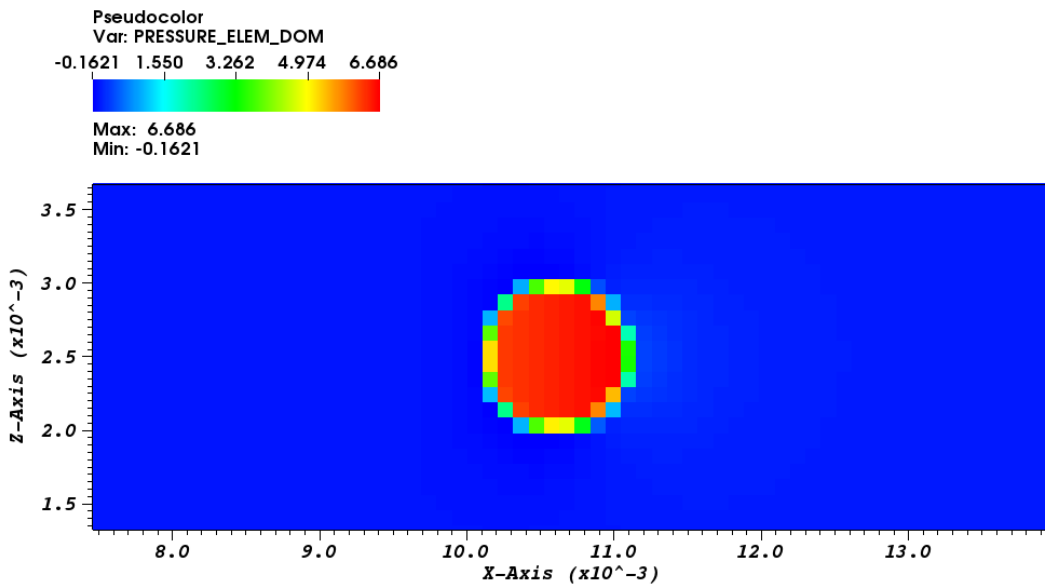
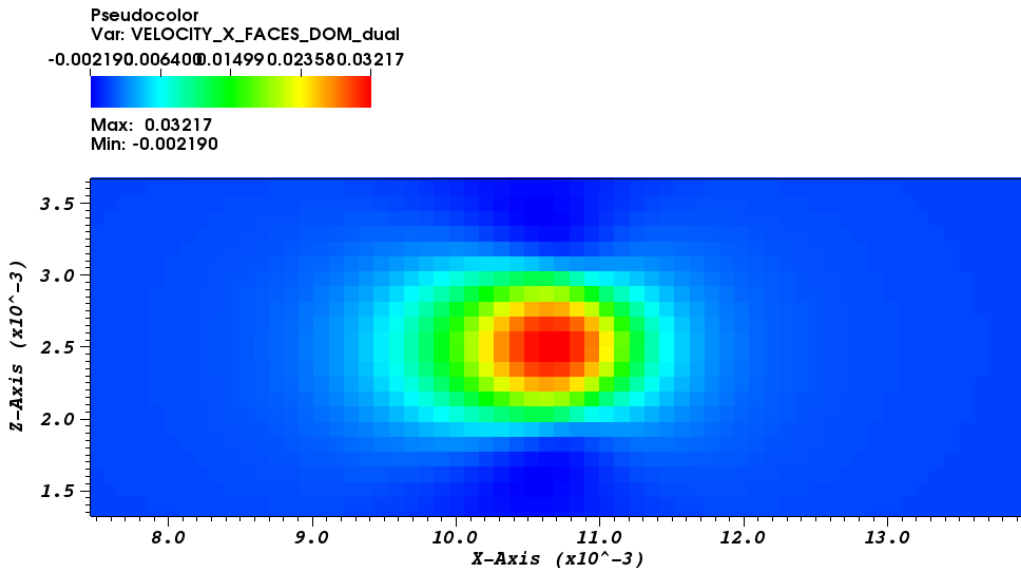


Figure 3.1: Pressure field solved by TrioIJK along the bubble.

The distribution assigned to the velocity field by the solved equation 3.2 is correct still because clearly the bubbles travel along with the liquid phase when phase change is not taken into account. The picture 3.2 displays the homogeneity of the x - component of this vector.

Figure 3.2: x component velocity field solved by TrioIJK along the bubble.

In conclusion, although the Front Tracking method is especially suitable to provide some relevant information in Direct Numerical Simulations, such as the exact position of the interface and the

jumps, it prevents us to properly evaluate the pressure of the single phase in all the cells that are not purely liquid nor purely vapor. An accurate description of these quantities is essential yet, as it directly contributes to the interfacial transfers.

3.3 Local instantaneous "Two-fluid" formulation

The summarized DNS performed by the code TrioIJK is capable of providing only the features of the mixture in the cells where both of the phases are present. Nevertheless a knowledge of the characteristics of each phase and in particular of the carrier liquid one is required to properly describe the evolution of the dynamics inside the flow. For this reason other mathematical approaches are available, although they are not directly implemented in the software. One of them is the local instantaneous *two-fluid formulation* of the governing equations. It relies on a mathematical model that treats the disperse phase (namely the vapor) as a second continuous field interacting with the continuous phase (the liquid). This formulation is intended to express the whole of the effects acting on the generic phase κ , including the ones due to the presence of the interface.

The one-fluid equations 3.1 and 3.2 reduce inside each phase (where the phase indicator function χ_κ is constant in time and space and equal to one) to:

$$\frac{\partial \rho_\kappa}{\partial t} + \nabla \cdot (\rho_\kappa \mathbf{u}_\kappa) = 0 \quad (3.10)$$

$$\frac{\partial \rho_\kappa \mathbf{u}_\kappa}{\partial t} + \nabla \cdot (\rho_\kappa \mathbf{u}_\kappa \otimes \mathbf{u}_\kappa) = -\nabla p_\kappa + \rho_\kappa \mathbf{g} + \nabla \cdot [\mu_\kappa (\nabla \mathbf{u}_\kappa + \nabla^T \mathbf{u}_\kappa)] \quad (3.11)$$

In addition, the jump conditions at the interface are obtained taking into account the spatial derivatives of χ_κ . In the present work, where the phase change is neglected, just one relation holds:

$$\sum_k \left(-p_\kappa \nabla \chi_\kappa + [\mu_\kappa (\nabla \mathbf{u}_\kappa + \nabla^T \mathbf{u}_\kappa)] \cdot \nabla \chi_\kappa \right) = \sigma \kappa \mathbf{n}_v \delta^i \quad (3.12)$$

Combining the equations 3.11 and 3.12 and resorting to the definition already given $\nabla \chi_\kappa = -\mathbf{n}_\kappa \delta^i$, the local instantaneous two-fluid formulation finally reads:

$$\frac{\partial \chi_\kappa \rho_\kappa \mathbf{u}_\kappa}{\partial t} + \nabla \cdot (\chi_\kappa \rho_\kappa \mathbf{u}_\kappa \otimes \mathbf{u}_\kappa) = -\nabla (\chi_\kappa p_\kappa) + \nabla \cdot (\chi_\kappa \tau_\kappa) + \chi_\kappa \rho_\kappa \mathbf{g} - p_\kappa \mathbf{n}_\kappa \delta_i + \tau_\kappa \cdot \mathbf{n}_\kappa \delta_i \quad (3.13)$$

where $\tau_\kappa = [\mu_\kappa (\nabla \mathbf{u}_\kappa + \nabla^T \mathbf{u}_\kappa)]$ is the viscous stress tensor for a Newtonian incompressible fluid. It should be noted that all the equations presented in this section are not explicitly solved by TrioIJK, but the solutions obtained should satisfy them. Conversely they are adopted exclusively to process the information given by the DNS after having re-built the two-fluid variables as $\phi_\chi = \chi_\kappa \phi$. This relation produces exact variables inside the phase, whilst along the front of the bubbles some error arise because of the discretization and of the unclear physical meaning of the values assigned to these cells. In order to better understand the motivations and the ways the two-fluid formulation is employed, the up-scaling process needs to be further detailed.

3.4 Up-scaling, turbulence and averaged formulation

3.4.1 Averaging operator

Both the one-fluid and the local two-fluids formulations as they have been presented in the previous paragraphs are intended to provide information on the instantaneous field at a microscopic level, including all the spatial and temporal details. The huge amount of scales involved and resolved may not be tractable. In order to acquire knowledge and useful models for practical situations the data obtained by the DNS need to be post-processed. The degrees of freedom involved in the description of the flow ought to be reduced and *macroscopic* equations should be derived to produce a relevant

analysis of the momentum balance and in particular of the interfacial effects. Moreover, since the final aim is to study realistic turbulent configurations, it is recalled that the ratio between the largest and smallest scale where turbulence is relevant increases with the Reynolds number according to the relations ???. Acquiring information on flows with high Reynolds number from DNS is then not possible without a proper "filter". The statistical approach (or RANS approach) is the most spread way to derive macroscopic governing equations. The variables they involve are obtained performing a Reynolds decomposition on the microscopic fields, which means splitting them into a fluctuating part and an averaged value. The last one is considered sufficient to depict the whole of the flow.

The strict definition of average is needed, since it is the link between the *microscopic* and *macroscopic* equations. All the simulations performed have been run for a sufficient time to ensure the independence of the statistics from the initial conditions and on domains periodic along at least two directions. In this circumstances the ergodicity hypothesis holds, hence the time and space averages along these directions might be assimilated to the statistical (or ensemble) average. Thus, indicating with ϕ the generic variable, its definition is:

$$\overline{\phi(y)} = \frac{1}{\Delta t L_x L_z} \int_{t-\frac{\Delta t}{2}}^{t+\frac{\Delta t}{2}} \int_0^{L_x} \int_0^{L_z} \phi(x, y, z, \tau) dx dz d\tau \quad (3.14)$$

where x and z are the generical periodic directions and Δt the averaging time which clearly depends on both the physical and the geometrical characterisitcs of the specific studied configuration. The final values obtained take into account the flow distribution on a plane parallel to $x - z$ (see figure 3.3) and are scalar functions of the coordinate along the direction y .

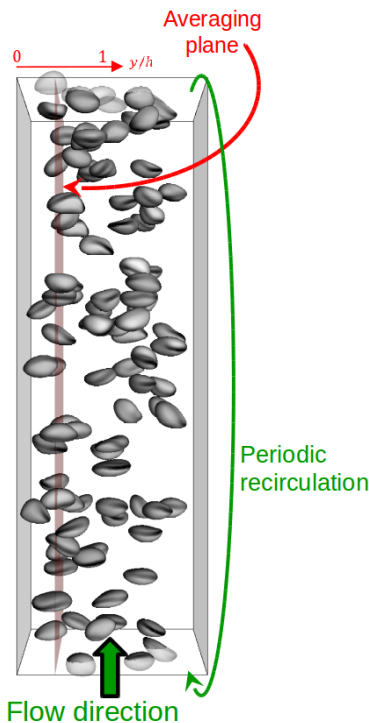


Figure 3.3: Planes of the average

It should be recalled that the present axis notation has be taken as an example to explain the procedure for the up-scaling that has been followed also when all the directions are periodic. The application of this definition is due to the fact that the ensemble average (always noted in the

following with an overbar) have some properties that simplify the final form of the equations.

$$\overline{\phi + \psi} = \overline{\phi} + \overline{\psi} \quad (3.15)$$

$$\overline{a\phi} = a\overline{\phi} \quad a = \text{const.}$$

$$\frac{\partial \overline{\phi}}{\partial s} = \frac{\partial \overline{\phi}}{\partial s} \quad s = (\mathbf{x}, t)$$

$$\overline{\overline{\phi}} = \overline{\phi}$$

$$\overline{\overline{\phi}\psi} = \overline{\phi}\overline{\psi}$$

$$\overline{\phi^*} = 0 \quad \phi^* = \phi - \overline{\phi}$$

$$(3.16)$$

Indeed it is a linear operator, the already averaged quantities are unaffected by a second application of the operator and it can be permuted with the spatial and temporal derivatives. As a consequence if the fluctuations are defined as the difference between the variable and its average, their average is zero.

3.4.2 Primary averaged equations

This definition leads to the re-writing of the equation 3.2 for the mixture. The new expression becomes:

$$\frac{\partial \overline{\rho \mathbf{u}}}{\partial t} + \nabla \cdot (\overline{\rho \mathbf{u}} \otimes \overline{\mathbf{u}}) = \nabla \overline{P_{num}} + (\bar{\rho} - \langle \rho \rangle) \mathbf{g} - \beta \mathbf{e}_x + \nabla \cdot \bar{\tau} - \nabla \cdot (\overline{\rho \mathbf{u}' \otimes \mathbf{u}'}) + \overline{\sigma \kappa \mathbf{n} \delta^i} \quad (3.17)$$

Solving 3.17 means that a particle-resolved approach is employed in the analysis. In contrast to what happens in a point-size approach (where inclusions are considered as pointwise, infinitely small and the surface tension effect is relevant only for the shape of the bubbles and its average is zero) in this case the last term of the previous equation $\overline{\sigma \kappa \mathbf{n} \delta^i}$ cannot be neglected at all. A better physical explanation of this term, indicated in the following as \mathbf{M}_σ , is provided in the following chapter.

The statistical averaging of the one fluid equation still does not enriches our knowledge of the single phase properties. As a consequence a different definition of phase average is introduced:

$$\overline{\phi}_\kappa^\kappa = \frac{\chi_\kappa \phi_\kappa}{\overline{\chi_\kappa}} \quad (3.18)$$

Averaging 3.13 and resorting to this definition the macroscopic two-fluid equations for incompressible flows are derived:

$$\begin{aligned} \frac{\partial \alpha_\kappa \rho_\kappa \overline{\mathbf{u}}_\kappa^\kappa}{\partial t} + \nabla \cdot (\alpha_\kappa \rho_\kappa \overline{\mathbf{u}}_\kappa^\kappa \otimes \overline{\mathbf{u}}_\kappa^\kappa) &= -\nabla(\alpha_\kappa \overline{p}_\kappa^\kappa) + \nabla \cdot (\alpha_\kappa \overline{\tau}_\kappa^\kappa) \\ &+ [\alpha_\kappa (\rho_\kappa - \langle \rho \rangle) \mathbf{g} - \alpha_\kappa \beta \mathbf{e}_x] - \nabla \cdot \left(\alpha_\kappa \rho_\kappa \overline{\mathbf{u}'_\kappa \otimes \mathbf{u}'_\kappa^\kappa} \right) - \overline{p_\kappa \mathbf{n}_\kappa \delta_i} + \overline{\tau_\kappa \cdot \mathbf{n}_\kappa \delta_i} \end{aligned} \quad (3.19)$$

where the $\alpha_\kappa = \overline{\chi_\kappa}$. Both in 3.17 and in 3.19 a new contribution arises because of the fluctuations of the velocity field. In the two-fluid formulation it is defined as $\mathbf{u}'_\kappa = \mathbf{u}_\kappa - \overline{\mathbf{u}}_\kappa^\kappa$. In contrast to the mixture approach they are centered on the phase average $\frac{\chi_\kappa \phi_\kappa}{\overline{\chi_\kappa}}$. Analytically the only dissimilarity between the governing equation for the total and the mean flow is expressed by this term. Hence, following a general explanation valid for the single phase flows too, it engenders the different behavior between a laminar and a turbulent flow and it can be physically interpreted as the contribution of the fluctuations, not solved by the macroscopic equations, on the flux of momentum through a control volume. Similarly to what has been discussed for single-phase flows, the contribution appearing in 3.19 is called Reynolds stress tensor and its component ij is indicated in the following as $R_{\kappa,ij} = \overline{u'_{\kappa,i} u'_{\kappa,j}^\kappa}$. The different definition of average adopted in the two-fluid formulation has a

consequence on the physical behavior it conveys: the distribution of the velocity field in the phase κ does not depend only on the chaotic behavior of the phase itself, but it is also due to the presence of inhomogeneities, thus being an indirect consequence of the mutual influence between the phases that will be detailed in the following section. Conversely this influence is directly expressed by the two terms averaged on the interface. They are collectively referred to as:

$$M_\kappa = -\overline{\mathbf{p}_\kappa \mathbf{n}_\kappa \delta_i} + \overline{\tau_\kappa \cdot \mathbf{n}_\kappa \delta_i} \quad (3.20)$$

. This term has been completely investigated by experiments and numerical simulations, so it is classically modelled as sum of drag, shear-induced and wall-induced lift, turbulent dispersion force, depending on the configuration and physical condition studied. In addition these forces satisfy the jump condition at the interface 3.12 in its averaged formulation:

$$\sum_{\kappa} \mathbf{M}_\kappa = \mathbf{M}_\sigma \quad (3.21)$$

The physical meaning of this term will be further discussed in the next section. It should be kept in mind that the above mentioned rebuilding of the microscopic variables is affected by an error each time the χ_κ is nor equal to one, nor equal to 0. In the conditions taken into account, where the phase change, coalescence and break-up are disregarded, the pressure p_κ is the field not available to directly recompute \mathbf{M}_κ in the up-scaling procedure and therefore it needs a dedicated algorithm for the post-treatment

3.4.3 Reynolds stress transport equation

In the chapter 2.3 the issues caused by the presence of the Reynolds stress tensor in the momentum balance have been introduced and they are involved in the macroscopic two-fluid formulation too. As a consequence, deriving a balance equation for $R_{\kappa,ij}$ is of the utmost importance in the up-scaling procedure. On one hand it can be useful to characterize the turbulence of the two phase flows analyzing classical quantities, such as the turbulent kinetic energy (noted as K in the following), on the other hand it may allow the formulation of new models for turbulence (see [1]). Indeed, in 2.3 the relevance of the RSM (Reynolds stress model) has been discussed for single phase flows, but the same model present different features for two phase flows. Although 7 equations are needed for it, in the present work the closure equation for the dissipation rate (or another equivalent parameter) is not analysed. The Reynolds stress transport equation is derived from the equations 3.13 and 3.19 exactly as happens for the single phase. As a matter of fact subtracting these equations one from the other leads to the balance equation for the fluctuating field u'_κ . Then, in order to highlight the correlation of velocity, as explained in [18] the obtained equation for the j-component is multiplied by the $u'_{i,k}$, then summed to its transposed and averaged. The result of this procedure when the phase-averaged variables are adopted, is:

$$\begin{aligned} \frac{\partial}{\partial t} \left(\alpha_\kappa R_{\kappa,ij} \right) + \frac{\partial}{\partial x_b} \left(\alpha_\kappa R_{\kappa,ij} \overline{u_{\kappa,b}}^\kappa \right) &= -\alpha_\kappa \left(R_{\kappa,ib} \frac{\partial \overline{u_{\kappa,j}}^\kappa}{\partial x_b} + R_{\kappa,jb} \frac{\partial \overline{u_{\kappa,i}}^\kappa}{\partial x_b} \right) + \\ &\quad \alpha_\kappa \frac{P'_\kappa}{\rho_\kappa} \left(\frac{\partial \overline{u'_{\kappa,i}}^\kappa}{\partial x_j} + \frac{\partial \overline{u'_{\kappa,j}}^\kappa}{\partial x_i} \right) - 2\alpha_\kappa \frac{\mu_\kappa}{\rho_\kappa} \frac{\partial \overline{u'_{\kappa,i}}^\kappa}{\partial x_b} \frac{\partial \overline{u'_{\kappa,j}}^\kappa}{\partial x_b} + \\ &- \frac{\partial}{\partial x_b} \left(\alpha_\kappa \overline{u'_{\kappa,i} u'_{\kappa,j} u'_{\kappa,b}}^\kappa - \nu_\kappa \frac{\partial \alpha_\kappa R_{\kappa,ij}}{\partial x_b} + \frac{\alpha_\kappa}{\rho_\kappa} (\overline{P'_\kappa u'_{\kappa,i}}^\kappa \delta_{bj} + \overline{P'_\kappa u'_{\kappa,j}}^\kappa \delta_{ib}) \right) + \\ &- \frac{1}{\rho_\kappa} \left[\overline{(P'_\kappa u'_{\kappa,j} n_{\kappa,i} + P'_\kappa u'_{\kappa,i} n_{\kappa,j}) \delta^i} + \nu_\kappa \left[\frac{\partial (\overline{u'_{\kappa,i} u'_{\kappa,j} n_{\kappa,b}} \delta^i)}{\partial x_b} + \frac{\partial (\overline{u'_{\kappa,i} u'_{\kappa,j}} n_{\kappa,b} \delta^i)}{\partial x_b} \right] \right] \end{aligned} \quad (3.22)$$

It should be noted that this equivalence only holds in absence of phase change, otherwise another interfacial term would be necessary. Among the interfacial averages two quantity are stressed in

red, namely the interfacial pressure fluctuations. They are defined as $P'_\kappa = P_\kappa - \overline{P_\kappa}^\kappa$, adopting the same method already used for the Reynolds stress tensor. Exactly as happens for the interfacial momentum exchange, in this case too the lack of a single phase pressure at the interface poses problems in the direct computation of this term. The previous formulation is written down for the generic phase κ , but in the context of the study already carried out and of the present work, it is only implemented for the liquid phase. Actually the vapor phase contains fluctuations too, but they usually are not investigated. Indeed they are assumed to be negligible because the dynamics of the flow is mostly attributed to the liquid phase when the vapor occurs in bubbles.

This equation is entirely built and recomputed in the post-processing, relying on the data provided by the DNS, following a procedure that allows to individuate several contribution characterized by a remarkable physical meaning. It should be noted that, for these reasons, a modified pressure field, extended to the interfacial cells too, is expected to have an impact on the other averaged term where pressure is involved. A general physical insight on the relevance of these contributions is provided in the following.

4 General physical remarks

4.1 Momentum balance and surface tension

In order to illustrate the importance of the interfacial terms appearing in the averaged equations the physical results already obtained by du Cluzeau et al. serve the purpose. They are obtained resorting to numerical experiments carried out with the code TioIJK and with an implicit method in the evaluation of the interfacial averaged terms. They focus on the classic case of a turbulent bubbly upflow in a vertical channel. As a matter of fact, it is one of the most studied configurations (see [6]) to comprehend how the presence of dispersed bubbles affects the turbulence in the liquid phase. Both the results presented by [1] and [6] thanks to the DNS pointed out that a very different turbulent behavior is shown depending on the bubble dimension and especially on the deformability, currently taken into account by means of the Eötvos number. This adimensional parameter is defined as the rapport between the gravity and the surface tension $E_o = \frac{\rho_l g d_b^2}{\sigma}$, where g is the gravitational acceleration, ρ_l is the homogeneous density of the liquid phase, d_b stands for the diameter of the bubble and represents the length scale of the problem and σ indicates the surface tension. This parameter provides information not only on the shape of the bubbles (less deformable as E_o decreases and the surface tension plays a major role), but above all, when the turbulent Reynolds number is the same, it is proved to affect the void fraction distribution and the characteristic lenght of turbulence.

Assuming the flow reaches a statistical steady state, the Navier-Stokes equation which governs this phenomenon, along the streamwise direction (please check) reduces to:

$$\frac{d\tau}{dy} - \beta - (\overline{\rho(y)} - \langle \rho \rangle)g = 0 \quad (4.1)$$

Here the term β is related only to the spatial average of the quantities on the whole domain, since it is defined as $\nabla \langle P \rangle - \langle \rho \rangle g$. Moreover the shear stress τ includes both the part due to the molecular viscosity $\tau_m = \mu(\frac{d\tau}{dy})$ and the one arising from the Reynolds decomposition because of the fluctuations in the velocity field $\tau_t = -\rho \langle u' v' \rangle$. Then the equation 4.1 means that the total driving force β , given by the imposed pressure gradient and by the hydrostatic pressure gradient due to the weight of the mixture, is balanced by the variation of the total shear stress in the fluid. This clearly affects the position of the bubble in the channel. All the DNS presented in [6] and [1] stress out how this position along the wall-normal direction depends on the Eötvos number and on the deformability of the bubbles. In particular the spherical bubbles, assumed as rigid ones, tend to assemble along the walls, whereas the deformable ones are concentrated in the middle of the channel. This phenomenon reveals significant differences in the lengthscale of the turbulent structures: the turbulent boundary layer can freely develop with deformable bubbles, while in the other case it is disturbed by the presence of the bubbles, therefore allowing only shorter lengths and forcing all the complexity of the flow to be constricted in a very thin layer along the walls.

Alongside this physical interpretation due to the hydrodynamic approach, a different point of view may be provided when the one fluid averaged equation 3.17 is solved at the statistical steady state. Since the finite size of the bubbles is taken into account, the position of the peak of void fraction could be seen as the center of gravity of the bubbles. Indeed, the work of [1] perfectly illustrates how the trend of the averaged void fraction along the cross-channel direction is similar to the profile of the averaged interfacial term $\mathbf{M}_\sigma = \overline{\sigma \mathbf{k} \mathbf{n} \delta^i}$ originated by the surface tension: it is responsible for the dispersion along the wall-normal direction as the pressure gradient, the global shear stress and the source term cannot balance anymore. The relevance if this approach is due to both the use of the averaged balance equation to describe the flow dynamics and to the presence of a swarm of finite-size bubbles that prevents the erasure of the wall-normal component in \mathbf{M}_σ . The trend of this term is found to change along with the bubble deformability and the physical phenomena it engenders need to be explored. The best way to pursue this aim is to resort to the two-fluid

averaged formulation, in order to investigate the behavior of each phase and then correctly direct further modelling efforts. The equations solved, once again at the statistical state for the liquid and the vapor phase were presented in the previous section in 3.19. The term highlighted 3.20 are the more relevant ones as it is linked to \mathbf{M}_σ by the equation 3.21.

The information needed to compute these terms are the viscous stress and the pressure in all the interfacial cells. As already explained in TrioIJK nor a purely liquid nor a purely vapor pressure field is available at the crossed cells. Moreover major interpolation errors are expected because of the presence of the discontinuity. Therefore in [1] \mathbf{M}_l and \mathbf{M}_v are not directly computed, but rather they are evaluated as the right hand side of the equation 3.19 specialized for the treated phase. Although the results obtained are physically consistent and lead to negligible errors, it is impossible to distinguish the numerical error from the one due to the model. This is the reason why at the present state of the study carried out by the STMF at the CEA, further physical analysis of this term have not been presented yet. In order to exclude any numerical errors in this investigation, the present work is aimed at implementing an algorithm to interpolate the monophasic pressure field to the interface and recompute these statistics.

As regards the viscous stress tensor at the interface the computation of the velocity field gradient $\nabla \mathbf{u}$ is needed too. It is evaluated in TrioIJK adopting a second order centred difference. Problems linked to discontinuities arise in this case too when the viscosity of the two phases is not constant, but they are limited by the neglecting of the phase-change (an hypothesis always adopted in the work of du Cluzeau summed up in this section). Moreover the viscous contribution has always been found not to be remarkable in the momentum balance for the turbulent channel. The settings and the hypothesis adopted in the present work for the viscous interfacial term will be exposed in the following, when the up-scaling procedure for the new terms will be detailed. (see section 6.2)

4.2 Reynolds stress tensor transport equations

In order to predict the velocity field and momentum, turbulence has to be studied too. As seen in the previous sections, the studies presented in [1], [2] and [3] focus on the balance of the Reynolds stress tensor. The equation 3.22 presented in the previous chapter is just one of the way the balance equation for the Reynolds stress tensor might be written. This choice, already followed in ??, is supposed to be the best to distinguish the physical mechanisms arising in the turbulence of the carrier phase and then to understand the impact the presence of the bubbles have on it. Referring to the equation 3.22 for the liquid phase, one can distinguish:

- $\frac{\partial}{\partial t} \left(\alpha_l R_{l,ij} \right) =$ Unsteady term. It describes the evolution in time of the Reynolds stress component. It is negligible when the system under investigation reaches the statistical steady state;
- $\frac{\partial}{\partial x_b} \left(\alpha_l R_{l,ij} \overline{u_l}_b^l \right) =$ Convective term. It conveys the non-linearity of this equation and, together with the unsteady term, it may be referred to as the material derivative $\frac{D \alpha_l R_{l,ij}}{Dt}$. The same notes made for the previous term hold at the statistical steady state;
- $-(\alpha_l R_{l,ib} \frac{\partial \overline{u_l}_i^l}{\partial x_b} + \alpha_l R_{l,jb} \frac{\partial \overline{u_l}_j^l}{\partial x_b}) =$ Production. It stands for the work done by the fluctuating field on the mean one because of its own strain, thus acting like a source of turbulent kinetic energy;
- $-2\alpha_l \frac{\mu_l}{\rho_l} \frac{\partial u'_{l,i}}{\partial x_b} \frac{\partial u'_{l,i}}{\partial x_b}^l =$ Dissipation. It is related to molecular viscosity and to the divergence of the rate of strain tensor based on the fluctuations of velocity and is responsible for the conversion of kinetic into internal energy;
- $-\frac{\partial}{\partial x_b} \left(\alpha_l \overline{u'_{l,i}} \overline{u'_{l,j}} \overline{u'_{l,b}}^l - \nu_l \frac{\partial \alpha_l R_{l,ij}}{\partial x_b} + \frac{\alpha_l}{\rho_l} (\overline{P'_l u'_{l,i}}^l \delta_{bj} + \overline{P'_l u'_{l,b}}^l \delta_{ib}) \right) =$ Diffusion. This conservative operator, responsible for the diffusion of the energy into the fluid, involves pressure, viscous contribution and turbulence;
- $\alpha_l \frac{P'_l}{\rho_l} \left(\frac{\partial u'_{l,i}}{\partial x_j} + \frac{\partial u'_{l,j}}{\partial x_i} \right)^l =$ Redistribution. It causes the energy to be redistributed between pressure and velocity and it is found out to be responsible for a migration of energy among the directions. Its trace is zero and consequently it has no impact on the turbulent kinetic energy equation;
- $-\frac{1}{\rho_l} (\overline{P'_l u'_{l,j}} n_{l,i} + \overline{P'_l u'_{l,i}} n_{l,j}) \delta^i =$ Interfacial production. It appears only in two phase flows and it is related to the work done by the interface on the liquid phase. The most spread theory states it is mainly related to the drag component of this force ([1], [18], [5]).

The two-phase flows turbulence engenders different physical phenomena with respect to the single-phase one since the interface provokes a disruption of the turbulent eddies on one hand and a production of vorticity at the interface on the other. As a consequence many authors proposed to describe turbulence as a superposition of several effects, some of them are typical of the single phase turbulence, other exists only because a dispersed phase is added. Following the nomenclature proposed by du Cluzeau in [2], one can identify the Single Phase Turbulence (SPT) and Bubble Induced Fluctuations (BIF). This name is used because it refers to a not completely chaotic phenomenon: a second temporal average of the instantaneous velocity fluctuations reveals the existence of a statistical steady distribution which depends only on the position and then of an unsteady contribution. The first one is called Wake-Induced Fluctuations and the latter Wake-Induced Turbulence since it is the only one that shows the complex phenomena turbulence is usually related

to in the single-phase flows. The DNS database build with TrioIJK and employed in [1] highlights only WIF, linked to the potential wakes every bubble induces in the carrier phase. Since an interaction between these contributions is demonstrated, it is clear that the presence of the bubbles results in a *modulation* of the existing turbulence in the liquid. The works of Santarelli too shows the impact of the dispersed phase on the averaged balance equation for turbulent kinetic energy (obviously related to the diagonal terms R_{ij}) and points out that the interfacial production is the main contribution. It introduces a disequilibrium and then affects the level of the other quantities, namely the dissipation, because production and diffusion, seen as classical single-phase contributions, are not relevant anymore in the bulk of the channel, where the bubble gather. This influence strongly depends on the dimension of the spherical bubbles injected (the turbulence level decreases when they are smaller than the Kolmogorov scale) and on the void fraction. In [1] the impact of deformability has been investigated too and in particular it has been pointed out that the effect of the bubbles acts on the magnitude of the diffusion and production (still related to the SPT), while the WIF are controlled especially by redistribution, Interfacial Production and dissipation. Having the chance of relying on an accurate values of this effects is pivotal to improve or develop efficient turbulence models. In this case too the results provided in [1] cannot resort to precise information for the interfacial cells, where no purely liquid pressure is available, and then the interfacial production is presented here as the residue of 3.22 at the statistical steady state for the liquid phase. In this case too the numerical errors can not be distinguished and then obtaining an extended field of pressure is necessary to explicitly evaluate the interfacial production, and in addition to recompute redistribution and pressure diffusion too in the equation 3.22. As a result the model proposed can be validated and a better insight on the relative importance of the different effects can be quantified, as it has already be done by [5] for the kinetic energy.

5 Pressure reconstruction

The numerical, mathematical and physical context described contains the motivation of the work exposed in this report. The pressure obtained respecting the Poisson equation solved by TrioCFD is not a continuous field on all the Eulerian points because of the presence of the surface tension contribution along the interfaces. The one fluid field includes some averaged value into the interfacial cells that do not correspond nor to the liquid, nor to the vapor one. An extrapolation of the single phase fields to the interfacial cells is evidently needed for the computation of the terms \mathbf{M}_l and \mathbf{M}_v in the averaged equations 3.19 and of the Interfacial Production in the liquid phase in 3.22 and it should be precise and stable enough to avoid numerical errors.

5.1 The Algorithm

The strategy followed in order to properly calculate the terms needed for the validation of the results is similar to the one proposed in [5], considered of interest since the new extended pressure value is computed directly on the Eulerian points of the crossed cells and relies on a small number of points close to the interface where the pressure is already known.

In its original implementation explained in [5], the algorithm is based on the definition of two different types of points, the so-called Ghost points and the Image points, stressed in the picture below:

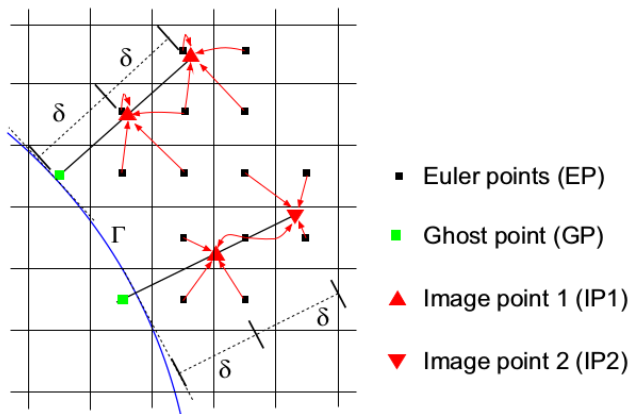


Figure 5.1: Different types of point defined for the pressure evaluation by Santarelli and al.

The Ghost points are simply all the points on the fixed grid crossed by interface, where the extension is needed, whereas the two image points are defined out of the grid along the radial direction normal to the interface at precise distance δ .

Once all these points have been established, two more steps are executed:

- trilinear interpolation of the liquid pressure in the Image points;
- linear extrapolation in the ghost cells resorting to the two values computed.

This algorithm has been slightly modified in order to satisfy the different aim of the present work and then implemented into IJK. It is not part of the Navier-Stokes solver itself, but rather is performed in the code after each time step, when the results are post-processed.

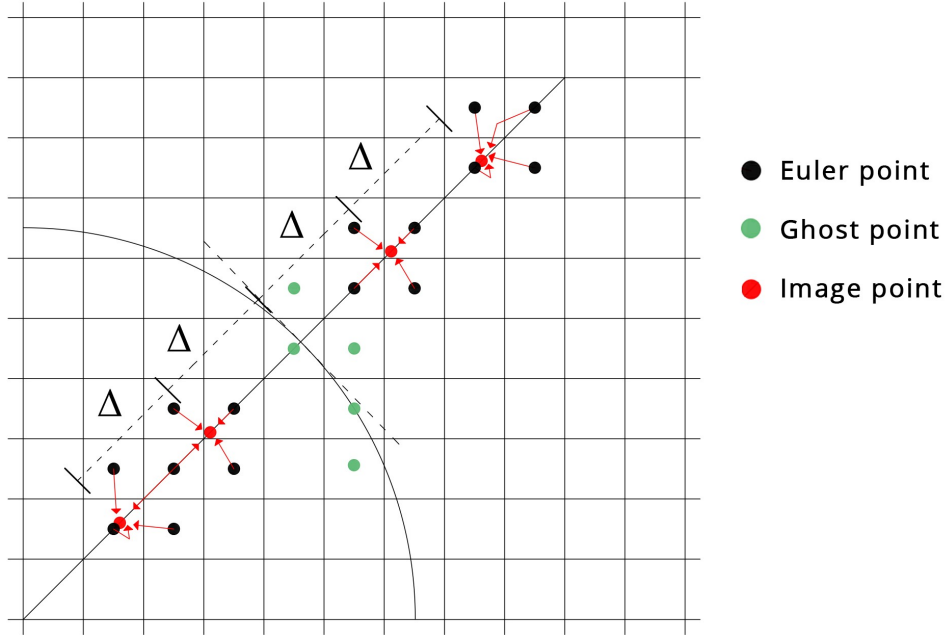


Figure 5.2: Example of the currently implemented algorithm.

The implemented algorithm is studied to be run over several processors, since a massive parallel calculation is the best way to perform a Direct Numerical Simulation. The first step consisted in identifying all the crossed cells where the pressure needs to be extended disregarding the relative position of the eulerian center and the interface in the cell.

Then the image points are identified resorting to the same definition explained above, and in order to do so both the position of the barycenter of the front and the normal to interface are computed for each interfacial cell. In this case two other points are indentified along the same direction, but inside the bubble, in order to extrapolate the vapor field in the crossed cells, and two different matrices, one for each of the phases, are used to store them. Clearly the aim of the work is different from the one presented in [5], as the statistics have to be computed for both phases to validate the results proposed in previous application. The chosen distance between the barycenter of the front and the first image point, called Δ , is not constant along the bubbles, but rather is calculated as the scalar product between the normal, always oriented toward the liquid phase, and a vector whose components are equal to the length of the cell in each direction and then properly multiplied by a coefficient κ slightly bigger than 1.5.

$$\Delta = \kappa \delta \cdot \mathbf{n} \quad (5.1)$$

It is noted that this distance is the same computed between the two image points, thus leading to a simple analytical function for the extrapolation.

These image points are not part of the Eulerian grid and therefore pressure needs to be interpolated by the closest ones, exactly as the code IJK does for the quantities along the front. The definition of Δ is a compromise between two requirements on the cells involved in the interpolation, since they should be at the same time sufficiently close to the interface to lead to a proper result and belong to the same phase computed in the extention. The pressure in the first image point will always be valid resorting to 5.1 for both the vapor and the liquid pressure.

Nevertheless, this algorithm cannot clearly work for all the points of the domain and a new interpolating function has been implemented for the liquid phase only in order to exclude from the final calculation the points where it relies on cells lying outside the domain or inside a bubble,

thus warping the liquid field. Because of the high regularity of this circumstance in the performed simulations, when at least the image point closest to the interface is valid, the values of the interpolated pressure is copied in the correspondent interfacial cell. The previous steps have been run on an extended, fictitious domain because of the presence of periodic boundary conditions and the resulting need for ghost cells and finally reduced to the physical domain. None of this exception is active in the procedure implemented for the vapor phase, as the definition of the image points inside the bubble itself is sufficient to guarantee the interpolation from purely vapor Eulerian points. The only interfacial cells regarded as invalid for the evaluation of the interfacial pressure terms in 3.20 are the ones crossed by more than one bubble, since the vapor field extrapolation relies on is not unique.

5.2 Validation

The algorithm has been performed on two simple configurations in order to validate it.

5.2.1 Single fixed bubble

The first configuration is a single fixed bubble characterized by a surface tension equal to $1\frac{N}{m}$, disregarding the presence of gravity: the pressure is constant for the two phases and so should be the extrapolated one too in the cells crossed by the interface. The calculation has been carried out on a rectangular domain, whose main geometrical parameters are summed up in the table 5.1:

L_x [m]	L_y [m]	L_z [m]	Δ [m]	d_b [m]
0.64	0.4	0.32	0.01	0.14

Table 5.1: Physical and geometrical parameters of the first test configuration. The grid is uniform.

The mesh is coarse as convergence is not in the main goal of this first test. This case has no physical relevance, but it suits the aim of checking the extrapolation performed by the algorithm. The results obtained are presented in the picture 5.3, visualized thanks to the software VisIt, the tool of TrioCFD devoted to the post-processing. In a plane normal to one of the periodic directions and crossing the bubble, the three pressures computed (the solved one, the extended liquid and the extended vapor) are plotted against the x coordinate: one can see that both the liquid and the vapor values of pressure are properly extrapolated in the interfacial cells.

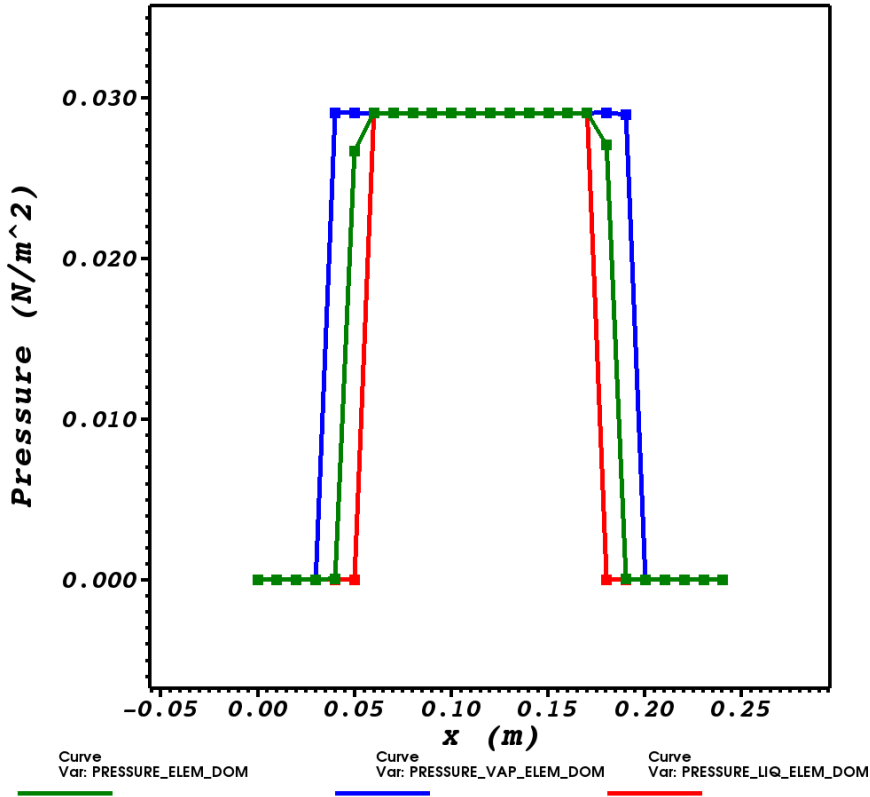


Figure 5.3: Trend of extended and computed pressure at $y = 0.131$ m and $z = 0.18$ m

5.2.2 Colliding bubbles

On the other hand, a second test has been performed in order to check the exceptions taken into account in the interpolation function for the liquid phase. The final target this works is supposed to reach is to extract the interfacial statistics in conditions where turbulence and bubbles interaction arise, such as a swarm of bubbles or a vertical channel. This test consisted in simulating two rising bubbles colliding with themselves and collapsing on the walls set along the z direction. Although the physical meaning of such a configuration is not significant too, it allows to check if all the exceptions to the research performed by the algorithm have been well implemented. The main geometrical and physical parameters of the simulation are listed in the following table:

$L[m]$	$\Delta[m]$	$d_b[m]$	$\sigma[\frac{N}{m}]$	$\rho_l[\frac{kg}{m^3}]$	$\mu_l[Pas]$	$\rho_v[\frac{kg}{m^3}]$	$\mu_v[Pas]$	$g[\frac{m^2}{s^2}]$
0.008	0.00025	0.0032	0.07	1000	0.001	800	0.01	9.81

Table 5.2: Physical and geometrical parameters of the studied configuration. The domain is cubic and the grid uniform.

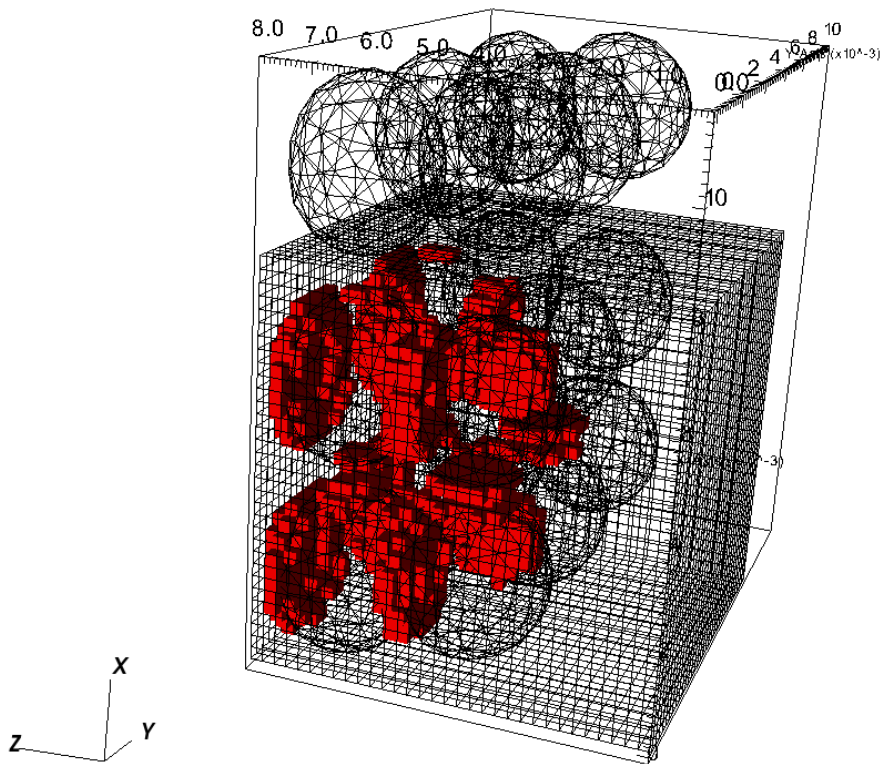


Figure 5.4: Pseudocolor of liquid pressure: only the values greater than 1000Pa are displayed in this 3D plot.

In the plot 5.4 only the cells where the extended liquid pressure is completely out of range are marked in red. All of these points will be excluded from the esteem of the averaged interfacial terms in the following steps of the up-scaling process. Moreover this simulation has been carried out adopting two processor for each direction in order to test the effective suitability of the implemented algorithm for a parallel calculation.

6 Computation of the statistics

The second part of the work is devoted to the computation of the interfacial terms in the equations 3.19 and in 3.22, respectively the interfacial momentum \mathbf{M}_k and the interfacial production noted as Π in the following. This is the main step of the up-scaling procedure and the need for the extention of the pressure field emerges from the adopted formulation of the macroscopic equations. The interfacial terms involves both an isotropic part related to pressure and a deviatoric one caused by the molecular viscosity and by the strain-rate tensor on the whole velocity field. The necessary averaged quantities are directly calculated in TrioIJK according to the general definition 3.14. In the case of the extended pressure fields the cells near walls and in between close bubbles are obviously disregarded. A Python code has been used in order to compute and plot all the terms appearing in the final equations.

6.1 Interfacial pressure force

The very first step of this procedure consisted in post-process all the statistics based on the new extended pressure fields. The validation has been firtly carried out only on the pressure interfacial force because of the ease in checking it and because it is a necessary step to validate the interfacial production too. Regarding the two-fluid momentum equation the term recomputed for both of the phases is the vector $\overline{P\nabla\chi}$. In addition the contribution due to the gradient of pressure $-\nabla(\alpha_\kappa\overline{P}_\kappa^\kappa)$, has been corrected too in order to smooth the original values. The results have been tested on the configuration already presented of the single fixed bubble: all the forces arising from velocity are disregarded and the averaged Navier-Stokes equation clearly reduces to:

$$0 = \underbrace{\overline{P_i\nabla\chi_\kappa}}_{P_\kappa} - \underbrace{\nabla\overline{\alpha_\kappa P_\kappa}}_{M_\kappa^P} \quad (6.1)$$

Moreover the pressure field in this case is constant and in particular is almost zero in the liquid phase. This is a perfect condition to visualize and test the computation of the averages since their trend should be equal to the one of the components of the normal to the interface. Indeed in IJK the accuracy in the definition of the gradient of the phase indicator function χ is reached by taking on its definition $\nabla\chi = -\mathbf{n}_v\delta_i$. In this way this value does not resort only on a local information as the δ_i function entails an average on the surraunding cells, thus caring for the various exsisting geometrical situations in the esteem of this interfacial quantities. In the case of the sphere their analytical expression integrated over the entire volume (PLEASE CHECK THIS TERM IN THE PDF DI GUILLAUME) is known and may be accepted as a reference:

$$\begin{aligned} aiNx &= \int_v N_x \delta^i dv = 0; \\ aiNy &= \int_v N_y \delta^i dv = 0; \\ aiNz &= \int_v N_z \delta^i dv = \frac{2\pi z}{L_x L_y} \end{aligned} \quad (6.2)$$

The results obtained computing all the terms of the equation 3.13 are displayed for the vapor phase only.

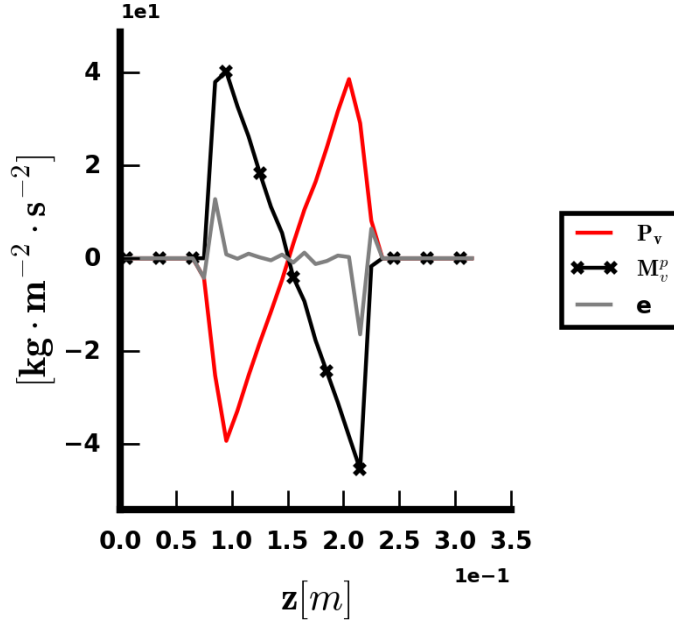
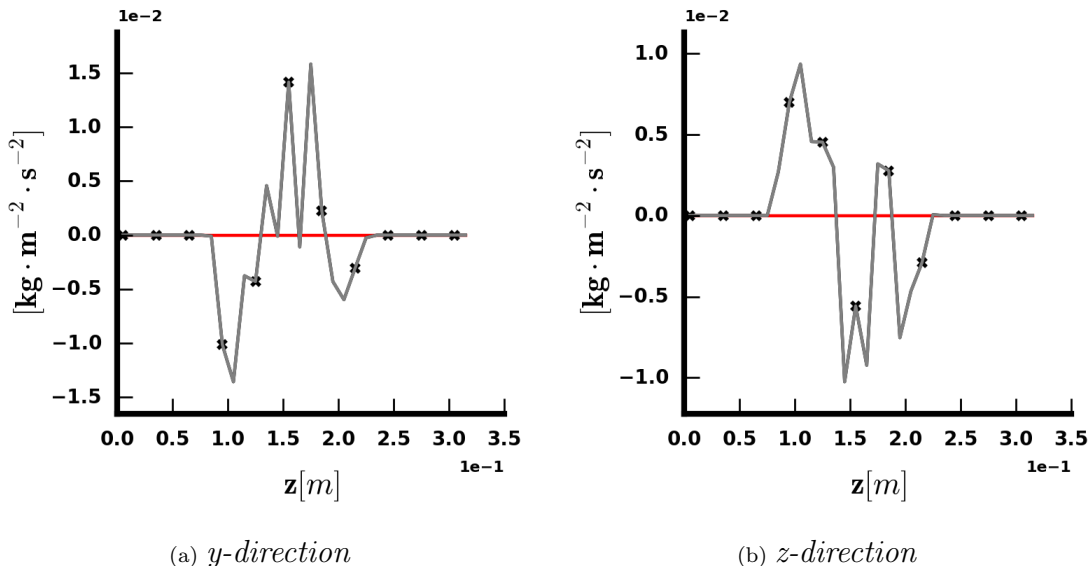
Figure 6.1: Averaged momentum equation along z - direction

Figure 6.2: Averaged momentum equation - vapor phase

It is noted that with respect to the definition provided of average (see equation 3.14) the peridotics direction are x and y and therefore the components of the vector $\overline{P_v \nabla \chi_v}$ are plotted against the wall normal direction, called z . As expected along the periodic direction the contribution of the interfacial pressure reduces to a noise, whose amplitude is still huge compared to the other quantites computed in the equation, wherese along the z - direction the slope is correctly approximated with some errors due to the choice of a coarse mesh.

As regards the interfacial terms arising in the Reynolds stress transport equation, the case studied is not evidently meaningful because of the absence of motion. They will be directly evaluated and compared to the reference [1] during the following simulations.

6.2 Interfacial viscous force

The force the phases exchange between each other are not simply generated by an hydrodynamic component of pressure, but evidently the gradient of velocity and viscosity play a relevant role too. Although many evidences are available in literature of their different weight in producing turbulent (or pseudo turbulent) structures, (see [5]) it is not always possible to assure the predominance of pressure *a priori*. As a consequence their computation and their average is as essential as for the pressure field.

The numerical issues connected to the computation of the interfacial pressure do not emerge for the velocity field as requested by the no-slip condition imposed on the bubbles and by the disregard of phase change. Notwithstanding the same conclusion cannot be drawn for the velocity gradient ∇u , since the velocity of the bubble(s) is not the same of the liquid carrier phase, as happens for instance for one or more bubbles arising into a stationary box of liquid. (See case of the rising bubble). Furthermore the definition of the viscosity at the interface implies an interpolation of the liquid and vapor values (neglecting temperature effects) which is not unambiguous as it seems to be strongly affected by the trend of the gradient and by the physics of the analysed case. Given that the following equality holds at the interface to ensure the continuity of the viscous shear stress,

$$\mu_v(\nabla u + \nabla^T u)_v = \mu_l(\nabla u + \nabla^T u)_l \quad (6.3)$$

the proper value of μ_l and μ_v have been suggested in [11] and [7] on the basis of an harmonic mean and on geometrical parameters in case both the viscosities are not negligible. Such conclusions rely on the strong hypothesis of a linear velocity profile, such as the one arising in a two-layer Couette or Poiseuille flow but not appropriate for the cases analysed. For these reasons in order to avoid issues connected to this interpolation, all the DNS have been carried out adopting a ratio between the dynamic viscosities equal to one.

In this simplified framework the gradient of velocity field results continuous too. Some numerical issues need to be discussed with regards to the post-processing of velocity: IJK provides the three components of this vector at the cell faces, in a suitable way for the formulation of the convective non-linear term into the momentum conservation equation. In contrast the scalar quantities such as pressure and density are defined at the cell centers. In order to avoid miscommunications between the grids and further computational effort, the velocity components are linearly interpolated at the cell center. On the other hand the velocity derivatives are evaluated directly at cell centers with a second order centered finite difference approximation, except in presence of walls where a second order directional scheme is needed. All the crossed terms $\frac{\partial u_i}{\partial x_j}$ implies a mean value of u_i along i direction. Consequently the stencil involved in this computation is larger than the others, thus it may affect the continuity of the gradient at the interface if the mesh is not sufficiently refined.

As regard the viscous interfacial term in the averaged momentum equation, because of the previous hypothesis it results $\tau_l = \tau_v$, but the vectors in 3.13 differ in the sign of the normal. Since no reason has been found for neglecting the transposed of the velocity gradient the final vector is:

$$\tau_k \cdot \nabla \chi_k = \begin{bmatrix} \frac{\partial u}{\partial x} \nabla \chi_x + \frac{\partial u}{\partial y} \nabla \chi_y + \frac{\partial u}{\partial z} \nabla \chi_z + \frac{\partial u}{\partial x} \nabla \chi_x + \frac{\partial v}{\partial x} \nabla \chi_y + \frac{\partial w}{\partial x} \nabla \chi_z \\ \frac{\partial v}{\partial x} \nabla \chi_x + \frac{\partial v}{\partial y} \nabla \chi_y + \frac{\partial v}{\partial z} \nabla \chi_z + \frac{\partial u}{\partial y} \nabla \chi_x + \frac{\partial v}{\partial y} \nabla \chi_y + \frac{\partial w}{\partial y} \nabla \chi_z \\ \frac{\partial w}{\partial x} \nabla \chi_x + \frac{\partial w}{\partial y} \nabla \chi_y + \frac{\partial w}{\partial z} \nabla \chi_z + \frac{\partial u}{\partial z} \nabla \chi_x + \frac{\partial v}{\partial z} \nabla \chi_y + \frac{\partial w}{\partial z} \nabla \chi_z \end{bmatrix}$$

whose components are directly averaged along the interface on the planes required in IJK.

7 Single rising bubble

Once the form of the total interfacial contribution in the two-fluid averaged formulation has been pointed out, a more meaningful case has been studied to further investigate the reliability of the method proposed. Since resolution plays a relevant role too, an additional mesh convergence study has been performed before proceeding with the analysis of the first and second order averaged equations.

The chosen configuration is a simple rising bubble in a periodic box of dimensions $20d_b \times 5d_b \times 5d_b$: in this framework all the interfacial effects arise and complex situations are avoided where the algorithm devoted to the pressure extention results in significant approximations, namely the presence of walls and of close bubbles. In addition it is straightforward to detect the position of the bubble and the influence of the interface on the equilibrium.

It should be noted that, due to the absence of walls, the equilibrium of the momentum along the streamwise direction assures that the hydrodynamic driving force (the pressure gradient averaged over the whole domain) is equal to the weight of the mixture averaged on the box. Thus, since the source term is defined as $\beta = \nabla \langle P \rangle - \langle \rho \rangle \mathbf{g}$, it is equal to zero.

In the chosen cartesian frame of reference x stands for the streamwise direction, y is the direction orthogonal to the planes of the average and z is the spanwise direction. The main physical and numerical parameters of the simulation are summarized in the table 7.1.

L_z [m]	0.02
L_y, L_z [m]	0.005
α_v [%]	1.047
d_b [m]	0.001
σ [N/m]	0.00163
ρ_l [kg/m ³]	986.51
ρ_v [kg/m ³]	845.44
μ_l [Ns/m ²]	0.00139
μ_v [Ns/m ²]	0.00139
Re_b	22

Table 7.1: Physical and geometrical parameters of the test case

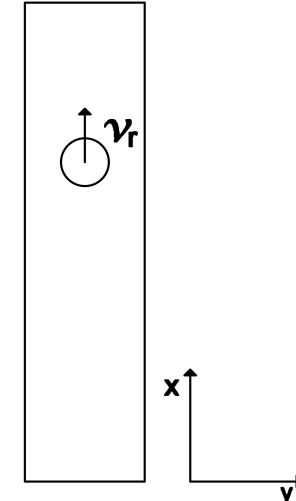


Figure 7.1: Configuration of the test case

It should be recalled that in the context of bubbly flows the Reynolds number is defined as the

bubble Reynolds number, namely $Re_b = \frac{d_b \langle u_r \rangle}{\nu_l}$, thus it based on the properties of the liquid phase and on the relative velocity, generally defined as $\langle u_r \rangle = \bar{u}_v^v - \bar{u}_l^l$ and that stands for the velocity of the bubble in the present configuration. The choice of this adimensional quantity, aimed at taking into account the features of both of the phases, is preferred in the description of the dispersed two-phase flows because the classical single-phase Reynolds number definition may not be univocal when the flow is not homogenous. With respect to the term of buoyancy, acting like an external forcing on the flow along the negative direction of the x axis, the constant acceleration of gravity g is assumed to be $9.81 m/s^2$.

7.1 Mesh convergence

The proper criterion to check the convergence of the mesh is not unequivocal in the up-scaling procedure where the scrutinized parameters are higher order statistics. In the studies already carried out resorting to TrioIJK, the terminal velocity of the bubble has been chosen as a strong convergence criterion to assure the adoption of a sound discretization (see [1]). Notwithstanding the current work is the first attempt of bringing to light the interfacial statistics, whose sensitivity to the mesh refinement has not been investigated yet.

For this reason the attention is focused on the new terms and in particular on the interfacial force \mathbf{M}_κ , whose definition has been provided in 3.20. The interfacial production has been analysed in a further stage since the Reynolds stress transport equations is not the averaged counterpart of a microscopic equation directly solved by the DNS and thus it is more exposed to imprecisions and errors. The results obtained in this case for three of the meshes are however presented in this section.

The mesh convergence study involves the mean value of the streamwise component of \mathbf{M}_l , i.e. the drag force exerted on the bubble. Its trend is expected to be similar to the one of the terminal velocity. The covariance of this field, namely the Reynolds stress $\overline{u'u'}$ is not adopted as it is not remarkable for the Reynolds number of the configuration, where only pseudo - turbulence due to the discontinuous fluid plays a role in the momentum equation.

Concerning the time interval to compute the statistics a long simulation on a coarse mesh has been run to let the system reach a steady state and settle on a proper time window to compare the results. The profile of the liquid and vapor velocity against time is provided below.

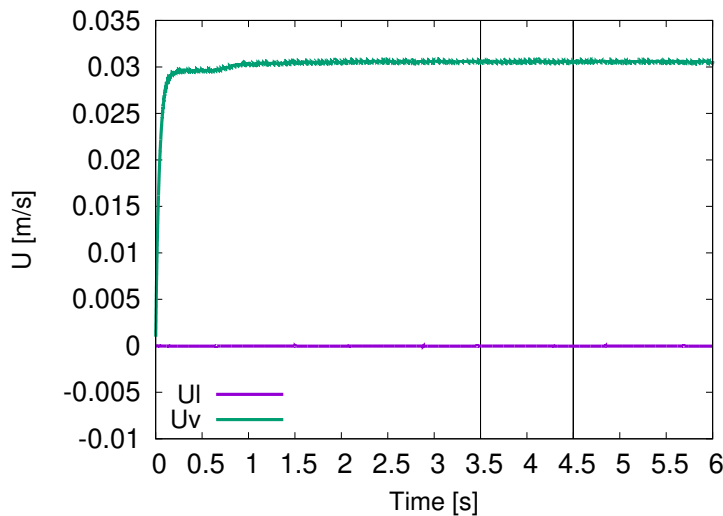


Figure 7.2: Evolution in time of liquid (U_l) and gas (U_v) velocity.

The single phase velocities have been easily obtained resorting to the definition of velocity and momentum of the mixture, the only available data provided by the Navier-Stokes solver. Although both of the curves show some oscillations in time, their amplitude is negligible with respect to the mean value computed for the vapor phase and equal to the bubble velocity when the liquid is not moving. The vertical lines in the previous figure mark the time interval $3.5 - 4.5[s]$ used to compute the ensemble average which is able to ensure the reaching of a statistical steady state. The study of the mesh convergence entailed five different staggered cartesian meshes characterized by a progressive refinement and was based on the classical Richardson extrapolation accurate at the third order. Accordingly to this method the value expected for a generical quantity f when

the mesh size h tends to zero is computed by the following equation:

$$f_{h=0} \cong f_1 + \frac{f_1 - f_2}{r^3 - 1} \quad (7.1)$$

where $r = \frac{h_1}{h_2}$ is the ratio between the characteristic dimension of the meshes, assumed equal to $\sqrt{2}$ in the present study.

The results obtained following this procedure are summed up in the following table:

Mesh	cells/diameter	u_r [mm/s]	M_l N/[m ³]	ϵ [%]
1	9.6	30.58	4.9060	26.8
2	14.4	30.96	5.9123	11.8
3	19.2	31.00	6.4769	3.46
4	27.2	31.10	6.6912	0.26
5	38.4	31.13	6.7027	0.09
∞	∞	31.15	6.7090	0

Table 7.2: Mesh converge study: the component along the streamwise direction is considered.

In order to better understand the previous results it is noted that, as explained in the chapters below, the statistics are computed on planes along the y – *direction* in the periodic box (see figure 3.3). All the terms of the momentum equation are therefore presented as functions of the y coordinate in such a way to clearly individuate the bubble and recognize the errors due to the presence of the new interfacial contributions. The values listed in the table 7.2 and used in the extrapolation formula 7.1 are the integrals of the curves referring to the interfacial momentum along the streamwise direction for the liquid phase. The RMS of the Reynolds stress and the terminal velocity are provided too for further information.

As a result of this convergence analysis one may notice that the interfacial force is the parameter most affected by the grid dimension. This trend might be explained by the computation of $\nabla\chi$ implemented in IJK. As explained in section 6.1, it resorts to the definition of the normal to the Front and on a cluster of close elements crossing a cell. It is clear that this number as well as the elements crossed by a single cell may change along with its dimension. This circumstance, although useful to manage changes in the front topology, is suspected to cause some imprecisions that decreases fastly along with the refinement.

The error relative to the values obtained for an infinitely refined mesh is listed in the last column of 7.2: the last two resolution tested are both amply sufficient to assure a negligible error in the momentum balance. The use of the coarser of the two could be suggested in more complex configurations, whereas the analysis carried out in the following paragraphs relies on the finest one to guarantee a proper validation of the up-scaling procedure. Finally, it is interesting to note how the explicit computation of the interfacial force makes clear the difficulty encountered in finding an unambiguous convergence criterion and how deeply it is affected by the numerical method followed as well as by the final aim of the analysis.

As regards the Reynolds stress balance equation, the impact of the mesh refinement is proved to be important too, but the same conclusions drawn thanks to the momentum analysis are reached. The trend of the first two diagonal components of R_{ij} is plotted for meshes 1, 3, 5.

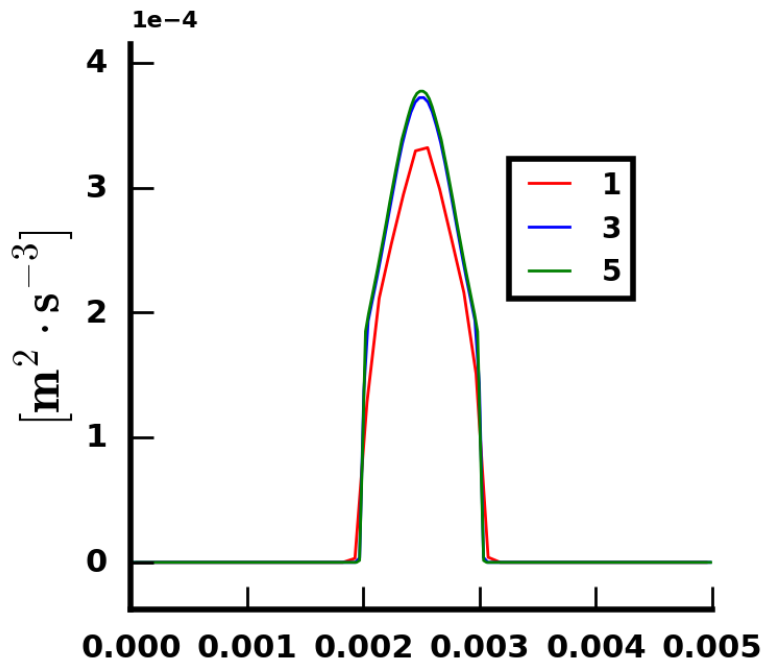
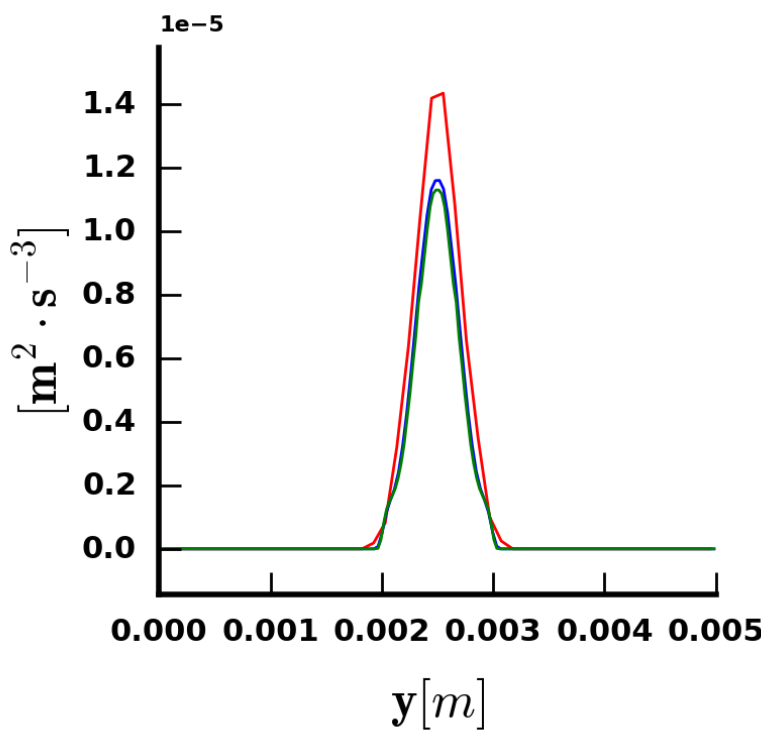
(a) Π_{xx} (b) Π_{yy}

Figure 7.3: Sensitivity of the interfacial production to the mesh refinement

7.2 Momentum budget

The simulation of the single bubble on the finest mesh has been then employed to analyse the momentum budget and validate the use of the averaged equations, now that all the terms are evaluated and a distinction might be done between modelling and numerical errors.

In the present configuration a laminar flow is simulated, therefore viscous effects emerge to balance the gradient of pressure and the inhomogeneous weight of the mixture in order to assure the steady state of the system. In the following plots a contribution formally defined as turbulent is present too. It should be stressed that it has nothing to do with the complexity, the high diffusivity coefficients turbulence refers to, but rather it simply arises because of the motion of the bubble relative to the liquid that causes fluctuations of velocity in the carrier phase. The convective scale is still the characteristic one of the system and the molecular features of the fluid still control its evolution. As a consequence emphasis is laid on the interfacial forces. Both the liquid and the vapor phase evolution is remarkable in this context and suits perfect the validation aim pursued in the section. The terms of the two - fluid averaged momentum equation 3.19 are displayed against the y direction for both the liquid and the vapor phase. Only the streamwise and the transverse y components have been investigated as in the second transverse direction z all the terms reduce to some numerical noise. An integration over the periodic direction y has been computed too expressly to easily rank the terms in the balance equation and supply a more precise insight on the real physical mechanisms acting on the flow. The integral formulation of the recomputed averaged two-fluid governing equation at the statistical steady state is noted here with an highlight on the new available interfacial pressure term:

$$\begin{aligned} \int_0^y \overline{P'_i \nabla \chi_\kappa - \tau_i \cdot \nabla \chi_\kappa} dy &= - \int_0^y \nabla (\alpha_\kappa \overline{P'_\kappa}^\kappa) dy + \int_0^y [\alpha_\kappa (\rho_\kappa - \langle \rho \rangle) \mathbf{g} - \alpha_\kappa \beta \mathbf{e}_x] dy \\ &\quad + \int_0^y \nabla \cdot (\alpha_\kappa \overline{\tau_\kappa}^\kappa) dy + \int_0^y \nabla \cdot (\alpha_\kappa \overline{\rho_\kappa \mathbf{u}'_\kappa \otimes \mathbf{u}'_\kappa}^\kappa) dy \end{aligned} \quad (7.2)$$

A recall of the terms appearing in the RHS of the equation 3.19 is reported too with a new notation to improve the readability of the plots. It is used in all the following sections and specialized for the phase treated. The numerical residue of the equation is noted with e in all the figures included in this section.

$$\begin{aligned} M_\kappa &= \overline{P'_i \nabla \chi_\kappa - \tau_i \cdot \nabla \chi_\kappa} \\ M_\kappa^\mu &= \overline{\tau_i \cdot \nabla \chi_\kappa} \\ M_\kappa^p &= -\overline{P'_i \nabla \chi_\kappa} \\ P_\kappa &= \nabla (\alpha_\kappa \overline{P'_\kappa}^\kappa) \\ T_\kappa^\mu &= \nabla \cdot (\alpha_\kappa \overline{\tau_\kappa}^\kappa) \\ T_\kappa^t &= -\nabla \cdot (\alpha_\kappa \overline{\rho_\kappa \mathbf{u}'_\kappa \otimes \mathbf{u}'_\kappa}^\kappa) \\ g &= \alpha_\kappa (\rho_\kappa - \langle \rho \rangle) \mathbf{g} \\ S &= \alpha_\kappa \beta \mathbf{e}_z \end{aligned}$$

7.2.1 Liquid phase

The results for the liquid phase are presented here.

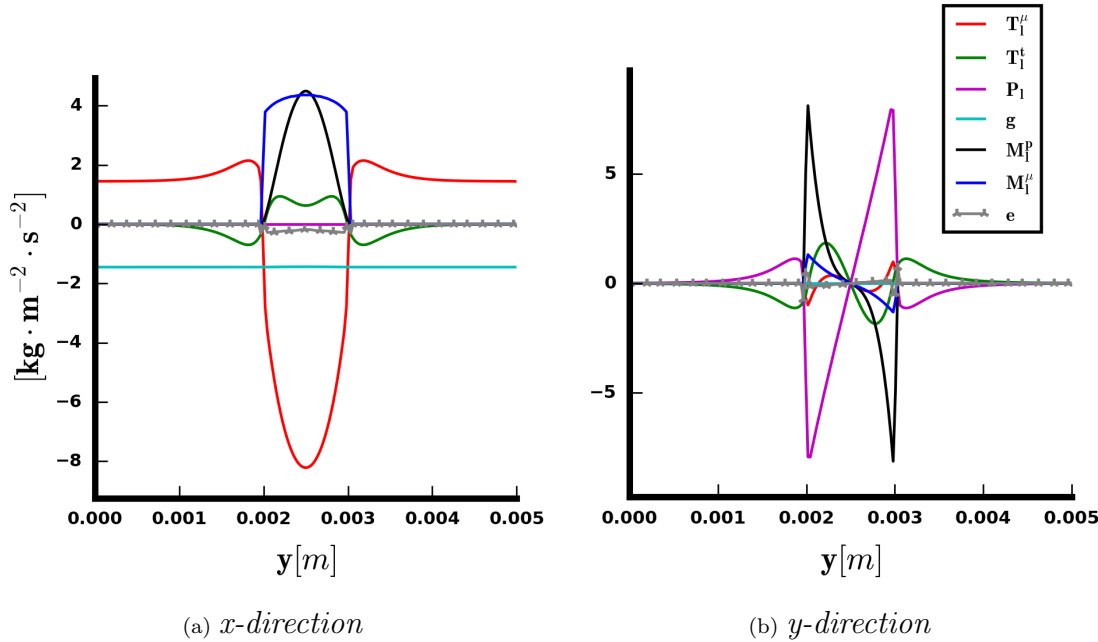
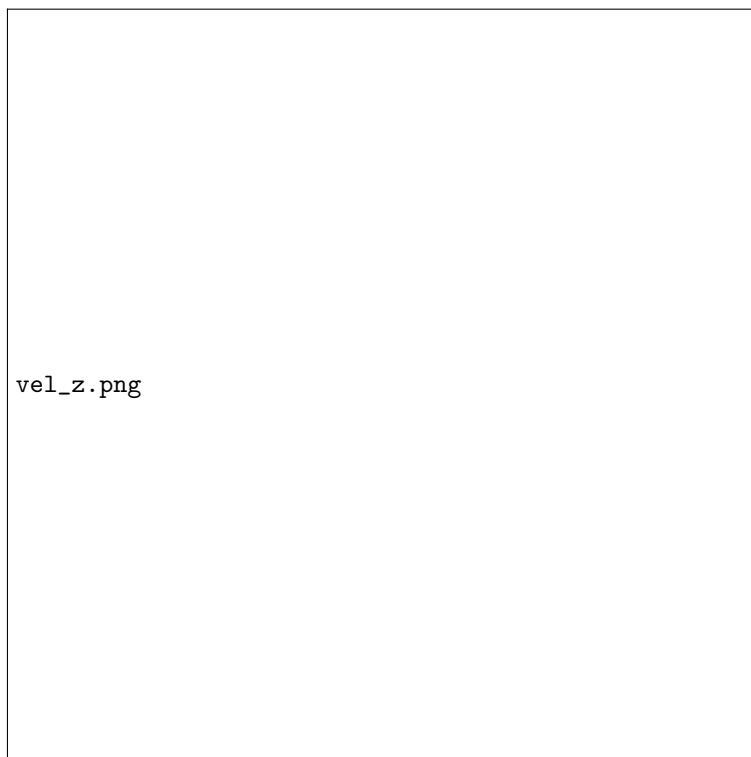


Figure 7.4: Averaged momentum equation - liquid phase

In figure 7.4a equation 3.19 at the statistical steady state is projected along the streamwise direction. Because of the low void fraction, the liquid indicator function averaged on the planes α_l is almost everywhere equal to one, then the bouyoancy force results nearly costant.

In the purely liquid region of the box it is balanced only by the predominant viscous stress produced by the movement of the liquid layers. Along the averaging planes close to the bubble ($0.001 \text{ m} < y < 0.002 \text{ m}$ \wedge $0.003 \text{ m} < y < 0.004 \text{ m}$) the magnitude of the gradients of the streamwise component of velocity tends to slightly increase since its microscopic value should reach the terminal velocity of the bubble at the interface. In this region the contribution due to the pseudo-turbulence T_l^t is observed, hence meaning the total average of the product of the liquid velocity $\bar{u}_l u_l \chi_\kappa$ is higher than then the product of the averages. The region inside the bubble $0.002 \text{ m} < y < 0.003 \text{ m}$ is marked by more noteworthy phenomena. It is the first time that the interfacial terms are explicitly computed and displayed in the up-scaling procedure. The pressure and the viscous contribution have been distinguished in order to provide a better first insight of their relative importance. Here the liquid velocity u_l decreases then causing the viscous stress T_l^μ to reach a negative peak at the center of the bubble, whereas the interfacial contribution pushes the liquid toward the top of the box. Both the pressure contribution M_l^p and the viscous one M_l^μ reach the same maximum, although their distribution is different: the latter seem to be predominant, as better pointed out by the analysis of the integrated equation (see figure 7.6a). As a matter of fact, in 6.2 has been reported that the streamwise component of the vector M_l^μ takes into account a great number of contributions, both due to the gradient of the streamwise component u along the three direction, and to the gradient of v , w along x . Although evidently the magnitude of the last two is less relevant when compared with u , they all undergo a sudden variation at the interface. As showed by the velocity distribution, the wake induced by the bubble into the flow is not symmetric along the streamwise component, thus explaining the major role played by $\frac{\partial u}{\partial x}$ and then the relative importance acquired by the two interfacial terms along this direction.

(a) u (b) w Figure 7.5: Velocity distribution on a plane $z = 0.0025$ m and $t=??$

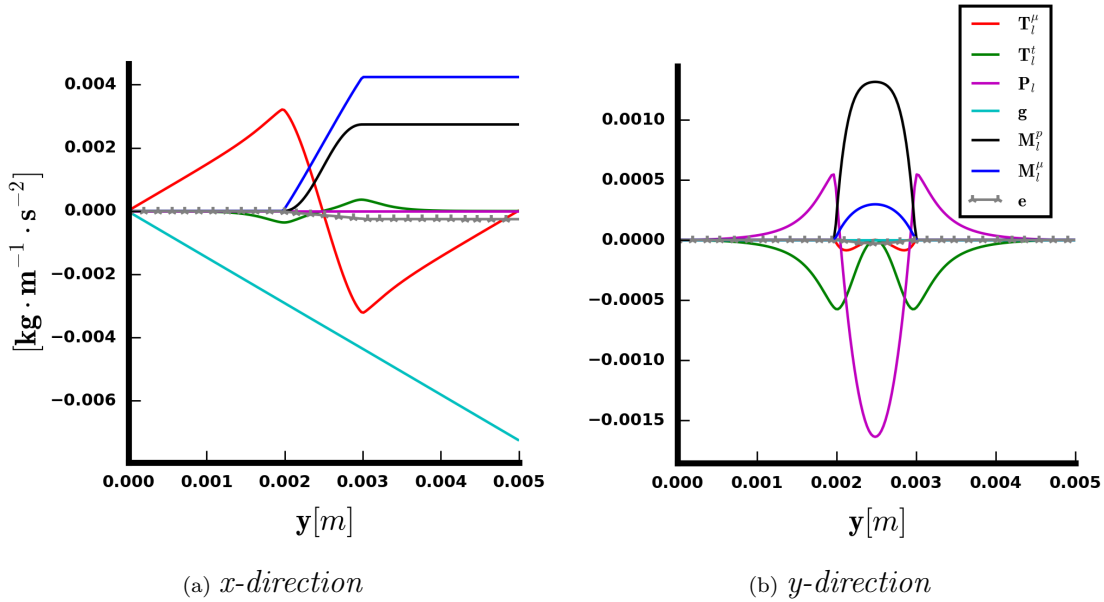


Figure 7.6: Integral of the momentum equation - liquid phase

Regarding the evolution along the y direction shown in figure 7.4b, the gradient of the averaged pressure is significant, both in the vicinity of the interface and inside the bubble. While in the first case it is balanced by the pseudo-turbulence, in the latter the predominant role is played by the interfacial pressure force. As happens for the fixed bubble, in this case too the quantity has a linear trend, extremely smooth because of the high definition of the mesh. Both the viscous contribution and the shear stress in this case are less relevant, as expected along the direction of the average (where the wake induced by the bubble is symmetric and not as wide as in the streamwise direction). In this direction a small error is detected at the very interface and it is due to imprecisions in the Front - tracking algorithm. On the other hand the streamwise component of the total residual is more relevant, thus suggesting that some numerical errors are still present in the computation of the averaged gradient of velocity and appear when the viscous effects are predominant.

In this respect it is recalled that a minor change has been introduced in the definition of the average $\overline{\tau_\kappa \chi_\kappa}$. The current implemented formulation of this term, holding that the viscosity is a constant, is:

$$\overline{\tau_\kappa \chi_\kappa} = \mu \left(\overline{\chi_\kappa \nabla u_\kappa} + \overline{\chi_\kappa \nabla^T u_\kappa} \right) \quad (7.3)$$

whereas it was previously evaluated as:

$$\overline{\tau_\kappa \chi_\kappa} = \mu \left(\nabla \overline{u_\kappa \chi_\kappa} + \nabla^T \overline{u_\kappa \chi_\kappa} \right) \quad (7.4)$$

thus neglecting the contribution due to the gradient of the phase indicator function, as evidently $\overline{\chi_\kappa \nabla u_\kappa} = \nabla \overline{u_\kappa \chi_\kappa} - \overline{u_\kappa \nabla \chi_\kappa}$.

Nevertheless, the idea previously followed in [1], [4] and [2] of computing \mathbf{M}_κ as the right hand side of the equation 7.2 led to highly accurate results, validated by the study carried out in this work. The comparison between the explicit (noted in legend as \mathbf{M}_l) and the implicit (noted as **RHS**) estimate of the total interfacial force on the liquid is provided in the picture 7.7 along the two directions studied:

The two curves along the y direction perfectly superpose, whereas a small difference in magnitude of the order of the 3% of the maximum could be detected in 7.7a, as a further consequence of the

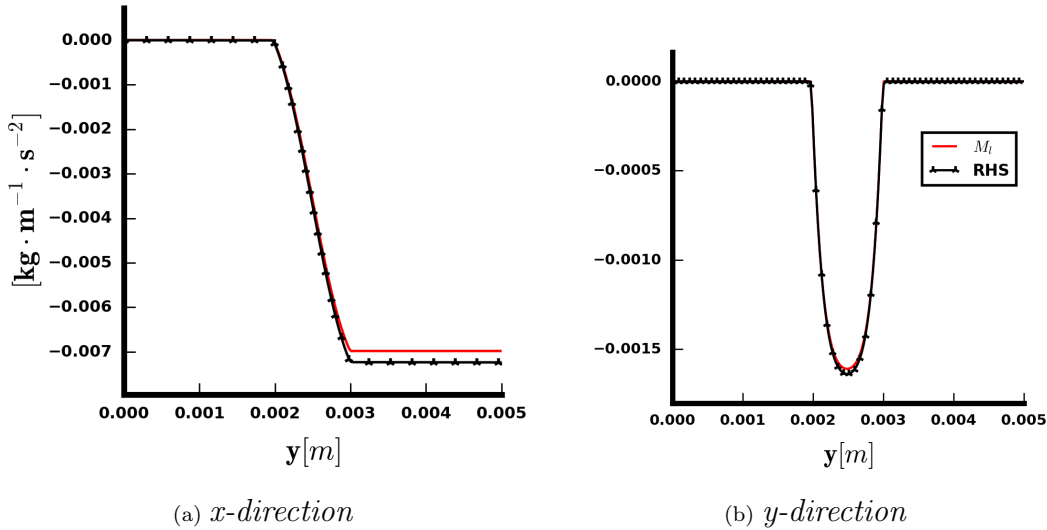


Figure 7.7: Confront between the two methodology

numerical errors still unavoidable in the reconstruction of the viscous terms.

7.2.2 Vapor phase

Depending on the framework studied and on the aim of the research, usually more focused on the characterization of the carrier phase, the resolution of the averaged equations for the vapor may not be pivotal. Nevertheless in the present work an accurate analysis of the momentum equation has been considered significant too in order to validate the reconstruction of the interfacial force. The results obtained for the vapor phase are reported and commented in this section.

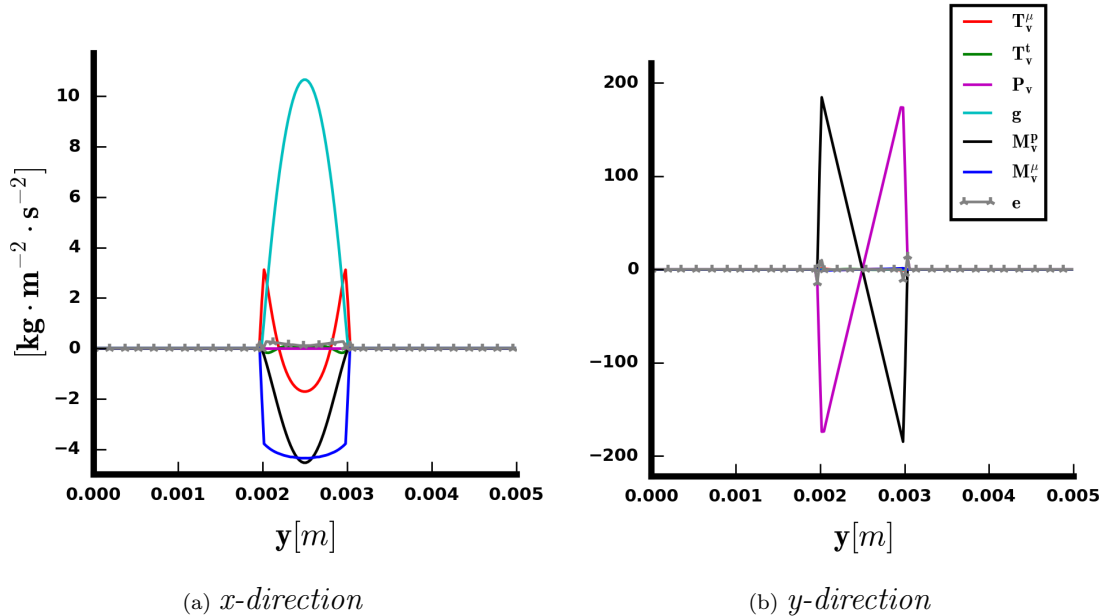


Figure 7.8: Averaged momentum equation - vapor phase

In this case only the planes inside the bubble ($0.002m < y < 0.003m$) show a considerable dynamics, as expected from the definition of phase averaged variables. Regarding the projection of the equation along the streamwise direction (7.8a), the buoyancy has a symmetrical trend which reaches its maximum at the position of the bubble diameter, then following the trend of the vapor indicator function. This contribution is predominant and induces the bubble to rise toward the top of the box because of its smaller density. Regarding the psuedo-turbulence T_v^t no effect of this kind may arise fot the gas phase. As explained in the previous section, it is a expression of the influence the bubbles exercise on the liquid. Conversely, the influence of the liquid on the vapor phase in dispersed flows induces only changes in the trajectory of the bubbles. This phenomenon is remarkable when the mean velocity of the liquid and the void fraction are high, thus causing multiple interactions able to affect liquid turbulent stuctures, whereas in the current configuration (the mean liquid velocity is zero), this effect does not arise at all. The remaining remarkable actions for the vapor phase are mainly due to the viscous shear stress T_v^μ caused by the velocity distribution inside the bubble, and to the interfacial force. It should be kept in mind that when the hypothesis explained in 6.2 hold, the viscous contribution M_l^μ and M_v^μ are equal but have opposite sign because of the opposite orientation assigned the normal. (\mathbf{n}_v , computed by TrioLJK is oriented toward the liquid, whereas $\mathbf{n}_l = -\mathbf{n}_v$ is oriented inside the bubble). In contrast M_l^p and M_v^p are different but they have the same order of magnitude, although the pressure in the vapor phase is higher than the liquid one. This happens because $\frac{\partial \chi_v}{\partial x}$ is symmetric along the plane of the average, thus the interfacial pressure contribution is more affected by the pressure distribution, equal for both of the phases at the interface, than by its magnitude.

It is evidently not the case of the other relevant component $P_v \frac{\partial \chi_v}{\partial y}$. The high vapor pressure leads to values of the momentum equation along the direction of the average that are two order of magnitude bigger than the others, as shown in figure 7.8b. The statistical steady state is here assured by the pressure terms P_v and M_v^p , while all the viscous contributions become negligible. The total residue is caused by the singular points at the interface, but it is not remarkable as results in the analysis of the integrated equation 7.9b and in the exact superposition of the curves referring to the explicit and implicit method for the esteem of the interfacial force 7.10b.

As regards the viscous term T_v^μ displayed along the streamwise direction, it has been computed as explained for the liquid counterpart and numerical errors arise in this case too (see 7.10a).

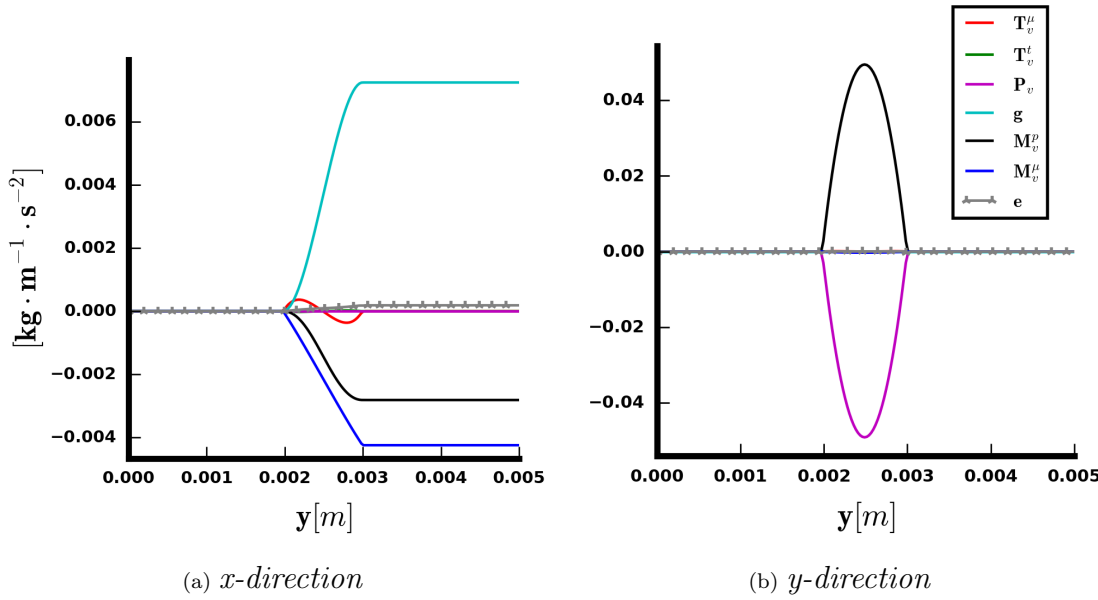


Figure 7.9: Integral of the momentum equation - liquid phase

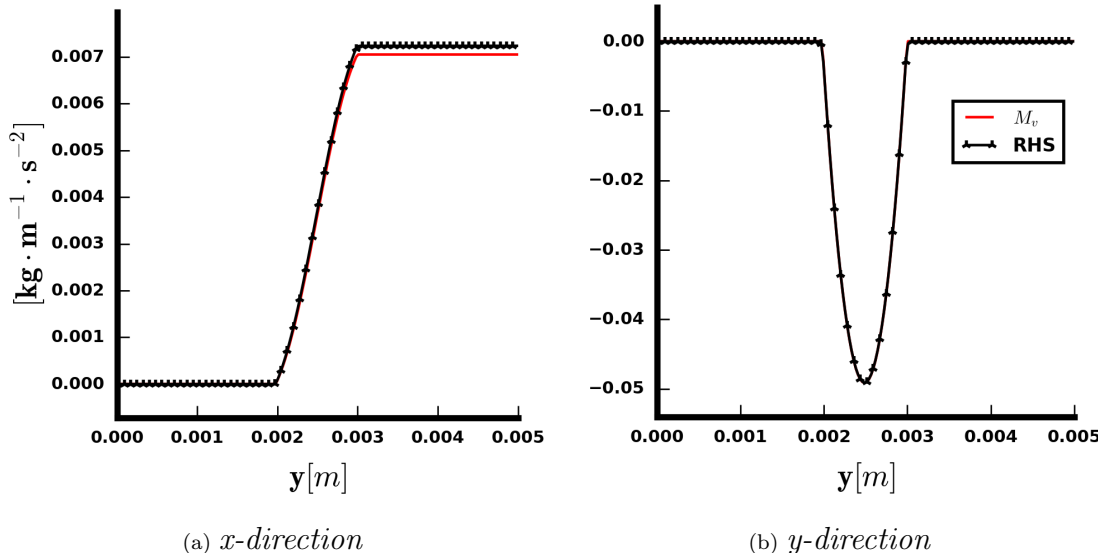


Figure 7.10: Confront between the two methodology

7.2.3 Jump condition and Drag force

Finally in order to conclude this analysis of the momentum balance, the jump condition 3.21 has been checked and validated resorting to the averaging procedure performed on the one-fluid equation. The term \mathbf{M}_σ has been evaluated adopting its definition as $\sigma \bar{\kappa} \bar{\mathbf{n}}_v$. It should be noted, as already pointed out by du Cluzeau in [2], that in the current configuration of a single bubble in a uniform flow, the statistical approach and the particle approach could be considered equivalent since each part of the finite-size bubble passes through a plane at $y = \text{const}$ when a sufficient time is taken for the average. Thus the choice of the averaging parameters justifies the assimilation of the mean value of the momentum transfer \mathbf{M}_κ to the force experienced by the bubble per unit

of volume. The contributions to the equation 3.21 are portayed in the integral version too in the current section.

In the first place some remarks on the value of the vector \mathbf{M}_σ are needed to understand how the surface tension affects the momentum balance of the mixture. As usual the study will be carried out for the components along the streamwise and the transverse directions. In the first case the contribution due to the inhomogeneity of the fluid is not remarkable, as expected because of the symmetry of the x component of mean curvature. This means that the surface tension source has no impact in determining the stationary kinematic features of the bubbles, as shown in the figure 7.11a. It should be noted that the same conclusion was drawn by du Cluzeau et al. for an higher void fraction in a vertical channel. In the second case, displayed in 7.11b the component of \mathbf{M}_σ follows a linear trend along with the curvature and it is balanced by the one-fluid pressure gradient.

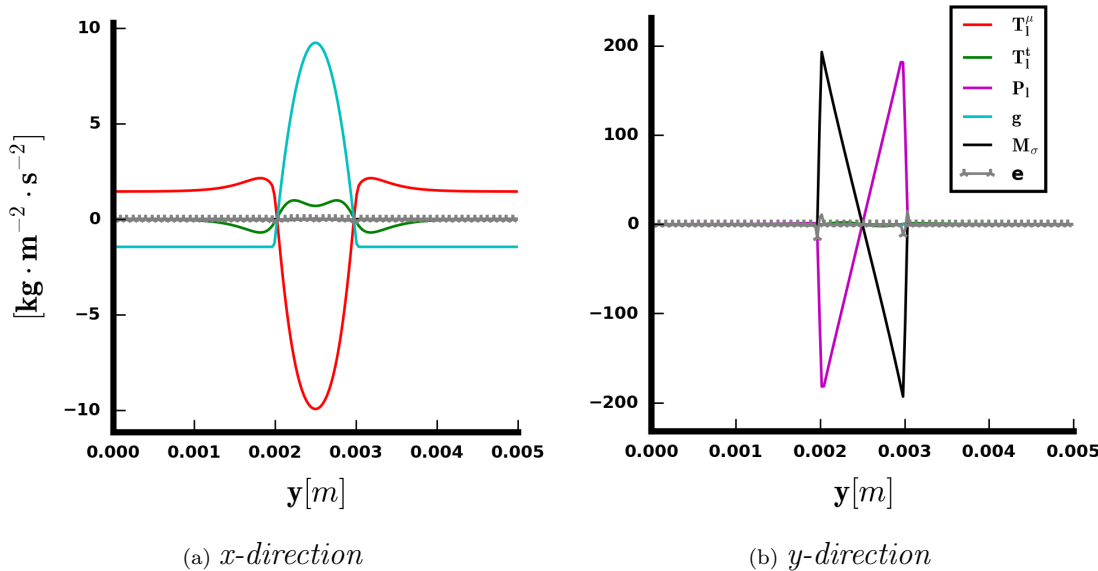


Figure 7.11: Momentum equation for the mixture

Looking to the picture 7.13b, its integral value has the same trend of the local void-fraction α_v , as pointed out in more significant cases (swarm of bubbles in wall bounded domains) by several publications. The mean value of this force is zero because a single bubble is present in the domain, so the surface tension, just like the other quantities in the direction y , is not responsible for a bubble migration in this simple test case. Once more it is recalled that the spanwise direction z does not undergo any investigation because of the definition of average 3.14 and the absence of motion along this direction. All the terms in the balance equation, both in the two-fluid and in the one-fluid formulation, have a low magnitude that could be rightly seen as a numerical error.

Furthermore the role of the momentum transfer \mathbf{M}_κ could be detailed. In the current configuration since the domain is periodic, there are no effects due to the presence of boundary layers. Moreover the velocity fluctuations included in the psuedo-turbulent contribution are almost negligible. Consequently the interfacial momentum exchange could be ascribed to the local pressure distribution at the very interface. It should be noted that in the current configuration the local velocity field at the interface is symmetrical with respect to the direction y and so is the local pressure distribution. As a consequence no shear-induced stress is exerted on the bubble along the direction y . Thus this contribution only gives rise to a drag force. As seen in the previous sections it is due to the asymmetry of both the liquid and the interfacial pressure field with respect to the direction x . A principle of action-reaction is valid and then, since $\mathbf{M}_v = -\mathbf{M}_l$, the jump relation is verified, as

shown in the figure 7.13a.

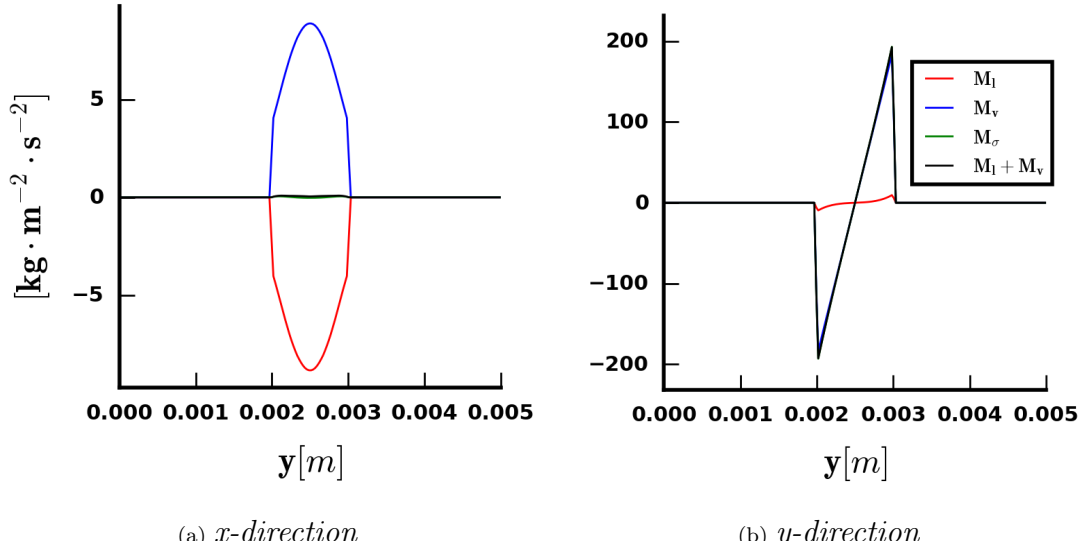


Figure 7.12: Contributions in the equation 3.21

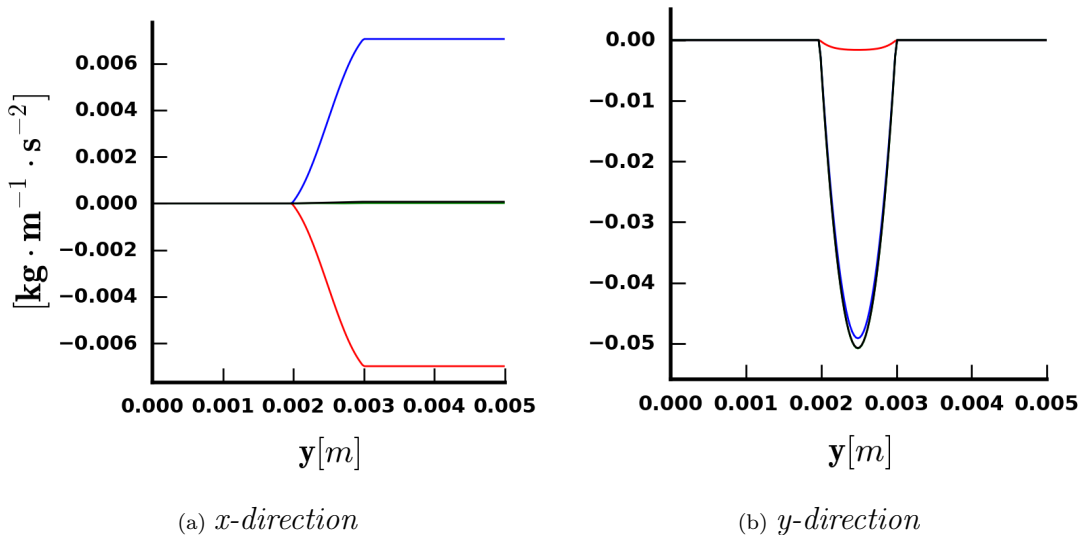


Figure 7.13: Contributions in the equation 3.21-Integral version

On the other hand, the transverse component, that could be still be interpreted as a Lift force is in principle more interesting because it is responsible for the bubble migration along the minor dimensions of the box. However in the current configuration this role can not be explored. Exactly has happens for the surface tension effect, the plots 7.4b and 7.8b, put in evidence that all the contribution related to the presence of the bubble have a zero mean value and consequently no Lift force acts on the bubble, whose position stays always the same along this direction. In spite of this absence one can still observe the distribution of \mathbf{M}_κ , in particular in its integral formulation, where the stress is displayed. It should be recalled that the sign of the interfacial contributions are different in 7.4 and in 7.7: in the first case they are taken into account as the stress exerted by

the vapor on the liquid phase, whereas in the latter an interpretation as the stress the liquid phase exerts on the bubble seems to fit better. The same note could be made for the results displayed in 7.8 and 7.10 too. The convention adopted in the confront between the methods has been used in the current section. As shown in figure 7.13b the stress exerted by the vapor on the liquid phase is found to be much more relevant than its liquid counterpart, and it is the major contribution to the surface tension effect.

In conclusion the analysis carried out in this section validate the method of the up-scaling and the improvement due to the explicit computation of the interfacial forces. Although it prevented us to observe new and relevant physical phenomena, a new instrument is now at our disposal to investigate more complex configurations and analyse the role each phase has in the definition of \mathbf{M}_σ . More information on the transverse direction in particular might be collected, as requested because of its importance in the bubbles migration, a feature that could affect the thermodynamics of the flow too. It should be kept in mind that when a swarm of finite-size bubbles is studied this component of \mathbf{M}_σ is not anymore cancelled and the analysis of \mathbf{M}_κ is of main relevance. In particular both the results obtained on this example case and the ones presented in [1] and now validated, the role of the vapor contribution seems to be crucially affected by the Eötvos number and thus requires additional investigations.

7.3 Reynolds stress budget

The final step in the validation was the reconstruction of the average Reynolds stress transport equation. Although this is the main aim of the pressure extention, such reconstruction was not at all easy to make: the chance of relying on the interfacial terms let us distinguish the numerical errors, so the entire post-processing script has been re-written resorting to the exact definition of fluctuations in order to minimize them. A list of the contributions present in the equation 3.22 at the statistical steady state and of their legend is presented here:

$$\begin{aligned}
 P_{ij} &= -\alpha_l \left(R_{l,ib} \frac{\partial \bar{u}_{l,j}^l}{\partial x_b} + R_{\kappa,jb} \frac{\partial \bar{u}_{l,i}^l}{\partial x_b} \right) \\
 \Phi_{ij} &= \alpha_l \frac{P'_l}{\rho_l} \left(\frac{\partial u'_{l,i}}{\partial x_j} + \frac{\partial u'_{l,j}}{\partial x_i} \right) \\
 \epsilon_{ij} &= -2\alpha_l \frac{\mu_l}{\rho_l} \frac{\partial u'_{l,i}}{\partial x_b} \frac{\partial u'_{l,j}}{\partial x_b}^l \\
 D_{ij}^t &= -\frac{\partial}{\partial x_b} \left(\alpha_l \bar{u}'_{l,i} \bar{u}'_{l,j} \bar{u}'_{l,b}^l \right) \\
 D_{ij}^\mu &= +\frac{\partial}{\partial x_b} \left(\nu_l \frac{\partial \alpha_l R_{l,ij}}{\partial x_b} \right) \\
 D_{ij}^p &= -\frac{\partial}{\partial x_b} \left(\frac{\alpha_l}{\rho_l} (\bar{P}'_l u'_{l,i}^l \delta_{bj} + \bar{P}'_l u'_{l,j}^l \delta_{ib}) \right) \\
 \Pi_{ij}^p &= -\frac{1}{\rho_l} (\bar{P}'_l u'_{l,j} n_{l,i} + \bar{P}'_l u'_{l,i} n_{l,j}) \delta^i \\
 \Pi_{ij}^\mu &= \nu_l \left[\frac{\partial (\bar{u}'_{l,i} \bar{u}'_{l,j} n_{l,b} \delta^i)}{\partial x_b}^i + \frac{\partial u'_{l,i} u'_{l,j}}{\partial x_b} n_{l,b} \delta^i \right]
 \end{aligned} \tag{7.5}$$

Since the main aim pursued in this section is to verify the consistency of this balance equation, all the terms were kept aside in order to detect errors in the esteem of each of them. For the interfacial term this method is useful for a physical analysis of their relative importance too, exactly as happened for the momentum equation.

7.3.1 Pressure diffusion and redistribution

As stated in section ?? there are several terms where the liquid pressure field is included. The first step of the analysis presented here is aimed at highlighting the changes produced in the computation of the redistribution and of the pressure diffusive term. As regards the latter the only relevant components involve the derivative along the y direction. In 7.14 the improvements are evident especially for the term xy , as the discontinuities and the singularities at the interface are now avoided and replaced by a continuous profile.

The second term investigated is the redistribution Φ , proved to be essential by the researches carried out in [1]: any difference in its evaluation could be of great relevance for the study of turbulence in other frameworks, like the channel.

It is evident in 7.15 that in the liquid phase the two values of pressure field are equivalent and differences arise along the planes inside the bubble. A slight underestimation emerges in the calculation of the redistribution based on the solved pressure field, particularly evident for Φ_{zz} and Φ_{xy} . It should be recalled that redistribution, pressure diffusion and the pressure interfacial production Π^p come from the decomposition of a term involving the pressure gradient (see Appendix

for further details):

$$\begin{aligned}
 -\frac{\alpha_l}{\rho_l} \left(\overline{u'_{l,j}} \frac{\partial p'_l}{\partial x_i} + \overline{u'_{l,i}} \frac{\partial p'_l}{\partial x_j} \right) &= \underbrace{\alpha_l \frac{P'_l}{\rho_l} \left(\frac{\partial u'_{l,i}}{\partial x_j} + \frac{\partial u'_{l,j}}{\partial x_i} \right)}_{\Phi_{ij}} \\
 -\frac{\partial}{\partial x_b} \left(\frac{\alpha_l}{\rho_l} \left(\overline{P'_l u'_{l,i}}^l \delta_{bj} + \overline{P'_l u'_{l,j}}^l \delta_{ib} \right) \right) - \frac{1}{\rho_l} \underbrace{\overline{P'_l u'_{l,j} n_i + P'_l u'_{l,i} n_j} \delta^i}_{\Pi_{ij}^p} &
 \end{aligned} \tag{7.6}$$

The LHS of the previous equation is not explicitly evaluated in the present work for both numerical and physical reason. Firstly the gradient of the pressure can not be considered exact along the interface because of the discontinuities this field exhibits, therefore care should be taken when it is involved in the averaging and in the building of the macroscopic equations. Clearly the issues arising in the interfacial cells could be solved resorting to the reconstruction this work deals with, but the practical implementation of the gradient entails some problems whose solution is beyond the scopes of the current work and requires further investigations. Finally, as already pointed out in the previous paragraphs, this decomposition put in evidence some remarkable phenomena, linked to the presence of the redistribution, whose modelisation both for single and two-phase flows is essential.

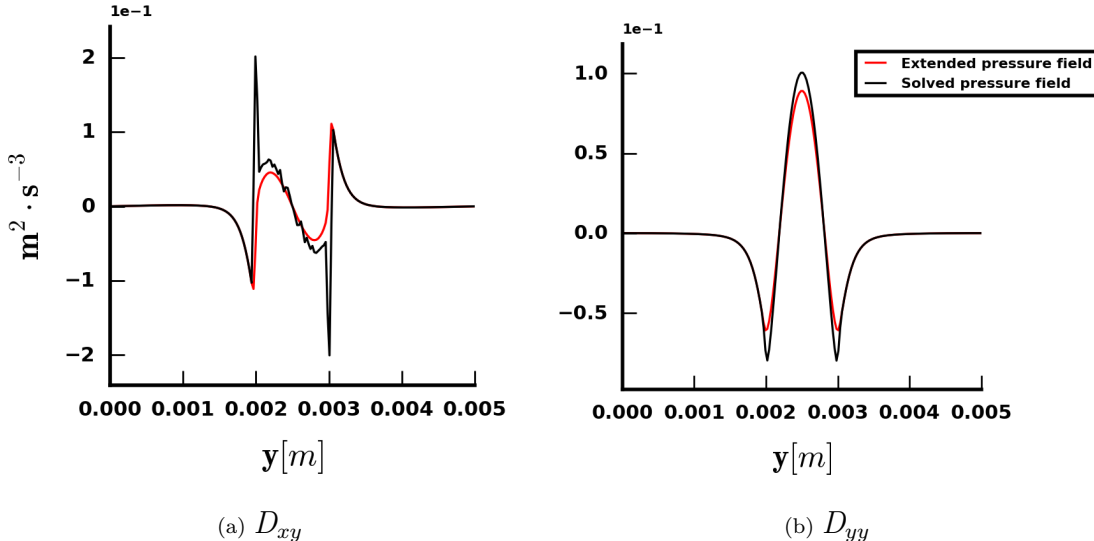


Figure 7.14: Influence of the liquid extended pressure field on the pressure diffusion

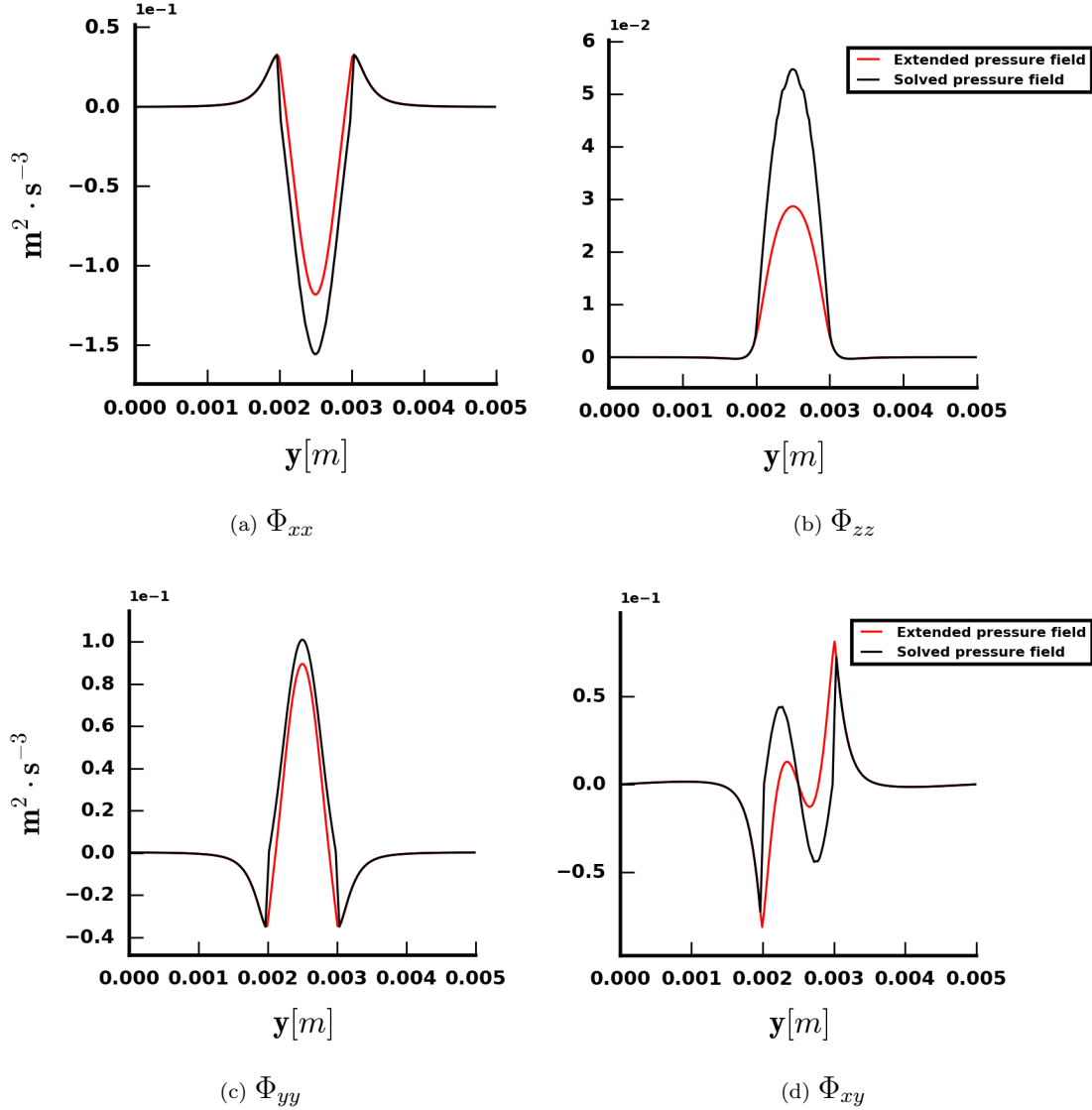


Figure 7.15: Influence of the liquid extended pressure field on the redistribution

7.3.2 Viscous terms

Similar considerations may apply to the viscous terms too, then the second step of this analysis consisted in carefully checking them. It is noted that a lot of work has been devoted to their esteem and implementation in the script because they are suspected of being the main source of errors. In this case it was possible to check the following equation, arising by several decomposition in the derivation of 3.22 (the reader is addressed to the [18] for the detailed developments):

$$\nu_l \alpha_l \left(\overline{v'_{l,j} \frac{\partial^2 v_{l,i}}{\partial x_b^2}}^l + \overline{v'_{l,i} \frac{\partial^2 v_{l,j}}{\partial x_b^2}}^l \right) = \underbrace{-2\alpha_l \nu_l \frac{\partial u'_{l,i}}{\partial x_b} \frac{\partial u'_{l,j}}{\partial x_b}}_{\epsilon_{ij}} \\ + \underbrace{\frac{\partial}{\partial x_b} \left(\nu_l \frac{\partial \alpha_l R_{l,ij}}{\partial x_b} \right)}_{D_{ij}^\mu} + \underbrace{\nu_l \left[\frac{\partial (\overline{u'_{l,i} u'_{l,j} n_b \delta^i})^i}{\partial x_b} + \frac{\partial u'_{l,i} \overline{u'_{l,j} n_b \delta^i}}{\partial x_b}^i \right]}_{\Pi_{ij}^\mu} \quad (7.7)$$

The plots 7.16 show that the LHS and the sum of dissipation, viscous diffusion and viscous interfacial production (referred to as 'RHS' in the legend are in perfect agreement, except for the component xx , where the LHS reaches a lowest value at the position of the diameter. It is stressed that the errors solely appear in the planes inside the bubble: the two contributions in Π^{mu} are then responsible for such a disagreement. At the current state of the job it wasn't possible to improve their implementation in the Python script devoted to the post-processing. Forthcoming investigations should focus on the role played by the gradient of phase indicator function $\nabla\chi_l$ as suggested by the presence of the error at the very interface too in the xx component. It is recalled that in the viscosity and the density are neglected in the study of the equivalence 7.7, so that the quantities displayed in 7.16 have a greater magnitude than the terms in the Reynolds stress equation.

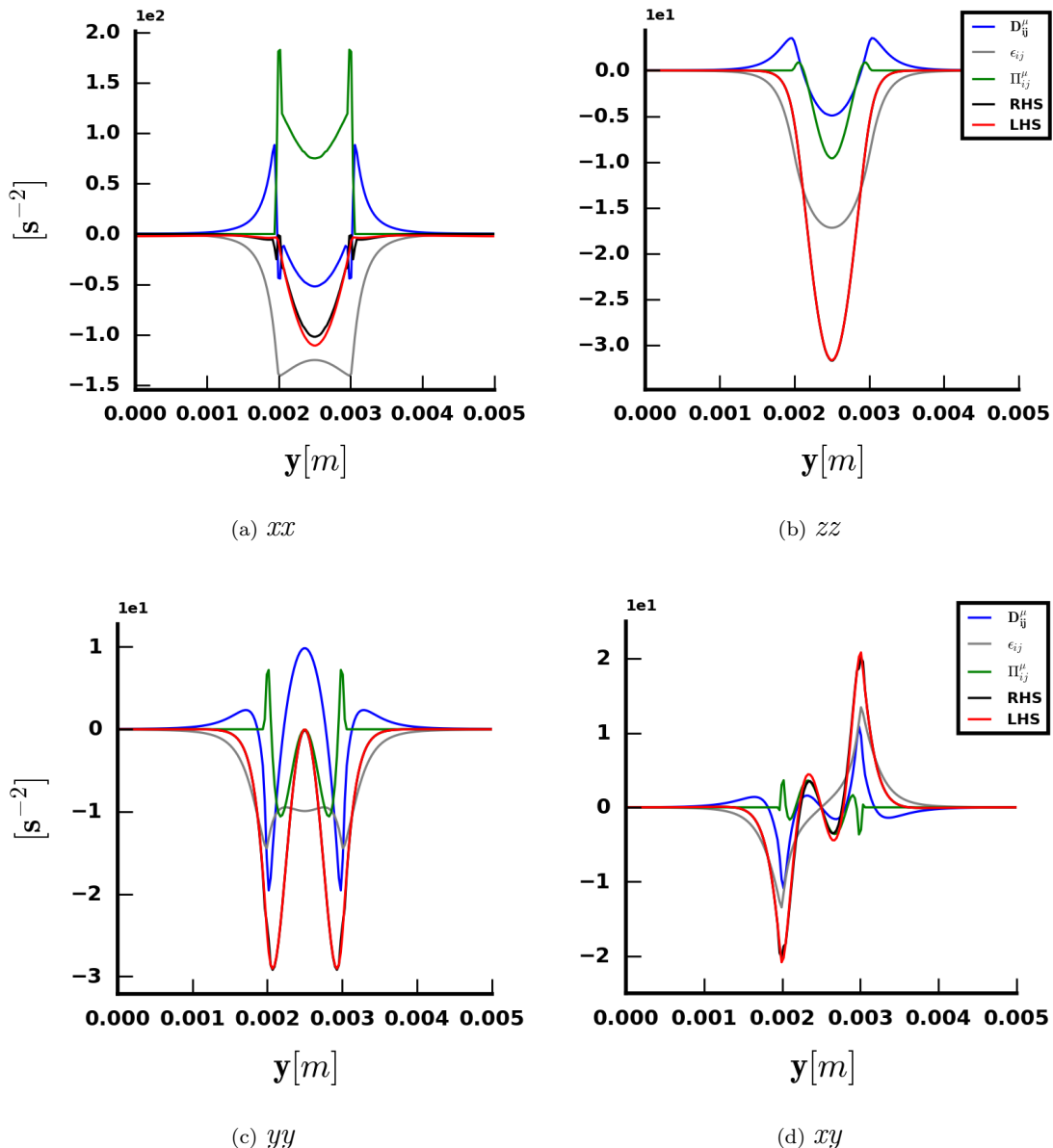
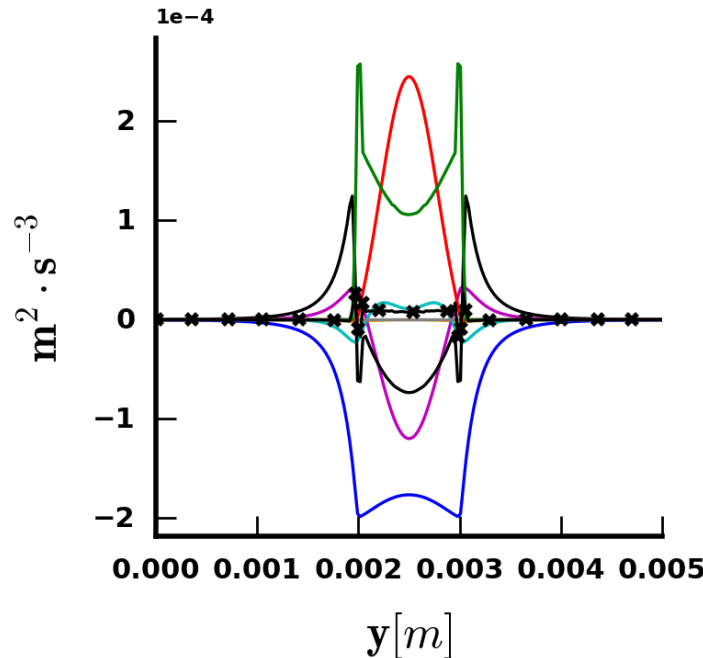
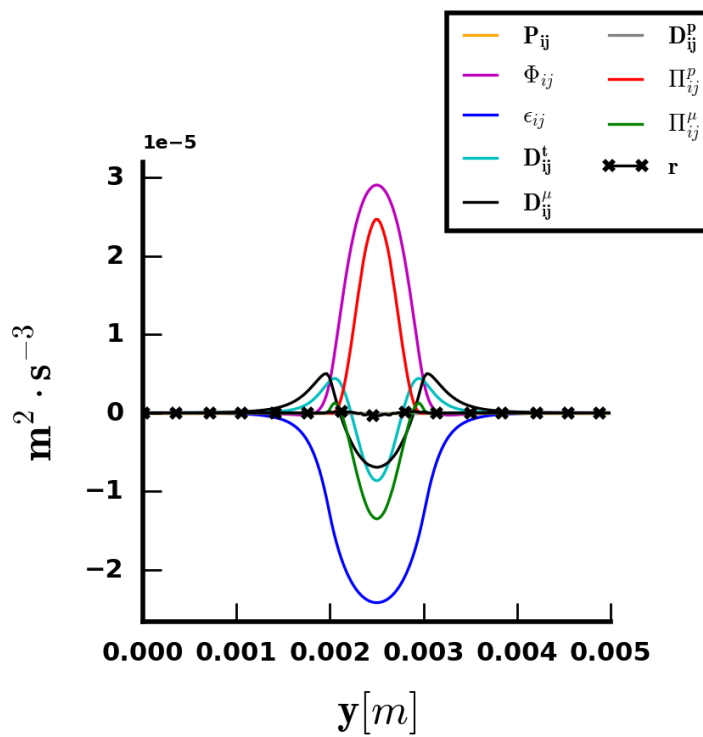
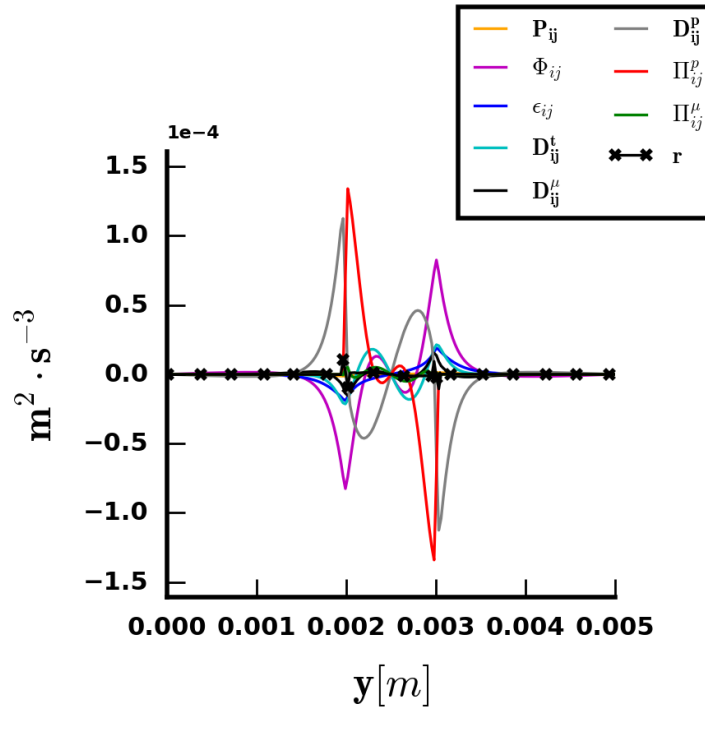
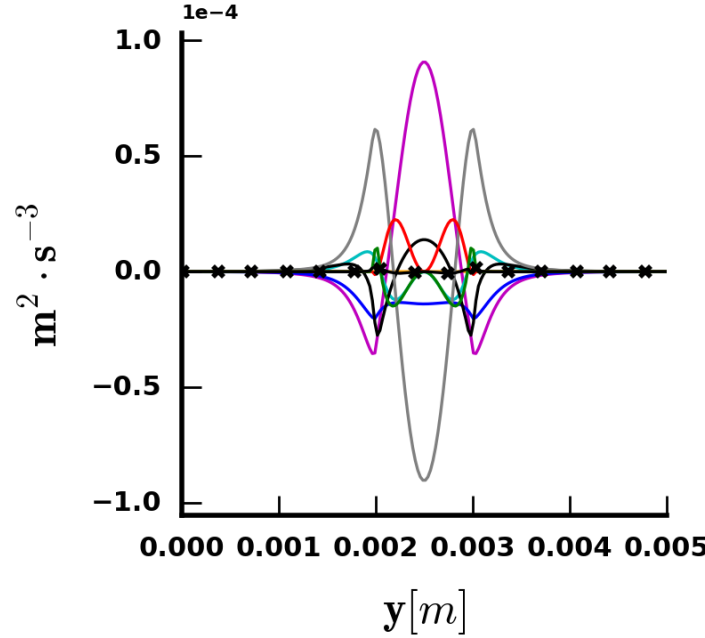


Figure 7.16: Check on the consistency of the viscous contributions in 3.22

7.3.3 Total balance

The third step of the present analysis involves all the term emerging in the balance equations 3.22 at the statistical steady state. The results obtained are portrayed in the following:

(a) R_{xx} (b) R_{zz}

Figure 7.16: Contributions to the R_{ij} balance equation

It should be kept in mind that the liquid flow is steady and its mean velocity is zero, thus no single-phase turbulent phenomenon arises. As a matter of fact the pseudo-turbulent effects, related to the presence of the bubble, are remarkable only in its vicinity and in the planes inside the bubbles itself. The production is negligible for all the components as the gradient of the averaged velocity is small. As regards 7.17a the remarkable effects are essentially due to viscosity, interfacial

production and redistribution. The triple velocity correlation arise too, but its magnitude is low. The redistribution in this case acts as the dissipation, subtracting energy that will be transferred to the two other principal components of the tensor (see 7.17b and 7.16c where this term is entirely positive). One sees that the viscous interfacial production Π^{μ} has an opposite trend as in this case it acts as a source of energy for the streamwise component whereas it plays a dissipative role for the other two cases. Conversely the pressure interfacial production Π^p has always a positive value, thus it is always responsible for an energy production in the balance equation. In the present case the interfacial production is pivotal in 7.17a and 7.17b, namely the cases where the dissipation is remarkable too and needs to be compensated for to assure the steady state. As regards the statistics along the direction y , orthogonal to the plane of the average, the balance is guaranteed by the pressure diffusion and by the redistribution, thus meaning only conservative effects arise for this component, since both the presence of the interface and the energy dissipation are negligible. Finally it is noted that both the viscous and the pressure diffusion are relevant in this laminar flow, while in more complex configurations they tends to disappear where the bubbles gather and only the bubble-induces effect hold. This could be explained arguing that the correlation of the fluctuations are not uniform in space in the region close to the interface, moreover the phenomena related to the presence of the bubbles are not enhanced as happens in a swarm.

In order to provide a deeper understanding on the kind of effect arising, the same results shown in 7.16 are proposed gathering all the diffusive terms in D_{ij} and all the interfacial terms in Π_{ij} . As expected, the interfacial production is always positive and in particular the cross-flows components are smaller than Π_{11} . This observation holds with the classical assumption that links this effect to the work of the drag force. (see [1]). In figure 7.17 the balance equation for the turbulent kinetic energy is displayed. It has been obtained resorting to its definition $K = \frac{1}{2}Tr a R_{ii}$. The redistribution has no effect in this case, and the results shown in [5] are confirmed: inside the bubble the balance is assured by the interfacial production (the source) and dissipation (the sink). In contrast to its result, conversely, the transport term is found to play a major role too for the above-discussed reasons, thus acting as a source of turbulent kinetic energy in the near of the bubble and then as a sink inside it. It is recalled the presence of a numerical error coming from the inaccuracy in the esteem of the viscous terms in xx component, the one that contributes most to the budget of K .

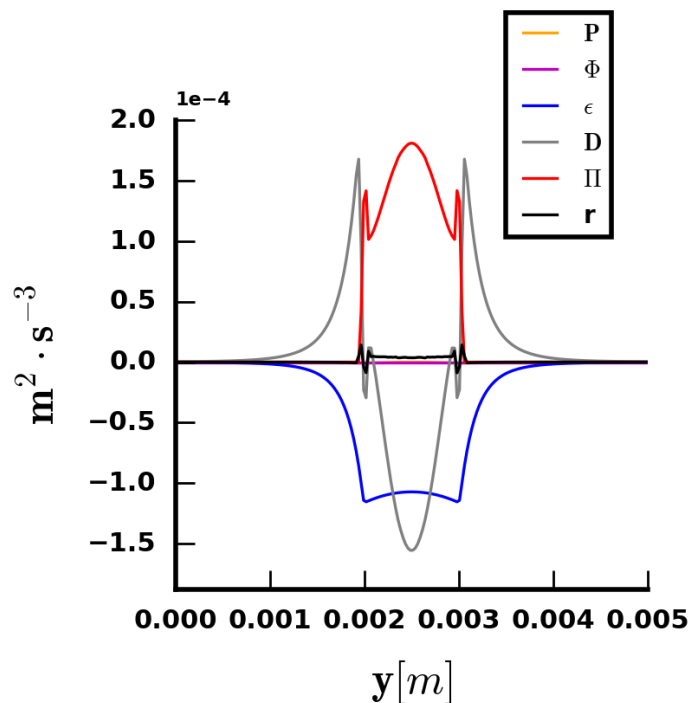
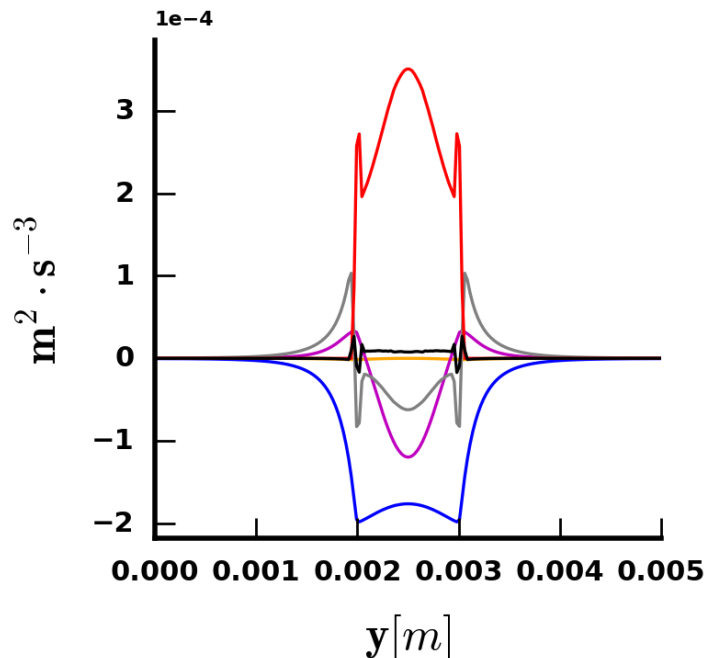
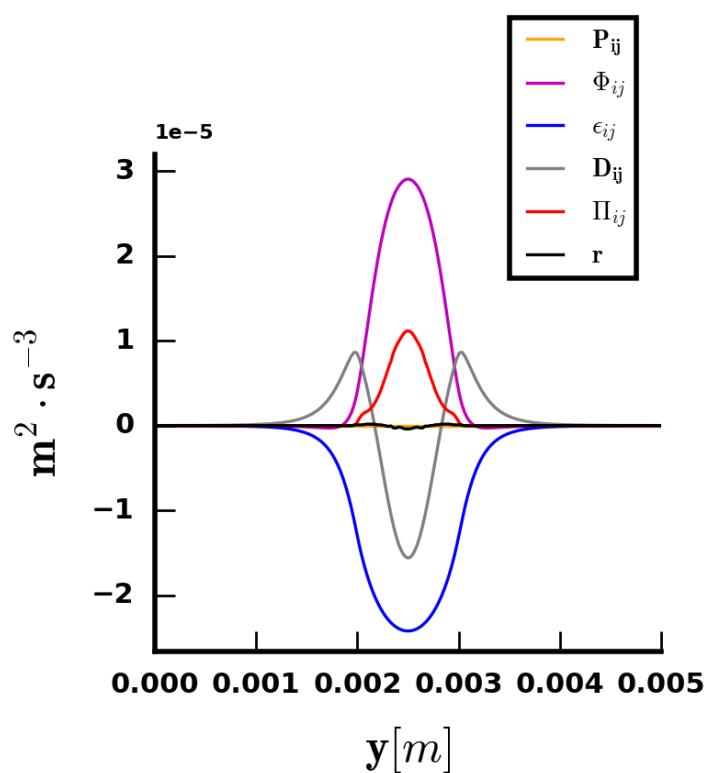
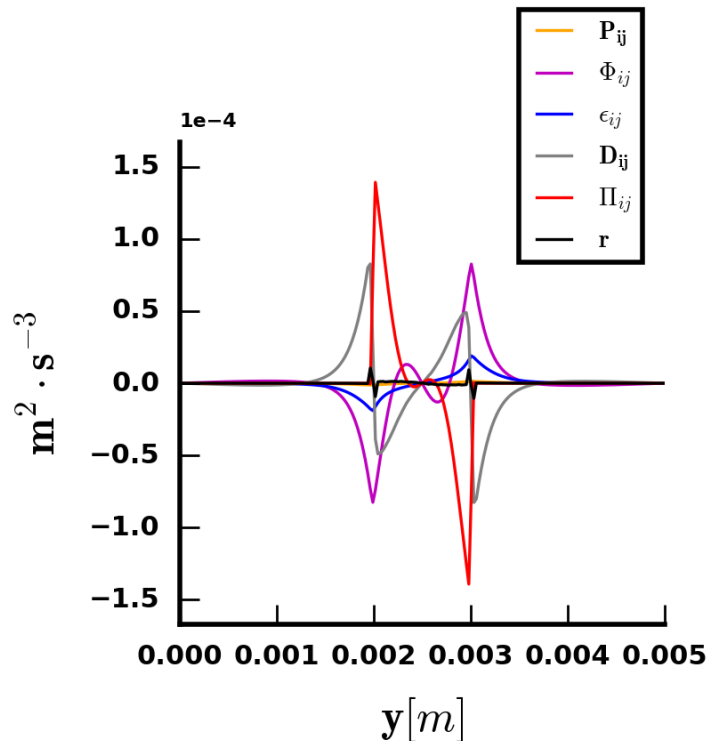
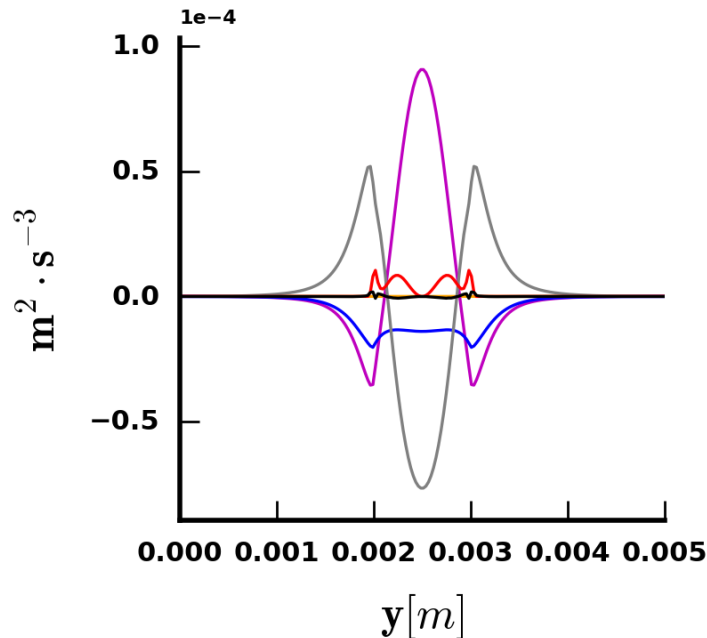


Figure 7.17: Contributions to the K balance equation

(a) R_{xx} (b) R_{zz}

Figure 7.17: Contributions to the R_{ij} balance equation

7.3.4 Confront with the implicit evaluation

The last step of the study of the Reynolds stress balance equation is the comparaison between the methodology developped in the present work to compute Π and the one exposed in [1]: as did for the interfacial force, in this case too it was evaluated as the residue of the equation 3.22 at the steady state. The results obtained are extremely positive: the two profiles have the same trend and small differences in magnitude could be detected in correspondence of the peak and of the interface.

In conclusion, although numerical errors are still present for the averaged quantites in the streamwise direction, the pressure reconstruction developped in the present work validate the results already obtained by the SMTF of the CEA in this field and stands as a perfomant tool for furher studies on more relevant configurations, where the impact of the bubble on the interface is essential in the modeling of the two-phase turbulence.

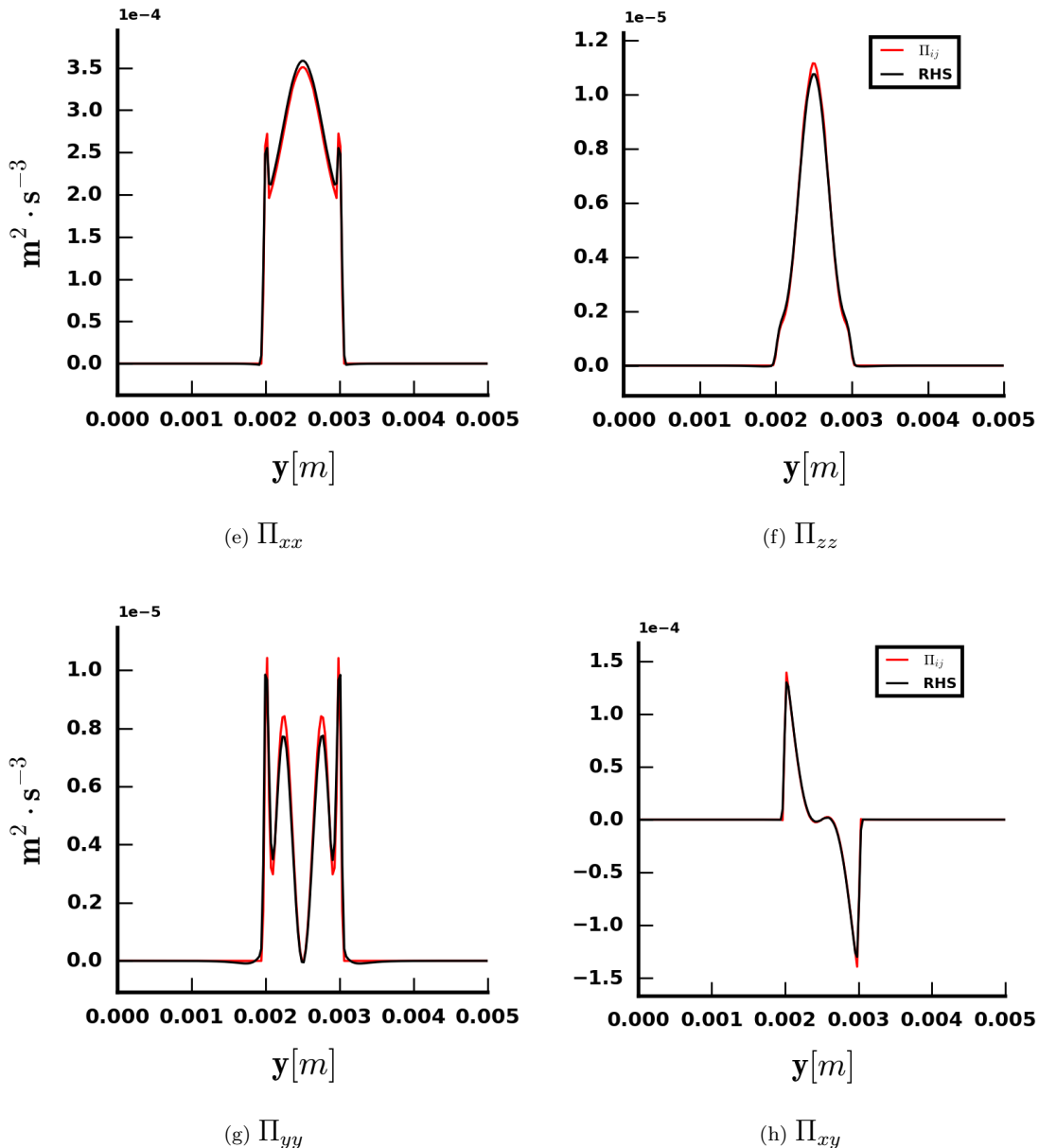


Figure 7.18: Confront between the explicit and implicit esteem of Π_{ij}

8 Swarm of bubbles

In this section a first application of the tools developped during this internship is presented. A swarm of random bubbles is investigated, the numerical settings and results obtained are presented.

8.1 Settings

The case analysed is one of the configuration already employed in [2] to better characterize the turbulent structures appearing in bubbly flows. It deals with a swarm of bubbles randomly dispersed in a tri-periodic box and rising along the x-direction in a liquid at rest. The phases are assumed incompressible, phase-change and heat transfer are neglected. The settings adopted are the same proposed in [2], except for the viscosity of the vapor phase, set equal to the liquid one. This choice is required to avoid issues with the interpolation of the viscosity at the interface and simplify the computation of the interfacial viscous terms.

L_x [m]	0.02
L_y, L_z [m]	0.005
α_v [%]	6
d_b [m]	0.001
σ [N/m]	0.018055
ρ_l [kg/m ³]	1171.3
ρ_v [kg/m ³]	87.545
μ_l, μ_v [Ns/m ²]	0.00035
Nb	57
Re_b	411

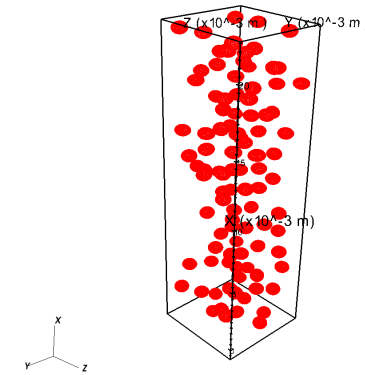


Table 8.1: Geometrical and physical parameters - swarm of bubbles case

Figure 8.1: Initial position of the bubbles in the box.

As regards the convergence in time, the simulations was run over about 4s. The velocity of the liquid and of the vapor phase are computed as for the single bubble. Their trend over the last 2.5s of the simulation is displayed below:

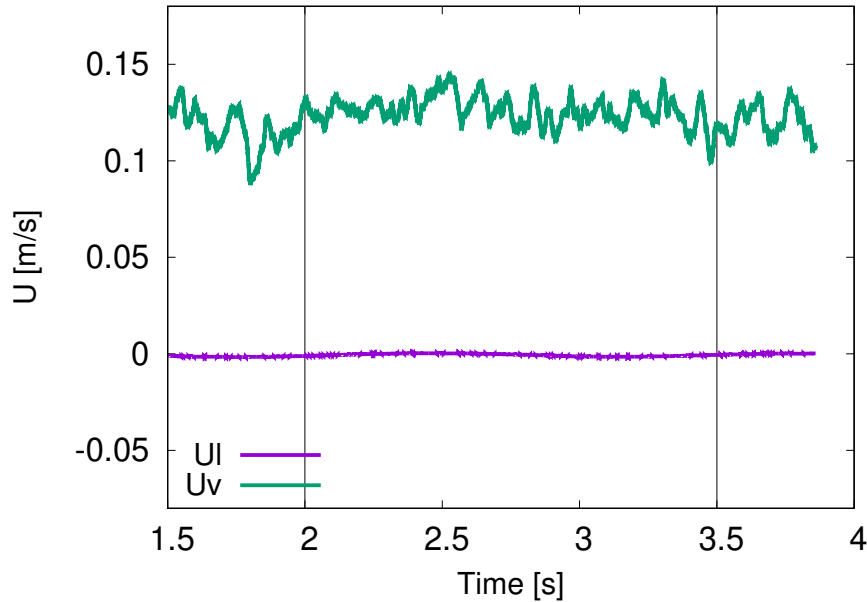


Figure 8.2: Evolution in time of liquid (U_l) and gas (U_v) velocity.

The liquid velocity show some oscillations around zero, as expected. On the other hand the velocity of the vapor phase is characterized by a greater amplitude of the fluctuations. However they are evidently centered on a value equal to 0.123 [m/s]. This is the relative velocity u_r involved in the definition of the bubble Reynolds number Re_b . The statistics are then computed on the time window $2 - 3.5s$ as shown in figure 8.2 by the vertical lines. In order to avoid issues due to the presence of these temporal fluctuations, the temporal derivative $\frac{\partial \alpha_\kappa \bar{u}_\kappa}{\partial t}$ is computed too in the averaged momentum equation 3.19. It is found out to be not exactly zero, but still negligible. Then the statistical steady state of the system is approximately reached. As regards the mesh convergence no further study has been carried out since the huge computational resources required do not allow a finer discretization than the one employed by du Cluzeau in [2], namely 25 cells/diameter.

8.2 Results

Although at the current state of the work a complete analysis of the results is not available, this case is remarkable for two main reasons: firstly the void fraction and the random positions taken by the bubbles lead to exceptions in the algorithm for pressure reconstruction. The impact the disregarding of the cells in between the bubbles have on the statistics may then be explored. Secondly this simulation is intended to check that the tools developed suit for a realistic configuration: the conditions analysed, namely the high void fraction and the high Reynolds number are closer to real industrial applications. In addition it is noted that the physical properties of the phases have been originally chosen by du Cluzeau to reproduce the density ratio of the flow in a reactor.

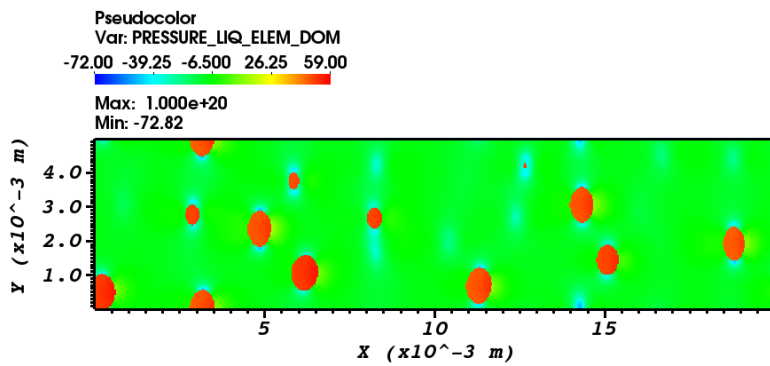


Figure 8.3: Extended liquid pressure field on a plane at $y = 0.0025m$ after 4 time-steps.

The averaging procedure adopted is the same explained above, although in this case the random position of the bubbles generates some curves that are not meaningful. Thus the total average has been taken into account computing the mean value of these curves. As regards the momentum transport, along the direction y and z no significant term in equation 3.19 is detected because of the random disposition of the bubbles and of the absence of motion. On the other hand along x the bouyoancy and the interfacial pressure force mainly contribute to the balance of the phase. It is noted that in absence of walls the source term β is zero. The results obtained for the interfacial pressure terms in both the momentum and the Reynolds Stress equation are reported. The redistribution term for the three diagonal components of R_{ij} is displayed too. It is noted that a numerical error appears in the momentum equilibrium of the liquid phase, as well as in the Reynolds stress balance for the $y - y$ and $z - z$ components. In the first case it is equal to 11% of M_l^P , whereas in the latter the residue has the same magnitude of the other terms in the equation 3.22

M_l^P	M_v^P	Π_{11}^P	Π_{22}^P	Π_{33}^P	Φ_{11}	Φ_{22}	Φ_{33}
592.04	-481.5	0.0995	0.0097	0.0096	-0.0672	0.0341	0.03318

Table 8.2: Interfacial pressure contributions and redistribution.

9 Conclusions and Perspectives

During this internship an algorithm for the pressure-discontinuity reconstruction at the bubble interface has been implemented in the open-source code TrioIJK. This reconstruction has been designed to compensate for the lack of single phase values in interfacial cells, caused by the resolution of the one-fluid equations and by the adoption of an Euler/Lagrange method. This aim has been accomplished by a linear extrapolation from the local fields for both the liquid and the vapor phase. Because of the shape of the bubbles the direction privileged for this extrapolation is the normal to the interface, which is accounted for thanks to a bidimensional Lagrangian mesh by the Front-Tracking. The absence of grid points along this direction has been supplied defining two new points along it and then interpolating here the pressure field. This algorithm has been proved to perfectly work: the interfacial cells become ghost cells for both the liquid and the vapor pressure. The points where local purely liquid information are not available, namely the cells close to the wall or in between two bubbles are excluded from this research. Whenever possible, if the layer of purely liquid cells exists around the bubble but is not thick enough for the algorithm to be fully performed, the pressure values available here are assumed as constant at the interface too. The extension for the vapor phase is straightforward and when bubbles are overlapping just one of the two pressures is taken into account in the extrapolation.

These extended fields based on the DNS results are involved in an up-scaling procedure in order to provide RANS two-fluid equations. They are derived for incompressible fluids in adiabatic condition, neglecting the phase change and assuming the two phases have the same, constant viscosity. All the terms occurring in these equations are explicitly computed, in contrast to what has been done with the previous applications of TrioIJK.

The simulation of a single bubble rising in a periodic box leads to the following conclusions in the analysis of the momentum balance:

- the interfacial force is extremely sensitive to the mesh refinement;
- the averaged shear stress $\overline{\tau_\kappa}$ requires a more accurate definition as $\mu \left(\overline{\chi_\kappa \nabla u_\kappa} + \overline{\chi_\kappa \nabla^T u_\kappa} \right)$;
- a non-zero residue arises in the projection of equation along the streamwise direction. It is significant especially for the liquid phase, where the viscous effects play a remarkable role;
- the jump condition $\sum_\kappa \mathbf{M}_\kappa = \mathbf{M}_\sigma$ is satisfied;

Additional comments are required by the computation of the Reynolds Stress balance equation for the liquid phase:

- the pressure diffusion is smoother when computed resorting to the extended field, the redistribution on the other hand exhibits a slightly different magnitude;
- the numerical error is always zero when the interfacial production Π is explicitly computed, whereas an error arise for the first component R_{xx} and it cannot be neglected since it has the same magnitude of the turbulent diffusion. The same error is found in the kinetic energy balance because R_{xx} mainly contributes to it.

In conclusion the up-scaling procedure has been checked through the explicit computation of the interfacial terms. They are in good agreement with the implicit esteem of M_κ and Π as the residue of the balance equations performed in the previous applications of TrioIJK. An error of 3 of the maximum is detected along the streamwise direction for M_κ , whereas the Reynolds stress components show a slight difference due to the different ratio between interfacial production and redistribution. The R_{xx} component is still not validated since an error in the evaluation of the viscous contribuition appears at the current state of the work.

To sum up the main goal of the stage has been accomplished since the algorithm implemented provides a perfect extension of the pressure to the interfacial cells. A new tool is now implemented in TrioIJK for further studies, although the averaged equations require a careful mathematical derivation to avoid the current inaccuracy along the streamwise direction. Additional works should aim at correcting this error, probably related to the presence of the source term along the streamwise direction and to the consequent difference between numerical and physical pressure. For the future this tool could be involved in the analysis of the turbulent up-flow in the vertical channel in order to validate the models presented in [1] and to provide a further insight on the interfacial dynamics. Moreover an extention of the velocity gradient too could be implemented to study more realistic conditions where phase-change is allowed and the ratio between the dynamic viscosities is not anymore equal to one.

A Alternative method

The algorithm implemented in the code and developped in this work is not the only possible strategy to reconstruct the pressure field at the interface. Another algorithm have been originally tested in order to avoid some of the problems related to the method proposed in case of swarm of bubbles. This second way tries to break free from the problems generated by the one-fluid formulation and in order to accomplish this aim it uses in the post-processing part some ideas of the free-surface method. This approach results in solving the equations for each phase separately and in taking into account the effect of the other phase through boundary conditions explicitely imposed. Examples of application of this method, like the ones proposed in [15] need to extend the properties of the computed fluid to one or more layers of Eulerian Cells. It should be borne in mind that in the present case, where the solved field is already provided by TrioIJK, a similar need emerges only in the post-treatment because of the up-scaling procedure the DNS are involved in. As a consequence the main idea is to *diffuse* the computed pressure to the boundary by means of an adequate equation. Essentialy a *Ghost Fluid* method is adopted as the interfacials cells are considered as fictitious liquid (or vapor) cells. In this case too the information will be available at the centers of the Eulerian cells crossed by the interface and not on the front itself, exactly as it has been done by the currently implemented algorithm. A similar approach is already coded in TrioIJK for the temperature in the solution of the energy equation. The main issue is to find a proper equation to impose when this *diffusion* is performed and it clearly must be deduced by the physical properties of the treated field. In the case of the pressure the Poisson equation has to be solved since both of the phases are treated as incompressible and the pressure is then in charge of projecting the velocity field into a divergence-free space. The main advatage of this strategy is that it allows to avoid problems when two bubbles are too close or they are too close to the walls, as it relies on the knowledge of the whole field. The procedure implemented is detailed here.

At the end of every time step, when the projection and the correction substeps are carried out and the one-fluid pressure field is known in every point of the grid, the Poisson solver is performed again for the two phases. In order to do so two new continuos fields have to be defined. The dynamic viscosity μ and the density ρ of the liquid phase are extended everywhere in the computational domain and the same procedure is followed for the vapor phase. As regards the velocity field it does not admit discontinuity in the one fluid equation since the bubbles travel with the liquid flow in absence of phase change, so that no re-initialisation is required. A new velocity projection is then computed resorting to the Poisson solver, accurately modified to suit for the single phase. All the source terms linked to the interfacial discontinuities, namely the surface tension and the spatial difference of density are neglected, leading to the following equation:

$$\dot{\mathbf{v}}_\kappa = -\mathbf{u}^n \nabla \cdot \mathbf{u}^n - \nabla \cdot (\mathbf{u}^n \otimes \mathbf{u}^n) + \frac{1}{\rho_\kappa} \nabla (\mu_\kappa \cdot (\nabla \mathbf{u} + \nabla^T \mathbf{u} - 2\mathbf{n}^n \otimes \mathbf{n}^n \nabla \cdot \mathbf{u}^n)) \quad (\text{A.1})$$

where κ stands for the phase considered. For the previous equation is used just a fictional and small time step and then the Poisson solver is called to have the two pressure extended fields. The expression to be solved imposing a divergence-free velocity field in all the domain is then presented below:

$$\nabla \cdot \left(\frac{1}{\rho_\kappa} \nabla P_\kappa \right) = -\nabla \cdot \dot{\mathbf{v}}_\kappa \quad (\text{A.2})$$

At the end of this step all the one-fluid variables have to be restored in order to run properly the Navier-Stokes solver at the following time step.

Then this method leads to the computing of two continuos fields extended to all the cells of the domain, even at the interfaces. In order to understand the results of this extention, a simple test case has been studied, simulating the rise of a single bubble in a small channel. The main parameters of the simulation are reported here:

L_x [mm]	6
L_y [mm]	6
L_z [mm]	3
Δ [mm]	0.125
d_b [mm]	1
ρ_l [kg/m ³]	1000
ρ_v [kg/m ³]	600
μ_l [Ns/m ²]	0.001
μ_v [Ns/m ²]	0.001
σ [N/m]	0.07

Table A.1: Physical and geometrical parameters of the studied configuration. The grid is uniform and the initial velocity profile for the component along x is quadratic.

The streamwise direction is marked by x and the transverse by y . The extended pressure fields obtained are presented in the following pictures.

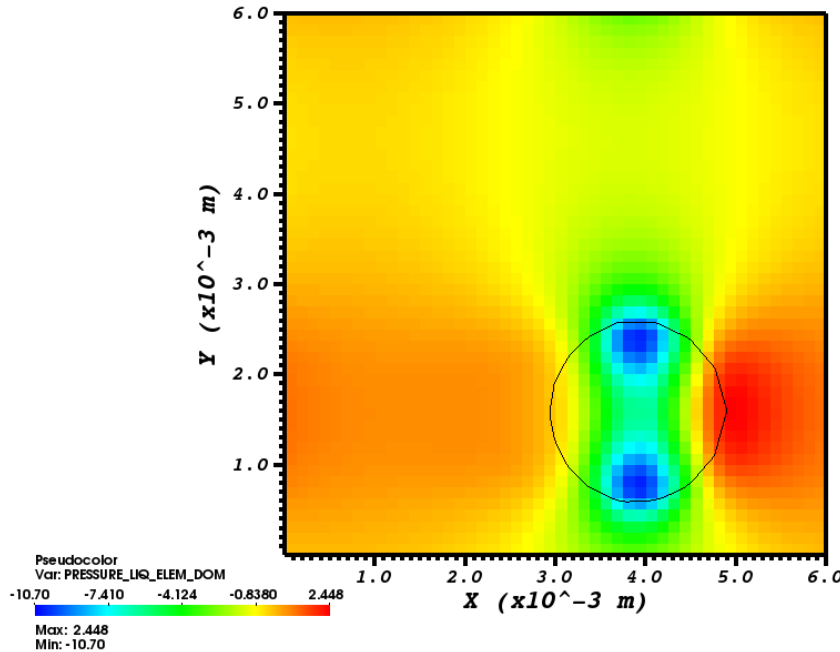


Figure A.1: Pressure extended field in the liquid phase on a slice along the z axis. Time step=100

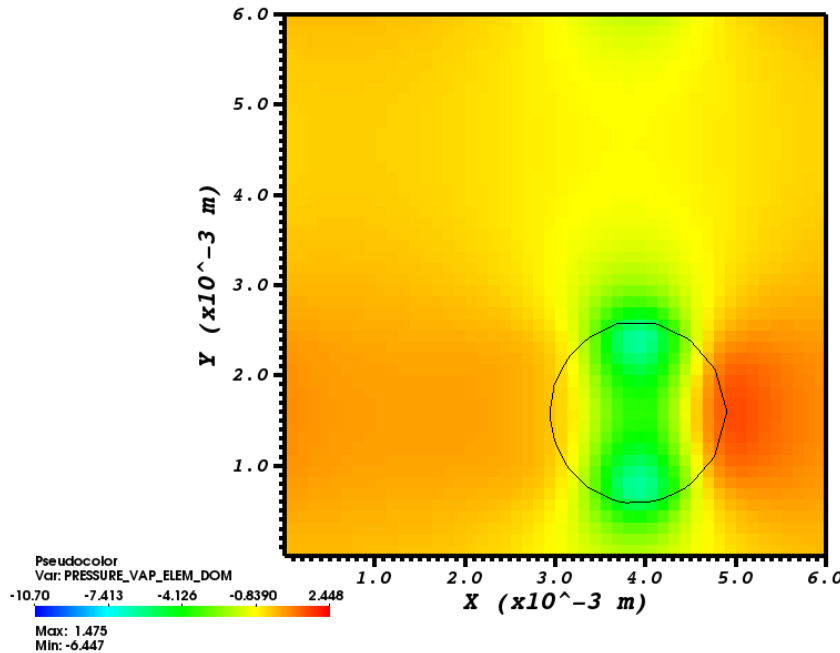


Figure A.2: Pressure extended field in the vapor phase on a slice along the z axis. Time step=100

The two fields are similar as they satisfy the same equation and they differ only for their magnitude. The distribution obtained is in good agreement with the theoretical results known for the flow past a sphere: an high pressure region is detected on the top of the bubble, responsible for the Drag force that hinders its motion. The major disadvantage of this calculation is that the existing difference between vapor and liquid pressure is not related to the source term and then to the surface tension of the bubble. Moreover the difference between the one-fluid pressure and the extended field in the liquid phase has been analysed.

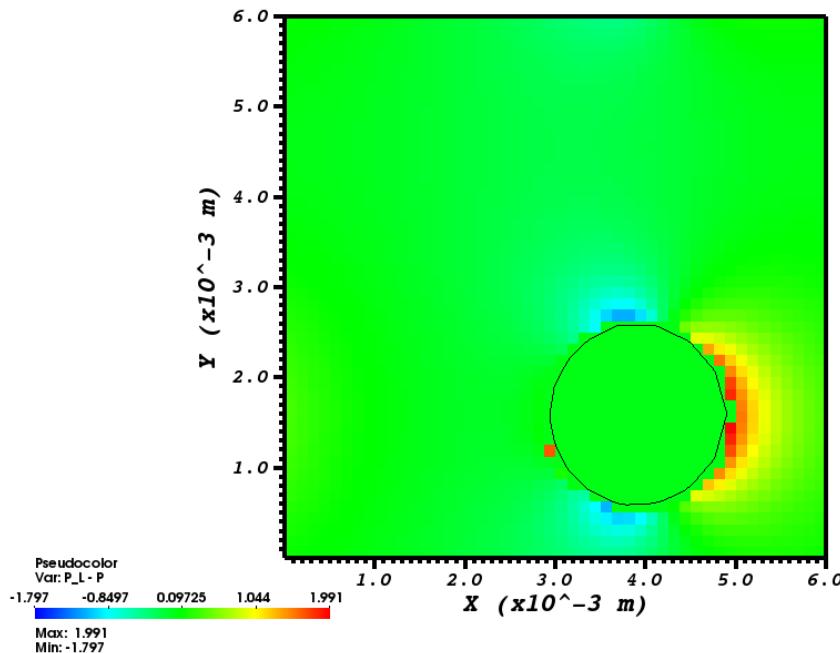


Figure A.3: Difference between the liquid extended field and the on-fluid pressure field on a slice along the z axis. Time step=100

This difference is expected to be uniform in space, since the two fields are supposed to respect the same conditions, but the results show exceptions along the bubble interface. This difference reveals that neglecting the surface tension leads to a pressure field whose physical relation with the real conditions of the simulation is not clear. To sum up these punctual reconstruction of the field is not allowed to be assumed as a trustworthy representation of the physics of the bubbly flow. An althernative way, inspired to the work exposed in [15], should involve in the pressure diffusion only the very interfacial cells. This strategy would be local as the one currently implemented, but at the same if the jump condition are properly accounted for, it may assure an higher physical consistency compared to the linear extrapolation currently implemented. In conclusion, the algorithm proposed in this appendix is not able of providing an istantaneous correct pressure field in the cells crossed by the interface and so it is not possible to include these results in the up-scaling to compute the interfacial terms in the averaged equations. Furthermore, the computational cost of such a procedure is high as the Poisson solver, which has to be performed three times per each time-step, is responsible of most of the computational power required by the entire Navier-Stokes solver. Nevertheless future perspectives and studies might focus on how to take into account the jump condition rapresented by the surface tension. As a matter of fact it is recalled that in the free-surface method it is employed as a boundary condition in the original solver and consequently the ghost pressure is related to it. In the code a first attempt has been carried out. Firstly the extended pressure fields have been interpolated on the Lagrangian mesh of the front, then an averaged value on each bubble has been computed, weighthed by the surface of each element of the domain of the front. The two scalar values obtained are not related, thus one of the two has been corrected so that their difference is equal to the source term $\sigma\kappa\delta^i$, where κ is an averaged value of the curvature of the single bubble obtained following the same procedure seen for the pressure. Future studies may provide a method to extend this scalar corrected values again to the Eulerian cells and provide a useful field for post-processing. Other strategies are evidently possible to directly compute the discontinous field with the Navier-Stokes solver, but they should rely on a different formulation of the equations for two-phase flows.

B Derivation of the Reynolds stress transport equation

The very first step to derive the equation 3.22 consists in finding the transport equation for the fluctuating velocity. It should be borne in mind that this quantity is defined as $u'_{\kappa,i} = u_{\kappa,i} - \overline{u_{i,\kappa}}^{\kappa}$, where $\overline{u_{i,\kappa}}^{\kappa} = \frac{u_{i,\kappa}\chi_{\kappa}}{\chi_{\kappa}}$ is the phase average. The technique originally proposed by [9] and then adopted in [18] too is followed. Only incompressible flows are taken into account. Disregarding the source term added in TrioIJK and resorting to the definition of shear stress tensor for a Newtonian fluid, the averaged momentum equation 3.19 could be rewritten as:

$$\begin{aligned} \frac{\partial \alpha_{\kappa} \bar{\mathbf{u}}_{\kappa}^{\kappa}}{\partial t} + \nabla \cdot (\alpha_{\kappa} \bar{\mathbf{u}}_{\kappa}^{\kappa} \otimes \bar{\mathbf{u}}_{\kappa}^{\kappa}) &= -\frac{1}{\rho_{\kappa}} \nabla (\alpha_{\kappa} \overline{p_{\kappa}}^{\kappa}) + \nu_{\kappa} \nabla^2 (\alpha_{\kappa} \bar{\mathbf{u}}_{\kappa}^{\kappa}) \\ &+ \alpha_{\kappa} \mathbf{g} - \nabla \cdot \left(\alpha_{\kappa} \overline{\mathbf{u}'_{\kappa} \otimes \mathbf{u}'_{\kappa}}^{\kappa} \right) - \frac{1}{\rho_{\kappa}} \overline{p_{\kappa} \mathbf{n}_{\kappa} \delta_i} + \overline{\nu_{\kappa} \nabla \mathbf{u}_{\kappa} \cdot \mathbf{n}_{\kappa} \delta_i} + \nu_{\kappa} \nabla \cdot \overline{\mathbf{u}_{\kappa} \cdot \mathbf{n}_{\kappa} \delta_i} \end{aligned} \quad (\text{B.1})$$

Multiplying B.1 for the phase indicator function χ_{κ} and then subtracting it from the equation 3.13, one can derive the evolution equation for the i - component of the fluctuating field \mathbf{u}'_{κ} :

$$\begin{aligned} \chi_{\kappa} \left[\frac{\partial u'_{\kappa,i}}{\partial t} + \overline{u_{\kappa,b}}^{\kappa} \frac{\partial u'_{\kappa,i}}{\partial x_b} + u'_{\kappa,b} \frac{\partial \overline{u_{\kappa,i}}^{\kappa}}{\partial x_b} + u'_{\kappa,i} \frac{\partial \overline{u'_{\kappa,i}}}{\partial x_b} - \frac{\partial}{\partial x_b} \overline{u'_{\kappa,i} u'_{\kappa,b}}^{\kappa} \right] = \\ \chi_{\kappa} \left[-\frac{1}{\rho_{\kappa}} \frac{\partial p'}{\partial x_i} + \nu_{\kappa} \frac{\partial^2 u'_{\kappa,i}}{\partial x_b^2} - \frac{1}{\alpha_{\kappa}} \left(-\frac{1}{\rho_{\kappa}} p_{\kappa} n_{\kappa,b} \delta_i + \nu_{\kappa} \frac{\partial u_{\kappa,i}}{\partial x_b} n_{\kappa,b} \delta_i \right) + \nu_{\kappa} \frac{\partial u_{\kappa,i} n_{\kappa,b} \delta_i}{\partial x_b} - \frac{1}{\alpha_{\kappa}} Q_{\kappa,i} \right] \end{aligned} \quad (\text{B.2})$$

$$\text{where } Q_{\kappa,i} = \left(-\frac{p_{\kappa}}{\rho_{\kappa}} \delta_{ib} + 2\nu_l \frac{\partial \overline{u_{\kappa,i}}^{\kappa}}{\partial x_b} - \overline{u'_{\kappa,i} u'_{\kappa,b}}^{\kappa} \right) \frac{\partial \alpha_{\kappa}}{\partial x_b} + \nu_l \overline{u_{\kappa,i}}^{\kappa} \frac{\partial^2 \alpha_{\kappa}}{\partial x_b^2}.$$

Then, multiplying B.2 by $u_{\kappa,j}$, adding the obtained equation to its transpose and averaging the result the evolution equation for $R_{\kappa,ij} = \overline{u'_{\kappa,i} u'_{\kappa,j}}^{\kappa}$ is found:

$$\begin{aligned} \overline{\chi_{\kappa} \left[\frac{\partial u'_{\kappa,i} u'_{\kappa,j}}{\partial t} + \frac{\partial u'_{\kappa,i} u'_{\kappa,j} \overline{u_{\kappa,b}}^{\kappa}}{\partial x_b} + u'_{\kappa,i} u'_{\kappa,b} \frac{\partial \overline{u_{\kappa,j}}^{\kappa}}{\partial x_b} + u'_{\kappa,j} u'_{\kappa,b} \frac{\partial \overline{u_{\kappa,i}}^{\kappa}}{\partial x_b} + \frac{\partial u'_{\kappa,i} u'_{\kappa,b} u'_{\kappa,j}}{\partial x_b} \right]} = \\ \overline{\chi_{\kappa} \left[-\frac{1}{\rho_{\kappa}} \left(u'_{\kappa,j} \frac{\partial p'_{\kappa}}{\partial x_i} + u'_{\kappa,i} \frac{\partial p'_{\kappa}}{\partial x_j} \right) + \nu_{\kappa} \left(u'_{\kappa,j} \frac{\partial^2 u_{\kappa,i}}{\partial x_b^2} + u'_{\kappa,i} \frac{\partial^2 u_{\kappa,j}}{\partial x_b^2} \right) \right]} \end{aligned} \quad (\text{B.3})$$

It is here recalled that the overbar stands for the statistical average and $\alpha_{\kappa} = \overline{\chi_{\kappa}}$.

The equation B.3 may be re-written introducing the phase indicator function into the derivatives, knowing that $\frac{\partial \chi_{\kappa}}{\partial t} + \mathbf{u}_i \cdot \nabla \chi_{\kappa} = 0$ holds. The results is:

$$\begin{aligned} \overline{\frac{\partial \chi_{\kappa} u'_{\kappa,i} u'_{\kappa,j}}{\partial t}} + \overline{\frac{\partial \chi_{\kappa} u'_{\kappa,i} u'_{\kappa,j} \overline{u_{\kappa,b}}^{\kappa}}{\partial x_b}} + \overline{\chi_{\kappa} u'_{\kappa,i} u'_{\kappa,b} \frac{\partial \overline{u_{\kappa,j}}^{\kappa}}{\partial x_b}} + \overline{\chi_{\kappa} u'_{\kappa,j} u'_{\kappa,b} \frac{\partial \overline{u_{\kappa,i}}^{\kappa}}{\partial x_b}} + \overline{\frac{\partial \chi_{\kappa} u'_{\kappa,i} u'_{\kappa,b} u'_{\kappa,j}}{\partial x_b}} = \\ \overline{\chi_{\kappa} \left[-\frac{1}{\rho_{\kappa}} \left(u'_{\kappa,j} \frac{\partial p'_{\kappa}}{\partial x_i} + u'_{\kappa,i} \frac{\partial p'_{\kappa}}{\partial x_j} \right) + \nu_{\kappa} \left(u'_{\kappa,j} \frac{\partial^2 u_{\kappa,i}}{\partial x_b^2} + u'_{\kappa,i} \frac{\partial^2 u_{\kappa,j}}{\partial x_b^2} \right) \right]} \end{aligned} \quad (\text{B.4})$$

In order to obtain the final form presented in 3.22 the phase average definition is employed and the terms on the RHS of B.4 are decomposed following the equations 7.6 and 7.7. These equalities base on the definition $\nabla \chi_{\kappa} = -\mathbf{n}_{\kappa} \delta^i$.

C Code for pressure reconstruction

```

void IJKFTPost :: compute_extended_pressures(const MaillageFTIJKmesh) if(!extended_pressure_computed) return; //  

    // The following calculation is defined on the extended domain ft const IJKsplittingSplitft =  

    splittingft; const int ni = splitft.get_nb_elem_local(DIRECTION_I); const int nj = splitft.get_nb_elem_local(DIRECTION_J);  

    const int nk = splitft.get_nb_elem_local(DIRECTION_K); const double dx = splitft.get_grid_geometry().get_constant_delta(DIRECTION_I);  

    const double dy = splitft.get_grid_geometry().get_constant_delta(DIRECTION_J); const double dz = splitft.get_grid_geometry().get_constant_delta(DIRECTION_K);  

    IJKField_double extended_p = phase == 1 ? extended_p : extended_pv; // The field we want to fill :  

    if(phase < 0 || phase > 1) Process :: exit();  

    Cerr jj extended_p(0,0,0) << finl;  

    interfaces.calculer_normales_taires_interfacing(ai,kappa_aj,normale_cell_ft,-1);  

    int nbsom = 0; ArrOfInt liste_composantes_connexes_dans_element; liste_composantes_connexes_dans_element.set_size(nbsom, 3); // Table of coordinates where interpolation need to be computed DoubleTab positions_vap(2*nbsom, 3); IntTab crossed_cells(nbsom, 3); // Table to store i, j, k of cells crossed by the interface. positions_iq.set_size(nbsom, 3);  

    // i,j,k are the indices of the cells in the extended domain, for each processor for (int k = 0; k  

    < nk; k++) for (int j=0; j < nj; j++) for (int i=0; i < ni; i++)  

    if ((indicatrice_ft(i, j, k) != 0) && (indicatrice_ft(i, j, k) != 1))  

        const int elem = splitft.convert_ijk_cell_to_packed(i, j, k); const int nb_compo_traversantes = interfaces.compute_list_compo(1)  

        num_compo = liste_composantes_connexes_dans_element[0]; interfaces.calculer_normale_elt_baryelelement_pour_compo(num_compo, elem, sqrt(normale[0] * normale[0] + normale[1] * normale[1] + normale[2] * normale[2])); dist = 1.52 * (fabs(dx * normale[0]) + fabs(dy * normale[1]) + fabs(dz * normale[2])) / norm;  

        // If the same cell is crossed by several bubbles the image points coincide with the crossed  

        cells // the interpolation function in these points will lead to invalid values. else num_compo =  

        liste_composantes_connexes_dans_element[1]; interfaces.calculer_normale_elt_baryelelement_pour_compo(num_compo, elem, sqrt(normale[0] * normale[0] + normale[1] * normale[1] + normale[2] * normale[2])); dist = 1.52 * (fabs(dx * normale[0]) + fabs(dy * normale[1]) + fabs(dz * normale[2])) / norm;  

        nbsom++; crossed_cells.resize(nbsom, 3, Arraybase :: COPY_INIT); positions_iq.resize(2*nbsom, 3, Arraybase :: COPY_INIT);  

        crossed_cells(nbsom - 1, 0) = i; crossed_cells(nbsom - 1, 1) = j; crossed_cells(nbsom - 1, 2) = k;  

        for (int dir=0; dir<3; dir++) // Four image points are calculated, two on each side of the  

        interface // liquid phase positions_iq(2 * nbsom - 2, dir) = bary_facades_dans_elm[dir] + dist *  

        normale[dir]; // 1st point to be done... positions_iq(2 * nbsom - 1, dir) = bary_facades_dans_elm[dir] +  

        2 * dist * normale[dir]; // 2nd point to be done... // vapor phase positions_vap(2 * nbsom - 2, dir) = bary_facades_dans_elm[dir] -  

        dist * normale[dir]; // 1st point to be done... positions_vap(2 * nbsom - 1, dir) = bary_facades_dans_elm[dir] -  

        2 * dist * normale[dir]; // 2nd point to be done...  

        // pressure field has to be extended from ns to ft  

        ref_ijkft.redistribute_to_splittingft(elem.redistribute(pressure, pressure_ft); pressure_ft.exchange_space_virtuel(pressure_ft));  

        // Interpolation on the image points // All the quantities are evaluated on the extended domain,  

        both the pressure field, both the image points coordinates  

        ArrOfDouble p_interp_iq(2*nbsom); ArrOfDouble p_interp_vap(2*nbsom); ijk_interpolate_skip_unknown_points(pressure  

        value_for_unknown_points *); ijk_interpolate_skip_unknown_points_bs(pressure_ft, positions_iq, p_interp_iq, 1.e5 /*  

        value_for_unknown_points */ , indicatrice_ft);  

        // initialisation  

        // The other points of the domain (the one outside the crossed cells are still equal to original  

        value of pressure) // This generates the discontinuities seen in Visit extended_p_ft = pressure_ft, extended_pv_ft = pressure_ft  

        // Extrapolation in the eulerian cells crossed by the interface for (int icell=0; icell<nbsom;  

        icell++)  

        const int i = crossed_cells(icell, 0); const int j = crossed_cells(icell, 1); const int k = crossed_cells(icell, 2); const int elem =
```

```

split_ft.convert_ijk_cell_to_packed(i, j, k); const int nb_compo_traversantes = interfaces.compute_list_compo_connexion_element;
2 * p_interp_v.ap(2 * icell) - 1 * p_interp_v.ap(2 * icell + 1);
if (nb_compo_traversantes != 1) extended_pv_ft(i, j, k) = 1.e20;
if (p_interp_iq(2*icell+1) == 1.e5) if (p_interp_iq(2 * icell) == 1.e5) // May changing the order affect the result??
extended_pl_ft(i, j, k) = 1.e20;
else extended_pl_ft(i, j, k) = p_interp_iq(2 * icell);
else if (p_interp_iq(2 * icell)! = 1.e5)
extended_pl_ft(i, j, k) = 2 * p_interp_iq(2 * icell) - 1 * p_interp_iq(2 * icell + 1);
else
extended_pl_ft(i, j, k) = p_interp_iq(2 * icell + 1);
// The previous evaluated extended pressure has to be recomputed on the real NS domain
ref_ijk_ft.redistribute_from_splitting_ft_elem.redistribute(extended_pl_ft, extended_pl); ref_ijk_ft.redistribute_from_splitting_ft_elem.redistribute(extended_pl, extended_pv.ghost());
extended_pl.echange_e_space_virtuel(extended_pl.ghost()); extended_pv.echange_e_space_virtuel(extended_pv.ghost());

```

References

- [1] A. DU CLUZEAU, G. BOIS, A. TOUTANT Analysis and modelling of Reynolds stresses in turbulent bubbly up-flows from direct numerical simulations. *Journal of Fluid Mechanics*, **866**: 132-169, 2019.
- [2] A. DU CLUZEAU *Modélisation physique de la dynamique des écoulements à bulles par remontée d'échelle à partir des simulations fines*. PhD Thesis, Université de Perpignan Via Domitia, 2019.
- [3] G. BOIS, A. DU CLUZEAU DNS of Turbulent Flows in Plane Channels Using th Front-Tracking Algorithm of TrioCFD. In: Proceedings of the ASME Fluids Engineering Division Summer Meeting. Waikoloa, Hawaii, USA. 2017.
- [4] G. BOIS Direct Numerical Simulation of a turbulent bubbly flow in a vertical channel: Toward an improved second-order reynolds stress model. *Nuclear Engineering and Design* **321**: 92-103, 2017.
- [5] C. SANTARELLI, J. ROUSSEL, J. FROHLICH Budget analysis of the turbulent kinetic energy for bubbly flow in a vertical channel. *Chemical Engineering Science* **141**: 46-62, 2016.
- [6] J.LU, G. TRYGGVASON Effect of bubble deformability in turbulent bubbly upflow in a vertical channel. *Physics of fluid* **20**:040701, 2008.
- [7] G.TRYGGVASON et al. Computations of multiphase flow by a finite difference/front-tracking method. *Journal of computational physics* **169**:708-759, 2001.
- [8] I.KATAOKA Local instant formulation of two phase flows. *International Journal of Multiphase Flow* **12**(5): 745-758, 1986.
- [9] I.KATAOKA and A. SERIZAWA. Basic equations of turbulence in gas-liquid two-phase flow. *International Journal of Multiphase Flow* **15**(5) 843-855, 1989.
- [10] M. ISHII, N. ZUBER Drag coefficient and relative velocity in bubbly, droplte or particulate flows. *AIChE J.* **25**(5): 843-855, 1979.
- [11] S. QUAN, D.P. SCHMIDT A moving mesh interface tracking method for incompressible two - phase flows. *Journal of Computational Physics* **221**: 761-780, 2007.
- [12] M.LANCE, F.BATAILLE Turbulence in the liquid phase of a uniform bubbly air-water flow. *Journal of Fluid Mechanics* **222**: 95-118, 1991.
- [13] W. DIJKHUIZEN, M. VAN SINT ANNALAND , J.A.M. KUIPERS Direct numerical simulation of the drag force in bubble swarm. In: Proceedings of the 6th International Conference on Multiphase flows. Leipzig, Germany. 2007.
- [14] J. KIM, D. KIM, H. PARK, J.H. LEE Modelling of interfacial momentum exchange for wall-bounded bubbly flows. In: Proceedings of the 16th NURETH conference. Chicago, Illinois, USA. 2015
- [15] M. SINGH, P.K. FARSOIYA, R.DASGUPTA Test cases for comparaison of two interfacial solvers. *International Journal of Multiphase flows-* In Press.
- [16] G.TRYGGVASON, R. SCARDOVELLI , S.ZALESKI *Direct Numerical Simulations of Gas-Liquid Multiphase Flows*. Cambridge University Press, 2011.
- [17] S. B. POPE *Turbulent Flows*. Cambridge University Press, 2000.

- [18] C. MOREL *Mathematical modelling of Two - Phase flows*. Springer 2015
- [19] C.E. BRENNEN *Fundamentals of Multiphase Flows*. Cambridge University Press, 2005.
- [20] J.- M. DELHAYE *Thermohydraulique des réacteurs*. EDP Sciences.